The Pennsylvania State University
The Graduate School
College of Engineering

OPTIMAL EARTH RETURN TRANSFERS FROM LAGRANGE POINT ORBITS USING PARTICLE SWARM OPTIMIZATION

A Thesis in
Aerospace Engineering
by
Mollik Nayyar

Submitted in Partial Fulfillment
of the Requirements
for the Degree of

Master of Science

December 2016

The thesis of Mollik Nayyar was reviewed and approved* by the following:

David B. Spencer
Professor of Aerospace Engineering
Thesis Advisor

Joseph F. Horn
Professor of Aerospace Engineering

Philip J. Morris
Professor and Interim Head
Department of Aerospace Engineering

*Signatures are on file in the Graduate School.

Abstract

A future where space mining and cargo transportation is fast approaching reality, for such a future, one needs a way to efficiently transport the materials gathered in space to Earth or other space based depots. The focus of this thesis is on such return trajectories from Lagrange point orbits to Earth. Since travel in space is currently very expensive, it is desired to utilize more efficient methods to travel through space. Current trajectory design methods require a lot of computational resource which contributes to mission cost. This thesis presents an approximate, computationally inexpensive method to scan the available search space and obtain the locations and trajectories associated the with lowest ΔV, which can be used as an initial guess that can be later used in advanced methods to obtain ΔV optimal trajectories. The use of invariant manifolds in the Earth-Moon system is proposed for this purpose. The three-body system is studied and a simplified methodology for the design of trajectories from the Lagrange point orbits is presented. The techniques to generate the invariant manifold associated with Lagrange point orbits is presented. To obtain the best possible trajectory based on ΔV requirements, an optimization scheme is introduced to select the best location on the manifold to initiate transfer. While gradient based methods have been previously used to study optimal trajectories in the three-body system, these are computationally very expensive. Therefore, this thesis tackles the computational requirements associated with design of the space trajectories in the Earth-Moon-spacecraft three-body system for space transportation. The solver used to survey the search space of the invariant manifold is presented. The two-body approximation is utilized to provide quick, preliminary study of the transfers in space, allowing the mission designer to be able to devise a suitable trajectory in the three-body system using the insights from the two-body approximation. Essentially, the burden of finding the location of the transfer point with the minimum ΔV transfer is offloaded to the particle swarm optimization algorithm that uses a simplified Lambert's solver to scan the search space on the manifold and provide the patch point with the lowest ΔV. The solver used here is validated using the results obtained from literature for transfers

from Earth to a Lagrange point orbit. Validation results show that the technique used is able to provide fairly accurate results for a two-impulse scenario at a very significant computational advantage. Then, the method is used to generate results for Earth return trajectories. The ΔV requirements from Lambert's solver for halo and Lyapunov orbits of $L_1,\ L_2$ points are presented. The trends obtained using this method shows the location of orbit insertion in the LEO that has the potential of providing the lowest ΔV. The present analysis suggests that it is possible to reach almost any inclination from the manifold of a halo LPO without incurring huge ΔV costs if the target location for insertion along the final orbit's true anomaly is either at the ascending or the descending node. ΔV was found to increase as the point of insertion approached a true anomaly corresponding to maximum z-component displacement from the equator. These trends seem to hold for higher inclinations of the final orbit. Similar trends seem to hold for transfers from Lyapunov orbit as well. The results and initial and final ΔV vectors obtained by this method has the potential to be used as an initial guess for gradient-based methods. Finally, ways to improve upon the solver and the optimization algorithm are suggested. The technique maybe combined with gradient-based methods to quickly and with reasonable accuracy locate the point on the manifold in the vicinity of the optimal point and then a detailed analysis may be pursued for better and more ΔV optimal results.

Table of Contents

List of Figures

List of Tables

Nomenclature

LPO	Lagrange Point Orbit
LEO	Low Earth Orbit
GEO	Geostationary Earth Orbit
DST	Dynamical Systems Theory
TOF	Time of Flight
ISEE-3	International Sun-Earth Explorer 3
SOHO	Solar and Helioshperic Observatory
WMAP	Wilkinson Microwave Anisotropy Probe
JWST	James Webb Space Telescope
DU	Cannonical Distance Units
TU	Cannonical Time Units
G	Universal Gravitational Constant
L_1	Collinear Lagrange point located between the two primaries.
L_2	Collinear Lagrange point located the on the far side of the smaller primary
L_3	Collinear Lagrange point located the on the far side of the larger primary
L_4	Equilateral Lagrange point located the on the positive side of the y-axis

L_5	Equilateral Lagrange point located the on the negative side of the y-axis
CR3BP	Circular restricted three-body problem
EOM	Equations of Motion
ECI	Earth Centered Inertial
KE	Kinetic Energy
PE	Potential Energy
U	Pseudopotential
STM	State Transition Matrix
MATLAB	Matrix Laboratory software package
TPBVP	Two-Point Boundary Value Problem
ISS	International Space Station
PSO	Particle Swarm Optimization
SS	Single Shooting Method
SOI	Sphere of Influence
RAAN	Right Ascension of the Ascending Node

Acknowledgments

The completion of this thesis is a result of efforts from numerous people in various ways. First of all, I would like to thank my advisor, Dr. David B. Spencer for his constant guidance, support and incredible patience with reading my thesis drafts. I know that through his efforts, I have become a better writer. I would like to thank him for motivating me towards taking up the three-body problem as my thesis topic. This has been an incredibly knowledgeable and satisfying experience. His guidance and support throughout the masters program has made this a very easy and enjoyable experience.

I would like to thank Dr. Andrew Abraham who has been taking the time to, help with and support me in my endeavor towards this thesis since its conception. His work has guided me every step of the way and has been a major factor responsible for the completion of this thesis.

My friends have been an invisible source of inspiration for me throughout my masters education. Their display of hard work and dedication towards their work has given me personal goals to achieve and habits to emulate to become a better professional.

My family has been the foundation, the pillars and the roof which has nurtured my education from the get go. My father's unwavering support, faith and motivation towards my education has been the reason that has made this possible. He has been the well of strength that I have drawn from, and the pillar of support that I have relied on always. My mother's unconditional love, wishes, support and motivation has given me the strength to carry on with my dreams. Her care has been responsible for making me a better human being. My sister's constant presence and her watchful eye has been the greatest source of comfort and support. I may still be a work in progress but her habit of showing me the mirror has helped me change for the better. I would like to thank them all for always being there for me, and for pushing me to better my future self.

Finally, I would like to thank God for giving me the family, friends and the opportunity to help me pursue my dreams and getting me to where I am.

Chapter 1
Introduction

1.1 Motivation

The high cost of space exploration is one of the biggest problems for space missions venturing out in the solar system. With traditional missions modeled on two-body dynamics and impulsive thrust and with an inherent high risk of failures, executing new mission concepts are rendered economically challenging. In the face of such challenges, Lagrange Point Orbits (LPOs) might be able to provide some necessary respite. As the world looks towards space as the next frontier coupled with the fact that technology that exists today is fast approaching the point where space travel or long-duration space missions seem likely in the near future. Missions currently under consideration seem particularly intriguing. One such mission may utilize asteroids moved into an LPO of the Earth-Moon system that can potentially be mined for essential elements. The mined material may be sent to a more stable/secure facility in an LPO or sent straight to Earth or perhaps quite possibly a combination of both. Such missions will have to rely on their minimum fuel consumption to maximize the payload on the spacecraft. With that constraint in mind, trajectories that utilize the natural gravitational environment (constant energy manifolds) of our solar system can be used as a standard trajectory design.

Envisioning such a future where continuous flow of materials using spacecraft to and from the LPOs is possible and the feasibility of such missions relies on the re-usability of the spacecraft in the long term, the focus of this work is on the design of optimal return trajectories from LPO to Earth as a sample return mission in the Earth-Moon system. The problem as described in this body of

work is essentially an extension of the work done by Abraham where he designed optimal trajectories from a Geostationary Earth Orbit (GEO) orbit to L_1 Lagrange point in the Earth-Moon system using particle swarm optimization as his primary optimization technique [2]. This thesis presents a return trajectory in the Earth-Moon system from a selected initial orbit. Utilizing the natural dynamics on the three-body system, the spacecraft is first perturbed from the initial orbit, placed onto an unstable manifold of the initial orbit which will take the spacecraft away from the initial orbit. At a location on the manifold closer to the final orbit, the spacecraft will then be taken from the manifold to the desired final orbit and placed in a Low Earth Orbit (LEO). Particle swarm optimization is used to select the optimal point of departure on the manifold of the LPO and to optimize the transfer from the manifold to the desired orbit.

Since solving for an optimal trajectory is computationally expensive, a major objective of this work is to obtain a computationally efficient method to obtain the results of the impulsive transfers in the three-body system. The method designed in this thesis uses the two-body approximation to obtain the ΔV values for the transfers from the manifold of a LPO to a LEO. The method is first validated against available solutions in the literature for transfers from a LEO to the manifold of a LPO and then extended to Earth-return transfers from LPOs. To understand the trends that exist in transfers from LPO to LEO and how these may be exploited to design efficient missions, analysis is performed on different LPO types and about different Lagrange points to observe variations in the ΔV requirements and the factors that influence them.

1.2 Background

The history of Lagrange point orbits began with the study and definition of N-body problem and subsequently the three-body problem by Isaac Newton. While the two-body problem provided powerful tools to study and design various orbits around a central body and allowed us to understand the orbits of planets around the sun, study of the N-body problem was essential to understand the long-term evolution of these orbits in the presence of multiple gravitational sources. Since the solar system is a representative of exactly such a system, motivation for this study followed naturally. The three-body problem was taken up by Leonard Euler and

Joseph-Louis Lagrange who managed to find families of periodic solution for the collinear points (1767) and equilateral points (1772) respectively [3]. It was later established by Poincaré [4] that analytical closed-form solution for systems with more than two bodies is not possible due to the unavailability of sufficient constants of motion. Subsequently multiple reductions to the generalized three-body problem were made. In the reduced form of the three-body problem, called the Circular Restricted Three-Body Problem (CR3BP), the periodic solutions result in five points and came to be known as Lagrange Points. Orbits around these points are known as Lagrange Point Orbits.

The existence of LPOs has been studied since the 18^{th} century, when Euler first discovered the collinear equilibrium points in the CR3BP. Since then, leading up to the past few decades, the interest in the CR3BP has seen a tremendous rise especially since now, missions based on the CR3BP are seen as a viable option for unmanned space exploration missions. Whether as a relay station for communication (Apollo missions) [5] or as a prospective way-point for longer missions such as a halo orbit (a type of LPO) space station [5], the potential utility of these mission is hard to miss. The study and application of DST has expanded the horizons of LPO based missions. It has allowed mission designers to plan low-cost missions utilizing the natural dynamics of the three-body system through the use of invariant manifolds also known as interplanetary superhighways [6]. Since time-of-flight (TOF) is not a strict constraint for unmanned missions, the use of constant energy manifolds opens up a strong possibility for low-cost, long-duration missions, such as asteroid mining and return, or sending supplies to a future moon base habitat. Apart from the potential utility of such mission, the study of these orbits and the dynamics associated with these orbits provides for a very interesting and challenging research area for researchers.

1.3 Earlier Work

Up until now, most of the focus on trajectory designs have been from Earth to LPO in the Earth-Moon system or Earth-Sun system. The International Sun-Earth Explorer 3 (ISEE-3) was the first mission to fly to a Sun-Earth L_1 halo orbit in 1978 [7]. Its objective was to study the Earth's magnetosphere, cosmic rays and solar flares. Since then, a number of missions have flown to LPOs, such as the

Solar and Heliospheric Observatory (SOHO) which was sent to Sun-Earth L_1 in 1995, and the Wilkinson Microwave Anisotropy Probe (WMAP) to Sun-Earth L_2 in 2001 [2]. In 2007, ARTEMIS/THEMIS became the first mission to reach the Earth-Moon Lagrange point. Another mission planned for the Sun-Earth L_2 is the James Webb Space Telescope (JWST) with a tentative launch date of October 2018 [2].

While the above mentioned missions were a designed as a one-way trip, Genesis, on the other hand, was designed as a long-term sample return mission which utilized the natural dynamics of the Sun-Earth system. It was sent to the Sun-Earth L_1 point to collect solar wind samples and returned to Earth using a low-energy trajectory. Relying heavily on dynamical systems theory, its trajectory was designed to make use of the manifolds and hetroclinic connection between the $L_1 - L_2$ points that exists in the Sun-Earth system to coast on the return trajectory [8].

1.4 Structure of Thesis

This thesis is divided into chapters which are arranged in the order of the flow of work and that was done. Chapter 2 begins with the study of the circular restricted three-body dynamics and developing the mathematical model of the system dynamics. The concept of zero energy curves is introduced which provides foreshadow of the manifold theory and their usage. The stability of the Lagrange points is discussed. The chapter ends with techniques to generate LPO using well established differential correction methods.

Chapter 3 focuses on the techniques that aid in design and analysis of the search space in an attempt to understand the environment of operation using Dynamical System Theory (DST). Basics of DST are discussed to understand the system behavior and application of manifolds to obtain constant energy pathways which, in turn, facilitate the design of low-energy transfers from desired LPOs. A general methodology for generating said manifolds for LPOs is introduced. Finally, concepts of optimization problem are reviewed along with a basic discussion on the techniques currently in use. One such technique is used in this work, namely, the particle swarm optimization.

In Chapter 4, individual techniques of analysis previously discussed are combined into one coherent method of generating optimized reliable trajectories. For this

purpose, the procedure to be employed is defined in terms of successive steps to accomplish tasks at hand. Results in terms of the optimized trajectories and their various qualities are presented.

In Chapter 5, a summary of the work is presented and conclusions are drawn from comparisons made with other similar trajectories available in the literature. Finally, some of the ideas that potentially follow from the current work are discussed as the next step in the analysis of similar missions and trajectories.

Finally, Appendix A and Appendix B includes the tables for the results displayed in chapter 4 for the L_1 and L_2 Lagrange point orbits respectively.

Chapter 2
Dynamics

2.1 Orbital Dynamics

To study the orbital dynamics of a spacecraft under the gravitational influence of two or more massive bodies, a mathematical model different from the two-body model needs to be constructed. Newton's N-body system of equations provides the foundation upon which such model is constructed. However, as already discussed, the N-body system doesn't lend itself to a convenient solution in its general form. One needs to look at ways to simplify the existing model in hopes of achieving a solution. The circular restricted three-body problem is one of the most widely used set of equations in modern astrodynamics as it gives a highly simplified model of the general three-body problem that simulates fairly realistic dynamics model without excessive modeling complexity. In essence, it describes the motion of a body with negligible mass (usually a spacecraft) around two primaries with masses.

The main simplifying factors, consider the third-body to be massless relative to the other two massive bodies. This implies that the gravitational effects of the third-body on the primaries are negligible. This is the restriction that is imposed on the problem otherwise, finding the solution tends to become a bit more complicated. The second assumption is that the two massive bodies revolve around the center-of-mass of the Earth-Moon system, called the barycenter, in a circular orbit with a constant rate of rotation. Hence the primaries always lie on the same line and this circular motion imposition allows for a highly simplified system of equations. The selected frame of reference rotates along with the primaries such that the primaries appears to be fixed in space. Further simplification is possible

when the system is non-dimensionalized and represented in the cannonical units of distance units [DU] and time unit [TU].

A major advantage of this system is that it allows us to realistically model the dynamics of the Earth-Moon system or the Sun-Earth system. It allows study of the Lagrange Points and the orbits around such points. Since an analytic solution is not possible, orbits thus obtained cannot be described by conic sections like in the case of a two-body problem. Therefore, to visualize the trajectories, numerical integration of the equations of motions needs to be performed.

2.2 Coordinate System and Equations of Motion

This section defines the coordinate system, basic description of the equations of motion of the CR3BP and provides an explanation of variables used in the equations and the non-dimensional parameters.

Let m_1 and m_2 be the mass of the two primaries and m_3 the mass of the spacecraft where, $m_1 \geq m_2 >> m_3$. The coordinate system is defined such that the barycenter of the primaries lies on the origin and the larger primary lies on left side of the barycenter on the negative x-axis and the smaller primary is on the right side of the barycenter as shown in Figure 2.1. The y-axis is orthogonal to the x-axis in the plane of rotation of the two primaries. The z-axis is orthogonal to the $x-y$ plane and completes the right handed system. The unit vectors $\hat{i}, \hat{j}$ *and* $\hat{k}$ are in the principal directions of the defined coordinate system. The position of the spacecraft or the third body is defined with respect to the two primaries.

Let μ be the mass ratio as

$$\mu = \frac{m_2}{m_1 + m_2} \tag{2.1}$$

which leads to

$$1 - \mu = \frac{m_1}{m_1 + m_2} \tag{2.2}$$

The distance between the primaries is non-dimensionalized to 1 distance unit (DU). For the Earth-Moon system,this is equal to 384,400 km. The locations of the primaries can be found using the equation of the center-of-mass (CM) described as

$$\vec{R}_{CM} = \frac{m_1 \ \vec{r}_{1_{CM}} + m_2 \ \vec{r}_{2_{CM}}}{m_1 + m_2} \tag{2.3}$$

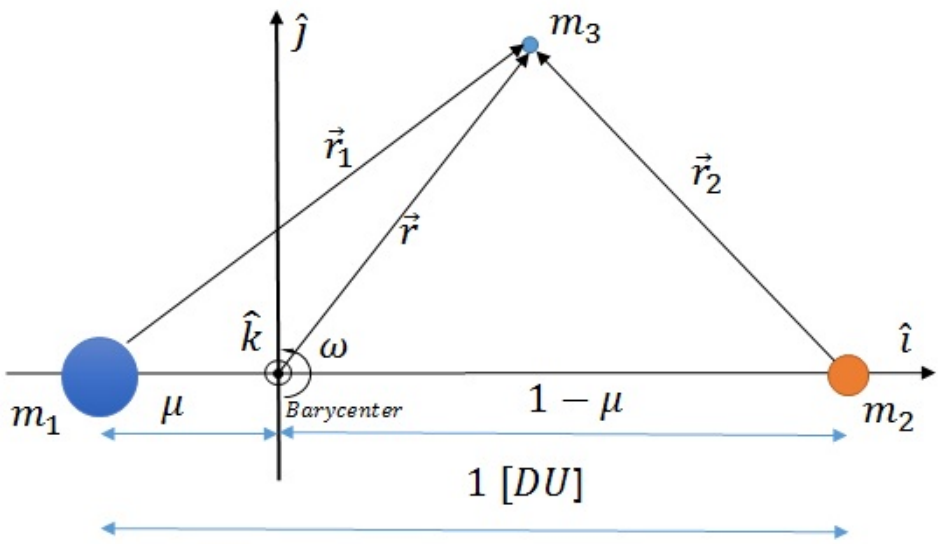

Figure 2.1. CR3BP Coordinate System.

where $\vec{r}_{1_{CM}}$ and $\vec{r}_{2_{CM}}$ are the position vectors of the two masses with respect to the CM. Substituting $r_{1_{CM}} = 0 \;\; and \;\; r_{2_{CM}} = 1$ in Eq.(2.3), we get the location of the CM with respect to m_1 as μ. Similarly, when $r_{2_{CM}} = 0 \;\; and \;\; r_{1_{CM}} = 1$, we find that the CM with respect to m_2 is $1 - \mu$. Hence, the position vectors of the three bodies with respect to CM are as follows

$$\vec{P}_{m_1} = \begin{bmatrix} -\mu \\ 0 \\ 0 \end{bmatrix}; \quad \vec{P}_{m_2} = \begin{bmatrix} 1-\mu \\ 0 \\ 0 \end{bmatrix}; \quad \vec{P}_{m_3} = \begin{bmatrix} x \\ y \\ z \end{bmatrix} \tag{2.4}$$

The distance of the third body m_3, from the two primary bodies m_1 and m_2, respectively, is

$$r_1 = \sqrt{(x+\mu)^2 + y^2 + z^2} \tag{2.5}$$

$$r_2 = \sqrt{(x-(1-\mu))^2 + y^2 + z^2} \tag{2.6}$$

The angular velocity of two masses in circular orbit is given as

$$\omega = \sqrt{\frac{G\,(m_1+m_2)}{r_{12}^3}} \tag{2.7}$$

where, r_{12} is the distance between the primaries which is equal to 1. The total mass of the primaries is also equal to 1. Therefore the equation becomes

$$\omega = \sqrt{G} \tag{2.8}$$

The time can be written in terms of cannonical time units (TU) by dividing the period of the orbit of the primaries around each other, T by 2π. The period is given by

$$T = 2\pi\sqrt{\frac{r_{12}^3}{m_1+m_2}} = 2\pi \tag{2.9}$$

$$1(TU) = \frac{T}{2\pi} \tag{2.10}$$

The angular velocity can be written as

$$\omega = \frac{2\pi}{T} = \frac{2\pi}{2\pi} = 1 \tag{2.11}$$

$$\omega = \sqrt{G} = 1 \Rightarrow G = 1 \tag{2.12}$$

From Newton's Law of Gravitation, the force between two arbitrary masses m_a and m_b is given as

$$\vec{F}_{ab} = \frac{G(m_a m_b)}{r_{ab}^3}\vec{r}_{ab} \tag{2.13}$$

where a and b are arbitrary variables representing two bodies. The positive or negative sign of the force is due to the direction of the relative position vector. The N-body equation then is given by

$$\ddot{\vec{r}}_3 = \frac{-G(m_1+m_3)\vec{r}_{13}}{r_{13}^3} + G\sum_{j=2,j\neq 3}^{N} m_j\left(\frac{\vec{r}_{3j}}{r_{3j}^3} - \frac{\vec{r}_{1j}}{r_{1j}^3}\right) \tag{2.14}$$

Equation (2.14) is the general series N-body equation of the relative acceleration of the spacecraft (body 3) with primary 1 as reference center [9]. For the three-body system like the one under consideration, replacing N with 3 gives the required expression. Since the system is in the synodic frame, the barycentric from of the

expression is more useful for the current work.

$$\ddot{\vec{r}} = -G \sum_{j=1, j\neq 3}^{N} \frac{m_j}{r_{j3}^3} \vec{r}_{j3} \tag{2.15}$$

Based on the Newton's Laws, the forces on the spacecraft in a two-body system can be written as follows

$$\vec{F}_{sc} = \vec{F}_{31} + \vec{F}_{32} \tag{2.16}$$

$$\vec{r}_1 = \vec{r} - \vec{r}_{B1} \tag{2.17}$$

Taking two time derivatives of Eq. (2.17) and substituting into Eq. (2.15) gives

$$\ddot{\vec{r}}_1 = \ddot{\vec{r}} - \ddot{\vec{r}}_{B1} \tag{2.18}$$

$$\ddot{\vec{r}}_1 = -\frac{Gm_1}{r_1^3} \vec{r}_1 + \frac{Gm_3}{r_1^3} \vec{r}_1 \tag{2.19}$$

$$\ddot{\vec{r}}_1 = -\frac{G(m_1 + m_3)}{r_1^3} \vec{r}_1 \tag{2.20}$$

where r_1 , r, m_1, m_3 are as defined in Figure 2.1, $\vec{r}_{B1}$ is the vector from the barycenter to m_1 and sc stands for spacecraft. Similarly

$$\ddot{\vec{r}}_2 = -\frac{G(m_2 + m_3)}{r_2^3} \vec{r}_2 \tag{2.21}$$

Combining the two equations to form the three-body model gives the following equation

$$\ddot{\vec{r}} = -\frac{G(m_1 + m_3)}{r_1^3} \vec{r}_1 - \frac{G(m_2 + m_3)}{r_2^3} \vec{r}_2 \tag{2.22}$$

Since the third body m_3 is of negligible gravitational influence, the mass of the third body is neglected, i.e. $m_3 = 0$. The above equation can be written in three dimensions as follows

$$\begin{aligned}(\ddot{x} - 2\omega\dot{y} - \omega^2 x)\hat{i} + (\ddot{y} + 2\omega\dot{x} - \omega^2 y)\hat{j} + \ddot{z}\hat{k} = & -\frac{\mu_1}{r_1^3}\Big[(x+\mu)\hat{i} + y\hat{j} + z\hat{k}\Big] \\ & -\frac{\mu_2}{r_2^3}\Big[(x-1+\mu)\hat{i} + y\hat{j} + z\hat{k}\Big]\end{aligned}$$

(2.23)

The terms on the left hand side are due to the fact that the synodic frame that is considered for the analysis is a rotational system with angular velocity rate of ω, hence centrifugal and Coriolis terms manifest in the equations of relative motion. Recall that μ is the mass ratio as defined in Eq. (2.1), rather than the gravitational parameter as is common in the literature. Finally, upon non-dimensionalization of the equations, the final form of the equations becomes

$$\begin{aligned} \ddot{x} &= 2\dot{y} + x - \frac{(1-\mu)(x+\mu)}{r_1^3} - \frac{\mu(x+\mu-1)}{r_2^3} \\ \ddot{y} &= y - 2\dot{x} - \frac{(1-\mu)y}{r_1} - \frac{\mu y}{r_2^3} \\ \ddot{z} &= -\frac{(1-\mu)z}{r_1^3} - \frac{\mu z}{r_2^3} \end{aligned} \tag{2.24}$$

Alternatively, a pseudopotential definition can also be used to generate the equations-of-motion (EOM). The kinetic energy, KE, and the potential energy, PE, of the spacecraft normalized with respect to the mass of the spacecraft is given as

$$\begin{aligned} KE = \frac{1}{2}v^2 &= \frac{1}{2}[(\dot{x}-\omega y)^2 + (\dot{y}+\omega x)^2 + \dot{z}^2] \\ PE &= -\frac{Gm_1}{r_1} - \frac{Gm_2}{r_2} \end{aligned} \tag{2.25}$$

Non-dimensionalizing Eq.(2.25) gives the following

$$\begin{aligned} KE &= \frac{1}{2}[(\dot{x}-y)^2 + (\dot{y}+x)^2 + \dot{z}^2] \\ PE &= -\frac{(1-\mu)}{r_1} - \frac{\mu}{r_2} \end{aligned} \tag{2.26}$$

The Lagrangian [2], L can be written as

$$\begin{aligned} L &= KE - PE \\ L &= \begin{cases} \frac{1}{2}[(\dot{x}-y)^2 + (\dot{y}+x)^2 + \dot{z}^2] \end{cases} \end{aligned}$$

$$+\frac{(1-\mu)}{r_1}+\frac{\mu}{r_2}\Bigg\} \tag{2.27}$$

Given the Lagrangian of a system, the EOM can be obtained by applying the Euler-Lagrange equation. Euler-Lagrange equation is given as

$$\frac{\partial L}{\partial x}-\frac{d}{dt}\frac{\partial L}{\partial \dot{x}} = 0 \tag{2.28}$$

The EOMs obtained using the Lagrangian are

$$\begin{aligned}
\ddot{x}-2\dot{y} &= -\frac{\partial PE}{\partial x}+x \\
\ddot{y}+2\dot{x} &= -\frac{\partial PE}{\partial y}+y \\
\ddot{z} &= -\frac{\partial PE}{\partial z}
\end{aligned} \tag{2.29}$$

A suitable arbitrary function can be defined such that the right side of the equations are obtained from the appropriate differential of the potential function. Since this function is not the exact potential as defined earlier, it is called the pseudopotential, and is of the form

$$U = -\frac{(1-\mu)}{r_1}-\frac{\mu}{r_2}-\frac{1}{2}(x^2+y^2) \tag{2.30}$$

The equations can then be represented as

$$\begin{aligned}
\ddot{x}-2\dot{y} &= -\frac{\partial U}{\partial x} \\
\ddot{y}+2\dot{x} &= -\frac{\partial U}{\partial y} \\
\ddot{z} &= -\frac{\partial U}{\partial z}
\end{aligned} \tag{2.31}$$

2.3 Dynamic Model and State Transition Matrix

The current section focuses on the definition of the state vector and the state transition matrix of the system. The system of equations developed previously are combined in the state space form to define the system as is used for numerical computation. While the selection of the states of the system can be arbitrary, generally it is better to select those states whose initial information can be easily obtained and is capable of defining the complete system. Since the position and velocity are the most commonly used states in a dynamical system, the current analysis considers the following state vector for all future computations

$$\vec{X} = \begin{bmatrix} x & y & z & \dot{x} & \dot{y} & \dot{z} \end{bmatrix}^T \tag{2.32}$$

Since a system can be generically defined as

$$\dot{\vec{X}} = \mathbf{F}(\vec{X}, t) \tag{2.33}$$

where $\mathbf{F}(X, t)$ simply states that the system is a nonlinear function of the state and time. For the current work, the given system is written as

$$\dot{\vec{X}} = \mathbf{F}(\vec{X}) = \begin{bmatrix} F_1 \\ F_2 \\ F_3 \\ F_4 \\ F_5 \\ F_6 \end{bmatrix} = \begin{bmatrix} \dot{x} \\ \dot{y} \\ \dot{z} \\ 2\dot{y} - \dfrac{\partial U}{\partial x} \\ -2\dot{x} - \dfrac{\partial U}{\partial y} \\ -\dfrac{\partial U}{\partial z} \end{bmatrix} \tag{2.34}$$

Equation (2.34) can further be reduced by linearizing the EOMs to give the

state space form as follows

$$\dot{\vec{X}}(t) = A(t)\vec{X}(t) \tag{2.35}$$

where $A(t)$ is the Jacobian matrix and is equal to $A(t) = \dfrac{\partial \mathbf{F}}{\partial \vec{X}}$. It is obtained from the Taylor series expansion of the system Eq. (2.33). The Jacobian for the desired system is defined as

$$\begin{aligned} A(t) &= \begin{bmatrix} \frac{\partial F_1}{\partial x} & \frac{\partial F_1}{\partial y} & \frac{\partial F_1}{\partial z} & \frac{\partial F_1}{\partial \dot{x}} & \frac{\partial F_1}{\partial \dot{y}} & \frac{\partial F_1}{\partial \dot{z}} \\ \frac{\partial F_2}{\partial x} & \frac{\partial F_2}{\partial y} & \frac{\partial F_2}{\partial z} & \frac{\partial F_2}{\partial \dot{x}} & \frac{\partial F_2}{\partial \dot{y}} & \frac{\partial F_2}{\partial \dot{z}} \\ \frac{\partial F_3}{\partial x} & \frac{\partial F_3}{\partial y} & \frac{\partial F_3}{\partial z} & \frac{\partial F_3}{\partial \dot{x}} & \frac{\partial F_3}{\partial \dot{y}} & \frac{\partial F_3}{\partial \dot{z}} \\ \frac{\partial F_4}{\partial x} & \frac{\partial F_4}{\partial y} & \frac{\partial F_4}{\partial z} & \frac{\partial F_4}{\partial \dot{x}} & \frac{\partial F_4}{\partial \dot{y}} & \frac{\partial F_4}{\partial \dot{z}} \\ \frac{\partial F_5}{\partial x} & \frac{\partial F_5}{\partial y} & \frac{\partial F_5}{\partial z} & \frac{\partial F_5}{\partial \dot{x}} & \frac{\partial F_5}{\partial \dot{y}} & \frac{\partial F_5}{\partial \dot{z}} \\ \frac{\partial F_6}{\partial x} & \frac{\partial F_6}{\partial y} & \frac{\partial F_6}{\partial z} & \frac{\partial F_6}{\partial \dot{x}} & \frac{\partial F_6}{\partial \dot{y}} & \frac{\partial F_6}{\partial \dot{z}} \end{bmatrix} \\ &= \begin{bmatrix} 0 & 0 & 0 & 1 & 0 & 0 \\ 0 & 0 & 0 & 0 & 1 & 0 \\ 0 & 0 & 0 & 0 & 0 & 1 \\ -\frac{\partial U_x}{\partial x} & -\frac{\partial U_x}{\partial y} & -\frac{\partial U_x}{\partial z} & -\frac{\partial U_x}{\partial \dot{x}} & 2 - \frac{\partial U_x}{\partial \dot{y}} & \frac{\partial U_x}{\partial \dot{z}} \\ -\frac{\partial U_y}{\partial x} & -\frac{\partial U_y}{\partial y} & -\frac{\partial U_y}{\partial z} & -2 - \frac{\partial U_y}{\partial \dot{x}} & -\frac{\partial U_y}{\partial \dot{y}} & -\frac{\partial U_y}{\partial \dot{z}} \\ -\frac{\partial U_z}{\partial x} & -\frac{\partial U_z}{\partial y} & -\frac{\partial U_z}{\partial z} & -\frac{\partial U_z}{\partial \dot{x}} & -\frac{\partial U_z}{\partial \dot{y}} & -\frac{\partial U_z}{\partial \dot{z}} \end{bmatrix} \end{aligned} \tag{2.36}$$

Here U_x, U_y *and* U_z are the partial derivatives of the pseudopotential in Eq. (2.30)

with respect to the $x, y \ \ and \ \ z$ directions, respectively. These can be written as

$$A(t) = \begin{bmatrix} 0 & 0 & 0 & 1 & 0 & 0 \\ 0 & 0 & 0 & 0 & 1 & 0 \\ 0 & 0 & 0 & 0 & 0 & 1 \\ -U_{xx} & -U_{xy} & -U_{xz} & 0 & 2 & 0 \\ -U_{yx} & -U_{yy} & -U_{yz} & -2 & 0 & 0 \\ -U_{zx} & -U_{zy} & -U_{zz} & 0 & 0 & 0 \end{bmatrix} \tag{2.37}$$

The state of the system at a any future time can be obtained from the state transition matrix (STM) given the state at present time, hence, it *transitions* the current state t_k to a state at a future time t. The state transition matrices are incredibly useful in gradient based studies of dynamical systems. Mathematically, the relations appears as

$$\vec{X}(t) \ = \ \Phi(t, t_k)\vec{X}(t_k) \tag{2.38}$$

where,

$$\Phi(t, t_k) \ = \ \frac{\partial \vec{X}(t)}{\partial \vec{X}(t_k)} \tag{2.39}$$

Substituting Eq. (2.38) in Eq. (2.33), gives a relationship between the time derivative of state transition matrix and the Jacobian as

$$\dot{\Phi}(t, t_k) \ = \ A(t)\Phi(t, t_k) \tag{2.40}$$

The expression in Eq. (2.40) becomes very useful for numerical computation. Through this equation, the STM can be numerically integrated along with the EOMs of the system for further use in various gradient based methods as will be seen in later chapters. The STM also exhibits some very useful properties such as

$$\Phi(t_a, t_a) \ = \ I \tag{2.41}$$

$$\Phi(t_c, t_a) = \Phi(t_c, t_b)\Phi(t_b, t_a) \tag{2.42}$$

$$\Phi(t_b, t_a) = \Phi(t_a, t_b)^{-1} \tag{2.43}$$

These expression allows for checks to ensure the numerical methods are functioning as expected.

2.4 Lagrange Points and their Stability

An essential aspect of the study of the dynamics of any system is the knowledge of the equilibrium points and the behavior around these. It allows us the necessary boundary conditions to linearize the system and study the stability modes of the system. This section will focus on the study of equilibrium points in CR3BP also known as Lagrange points and their stability characteristics. This is required to understand the motion of the spacecraft in the vicinity of these points and is the fundamental basis for the existence of Lagrange point orbits.

Equilibrium points, by definition, are points where a particle will remain stationary in the absence of disturbing forces. Setting the velocities and accelerations to zero in the Eq. (2.31), the required form of the equations are

$$\begin{aligned} 0 &= -\frac{\partial U}{\partial x} \\ 0 &= -\frac{\partial U}{\partial y} \\ 0 &= -\frac{\partial U}{\partial z} \end{aligned} \tag{2.44}$$

The derivative of the pseudopotential are given as

$$-\frac{\partial U}{\partial x} = 0 = -\frac{(1-\mu)(x+\mu)}{r_1^3} - \frac{\mu(x-1+\mu)}{r_2^3} + x \tag{2.45}$$

$$-\frac{\partial U}{\partial y} = 0 = -\frac{(1-\mu)y}{r_1^3} - \frac{\mu y}{r_2^3} + y \tag{2.46}$$

$$-\frac{\partial U}{\partial z} = 0 = -\frac{(1-\mu)z}{r_1^3} - \frac{\mu z}{r_2^3} \tag{2.47}$$

For Eq. (2.47) to be satisfied, z must be zero as the potential terms cannot be zero. For Eq. (2.46), there can be two kinds of solutions. The trivial solution, where $y = 0$, gives us collinear equilibrium points on the x axis namely, L_1, L_2 and L_3. The non-trivial solution gives us two more equilibrium points, L_4 and L_5 and these along with the collinear points are the five points obtained from the system dynamics commonly called the Lagrange points. Since for the collinear points, y and z are zero, r_1 and r_2 reduce to the form

$$r_1^3 = |x + \mu|^3 \tag{2.48}$$

$$r_2^3 = |x + \mu - 1|^3 \tag{2.49}$$

then solutions for the collinear Lagrange points involve solving Eq. (2.45) for the three regions of the space, namely, the far side of the two primaries with respect to the barycenter (*Regions II and III*) and in between the two primaries (*Region I*). The denominator for each of the regions is given as

$$\begin{aligned} &\textit{Region I } (L_1) \Rightarrow \\ &\qquad |x + \mu| &&= (x + \mu) \\ &\qquad |x + \mu - 1| &&= -(x + \mu - 1) \end{aligned} \tag{2.50}$$

$$\begin{aligned} &\textit{Region II } (L_2) \Rightarrow \\ &\qquad |x + \mu| &&= (x + \mu) \\ &\qquad |x + \mu - 1| &&= (x + \mu - 1) \end{aligned} \tag{2.51}$$

$$\begin{aligned} &\textit{Region III } (L_3) \Rightarrow \\ &\qquad |x + \mu| &&= -(x + \mu) \\ &\qquad |x + \mu - 1| &&= -(x + \mu - 1) \end{aligned} \tag{2.52}$$

The above substitution to Eq. (2.45) gives the following equations

$$L_1 \to 0 \;=\; -\frac{(1-\mu)}{(x+\mu)^2} + \frac{\mu}{(x+\mu-1)^2} + x$$

$$L_2 \to 0 \;=\; -\frac{(1-\mu)}{(x+\mu)^2} - \frac{\mu}{(x+\mu-1)^2} + x$$

$$L_3 \to 0 \quad = \quad \frac{(1-\mu)}{(x+\mu)^2} + \frac{\mu}{(x+\mu-1)^2} + x \tag{2.53}$$

Equations (2.53) are easily solved in MATLAB using the 'fzero' command. The remaining two collinear points are relatively easy to find if one realizes that r_1 and r_2 are equal as the remaining points lie on the vertices of the equilateral triangle between the two primaries. The terms r_1 and r_2 are of the form

$$\begin{aligned} r_1 &= \sqrt{(x+\mu)^2 + y^2} \\ r_2 &= \sqrt{(x+\mu-1)^2 + y^2} \end{aligned} \tag{2.54}$$

Upon equating the two equations, the x-coordinate is obtained to be

$$x = \frac{1}{2} - \mu \tag{2.55}$$

Hence, one can easily obtain the y-coordinate upon substituting Eq.(2.55) in the Eq. (2.54) as shown

$$y = \pm\frac{\sqrt{3}}{2} \tag{2.56}$$

where conventionally, L_4 lies on the positive side of y-axis and L_5 lies on the negative side of the y-axis. The Lagrange point locations in normalized form, for the Earth-Moon system are shown in Table 2.1.

Table 2.1. Collinear Lagrange Point locations in the Earth-Moon system

Point	x-Coordinate	y-Coordinate
L_1	0.8369	0
L_2	1.1557	0
L_3	−1.0051	0
L_4	0.4878	0.8660
L_5	0.4878	−0.8660

The Lagrange Points for the Earth-Moon system are plotted in Figure 2.2.

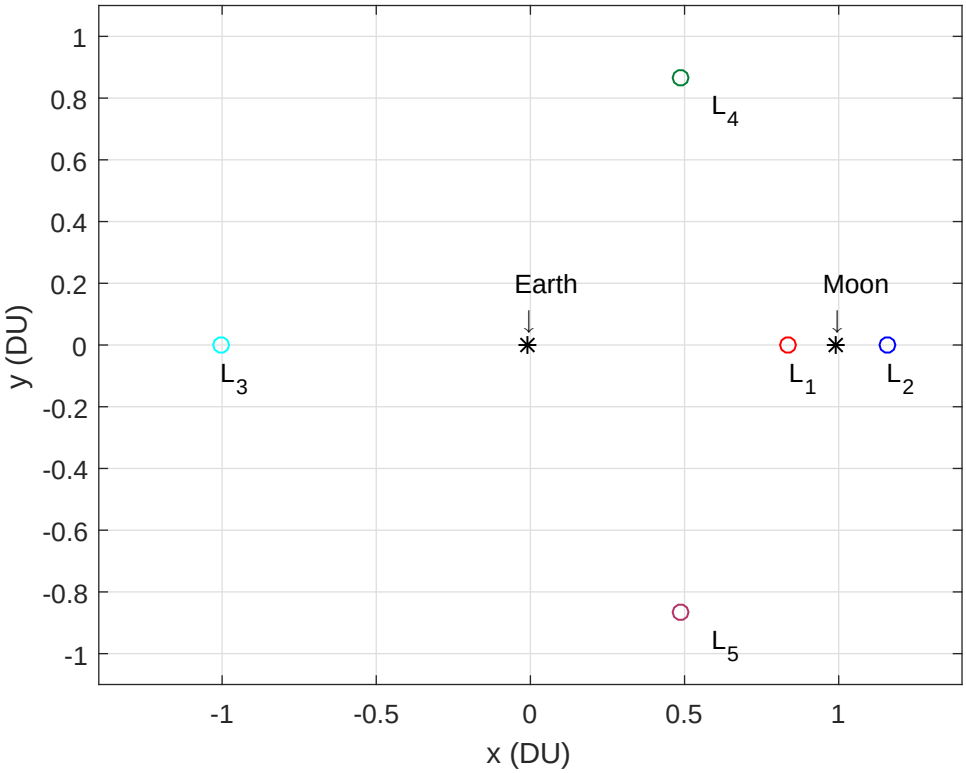

Figure 2.2. Lagrange Points in canonical units

Having obtained the Lagrange point locations, their stability analysis can be carried out. For a dynamic system, the stability of the system is obtained by observing the eigenvalues of the system matrix A. This is the same as the Jacobian matrix for the CR3BP. Eigenvalues are the roots if the characteristic equation of the system matrix. The roots of the characteristic equation are also called the poles of the system. A general characteristic equation is as given in the Eq. (2.57). For the system under consideration with six states, Eq. (2.58) gives the required form.

$$\begin{aligned} f(\lambda) = |\lambda I - A| &= 0 \\ \lambda^k + a_{k-1}\,\lambda^{k-1} + \cdots + a_0 &= 0 \qquad (2.57) \\ \lambda_6 + a_5\,\lambda_5 + a_4\,\lambda_4 + a_3\,\lambda_3 + a_2\,\lambda_2 + a_1\,\lambda_1 + a_0 &= 0 \qquad (2.58) \end{aligned}$$

Upon solving the Jacobian for each of the Lagrange Point values, the eigenvalues are obtained from MATLAB command 'eig'. Eigenvalues or poles of a system provide a unique insight into the stability characteristics and modes of the system near a stationary point. The system matrix must be a constant for eigenvalue

analysis. Eigenvalues with negative real parts tends to decay towards the stationary point exponentially and are considered stable. If the eigenvalue has a positive real part, then it tends to exponentially increase and diverge towards infinity and is considered to be unstable. If the eigenvalues occur in the form of complex conjugate pairs, then the imaginary part describes the oscillatory motion of the system. The real part governs whether the oscillatory motion is decreasing in magnitude (stable) or increasing in magnitude (unstable). In the case where the eigenvalue is on the imaginary axis, i.e. the real part is zero, then the system is neutrally stable.

Stability can also be understood as, if a particle placed near an equilibrium point is deviated from its path and it tends to regain it previous state as time progresses, then the particle is said to be in a stable equilibrium. If it tends to continue to move away from its previous state, it is said to be in an unstable equilibrium or at a saddle point.

The eigenvalues of the Lagrange points in the Earth-Moon system are shown in Table 2.2.

Table 2.2. Eigenvalues of the Lagrange Points in the Earth-Moon system

Points	λ_1	λ_2	λ_3	λ_4	λ_5	λ_6
L_1	2.9321	-2.9321	$-2.3344i$	2.3344i	-2.2688i	2.2688i
L_2	2.1587	-2.1587	-1.8626i	1.8626i	-1.7862i	1.7862i
L_3	-1.0104i	1.0104i	-0.17787	0.17787	-1.0053i	1.0053i
L_4	-0.9545i	0.9545i	-0.29821i	0.29821i	-1i	1i
L_5	-0.9545i	0.9545i	-0.29821i	0.29821i	-1i	1i

As can be seen above, each of the three collinear points have one positive real eigenvalue, this causes the collinear points to be unstable. The eigenvalues for the equilateral points are also shown. For convenience, the real parts of these eigenvalues are omitted as they were of the order 10^{-15} or lower which at the limit of machine precision which essentially means that they are zero as it can be caused due to numerical error. Notice that the since the real part of L_4 and L_5 are zero, these are then considered neutrally stable but recall that an actual system will be subject to perturbations due to other massive bodies in the solar system and hence, even these will be unstable points in reality. While the equilibrium points

themselves might be unstable, orbits around these points are slightly unstable and spacecraft placed there can be managed with minor trajectory correction maneuvers.

2.5 Jacobi Constant

In spite of being in the rotating frame of reference, there exists one constant of integration for the system of equations as discussed previously. It is equivalent to the energy of the system and is called the Jacobi constant(or Jacobi integral or Jacobi energy). It is useful in defining the available regions of motion in space as a function of the energy of the spacecraft. The expression for the Jacobi integral can be obtained by first analyzing the square of the velocity

$$v^2 = \dot{x}^2 + \dot{y}^2 + \dot{z}^2 \tag{2.59}$$

The time derivative of Eq. (2.59) gives,

$$\frac{d(v^2)}{dt} = 2\big(\dot{x}\ddot{x} + \dot{z}\ddot{z} + \dot{z}\ddot{z}\big) \tag{2.60}$$

substituting Eq. (2.34) into Eq. (2.60) gives

$$\frac{d(v^2)}{dt} = 2\big[\dot{x}\big(2\dot{y} - U_x\big) + \dot{y}\big(-2\dot{x} - U_y\big) + \dot{z}\big(-U_z\big)\big] \tag{2.61}$$

$$= 2\big[-U_x\dot{x} - U_y\dot{y} - U_z\dot{z}\big] \tag{2.62}$$

Time derivative of the pseudopotential can be obtained by applying chain rule

$$\frac{dU}{dt} = U_x\dot{x} + U_y\dot{y} + U_z\dot{z} \tag{2.63}$$

From Eq. (2.62) and Eq. (2.63) it follows that

$$\frac{d(v^2)}{dt} = -2\frac{dU}{dt} \tag{2.64}$$

$$\frac{d}{dt}\big[v^2 + 2U\big] = 0 \tag{2.65}$$

Integrating the Eq. (2.65) with respect to time gives the final expression for the Jacobi constant as,

$$v^2 + 2U = C \tag{2.66}$$

where U is given by Eq. (2.30). Equation. (2.66) is the Jacobi integral equation and C is the Jacobi constant. C only exists in the synodic frame of reference in the case of the restricted three-body problem [9]. The Jacobi constant can help define the regions of space which may be inaccessible to a given spacecraft of a give Jacobi energy. These regions are called Hill's Regions and are bounded by the curves known as zero-velocity curves [2]. It means that the motion of any spacecraft with a certain Jacobi energy is confined within the surface of that Jacobi energy and the outer limits of spacecraft's motion is defined by the zero-velocity curves as upon reaching this threshold, the velocity of the spacecraft will effectively be zero (i.e all the kinetic energy has been converted to potential energy) and will pulled back towards the center of attraction.

Setting the velocity equal to zero in the Eq. (2.66) gives the limiting value of the Jacobi constant as

$$2U = C \tag{2.67}$$

Setting the x and y for the Lagrange point gives the value of C at the equilibrium points. These are considered as the boundary conditions for the analysis of the zero velocity as ideally, the velocity at the Lagrange points should be zero. The zero velocity curves for the first three Lagrange points are shown in Figures 2.3-2.8. Earth is at the center of the figure marked with a black star. For convenience, the Lagrange points are not labeled. It is observed that as the Jacobi energy is increased, more and more regions of space becomes accessible to the spacecraft. For the Jacobi energy equivalent to that of L_1 and L_2 small sections open up in the vicinity of the Lagrange points that allow access to slightly greater regions of space. Since an orbit at L_1 is still able to access the Moon, it shows that such orbits are viable for sample return missions from the Moon as well.

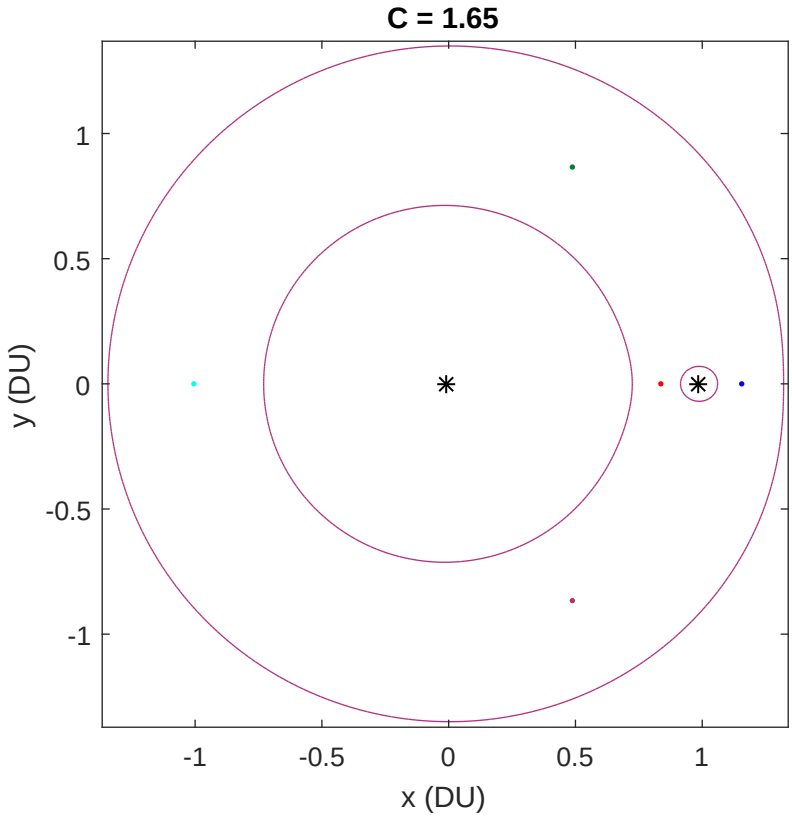

Figure 2.3. Zero Velocity Curves for Jacobi Energy of $C = 1.65$ in the Earth-Moon system

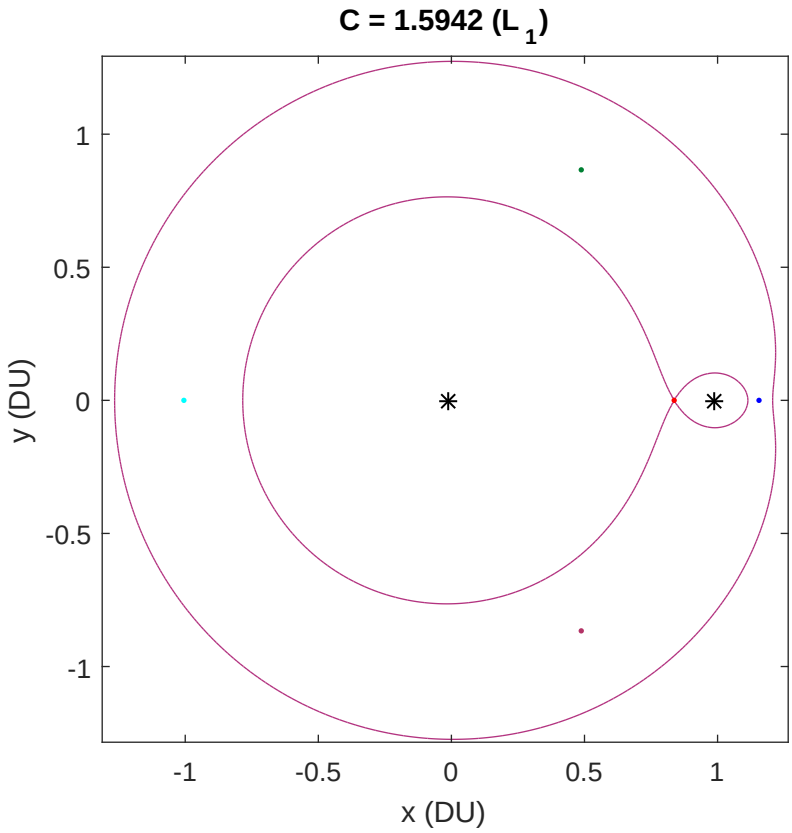

Figure 2.4. Zero Velocity Curves for Jacobi Energy of $C = 1.5942$ (L_1) in the Earth-Moon system

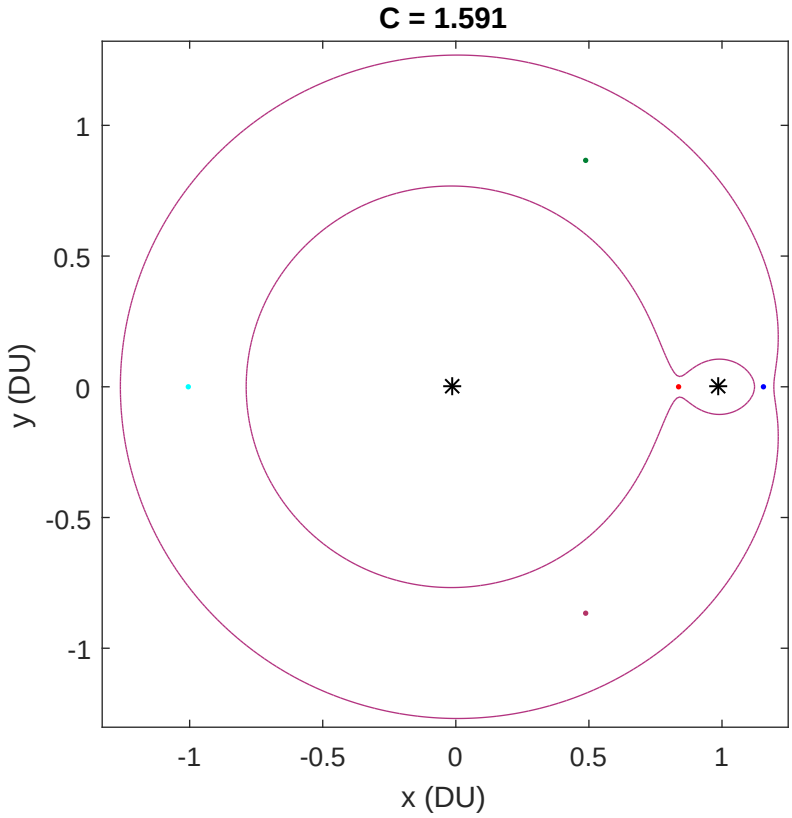

Figure 2.5. Zero Velocity Curves for Jacobi Energy of $C = 1.591$ in the Earth-Moon system

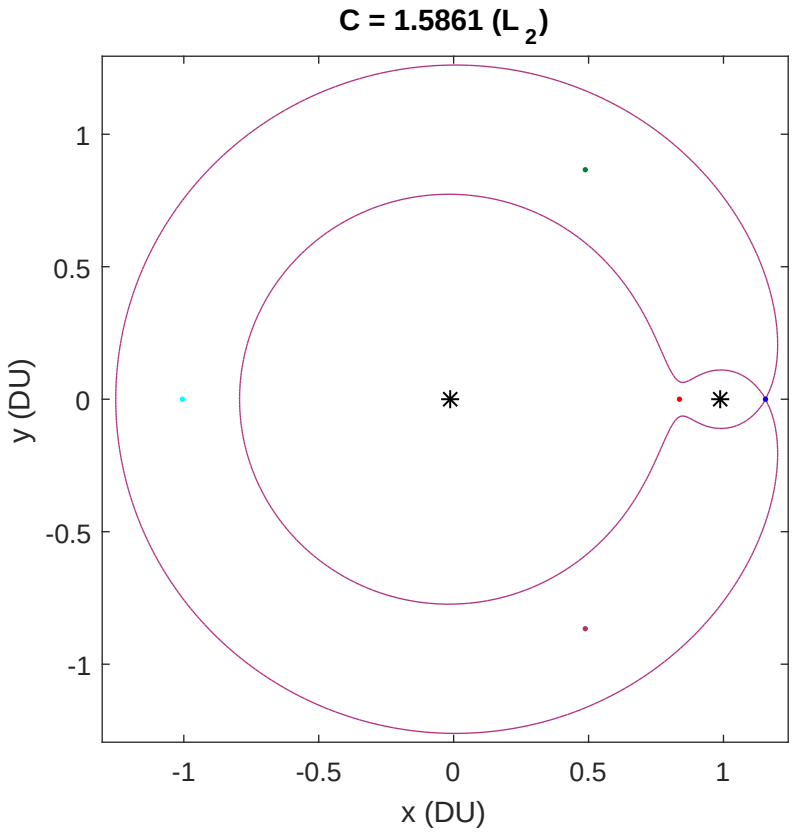

Figure 2.6. Zero Velocity Curves for Jacobi Energy of $C = 1.5861$ (L_2) in the Earth-Moon system

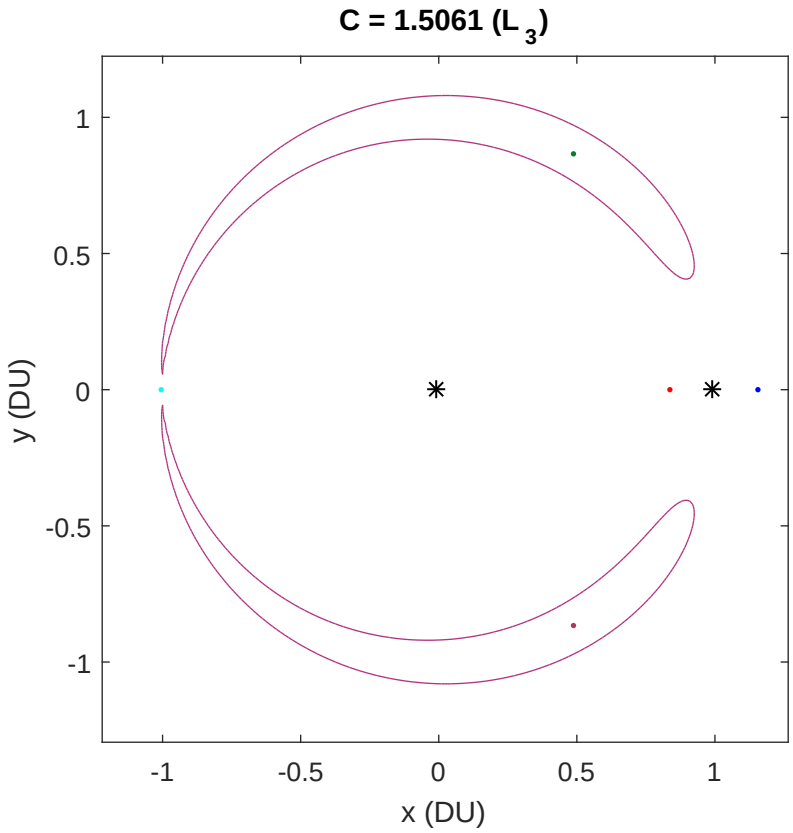

Figure 2.7. Zero Velocity Curves for Jacobi Energy of $C = 1.5061$ (L_3) in the Earth-Moon system

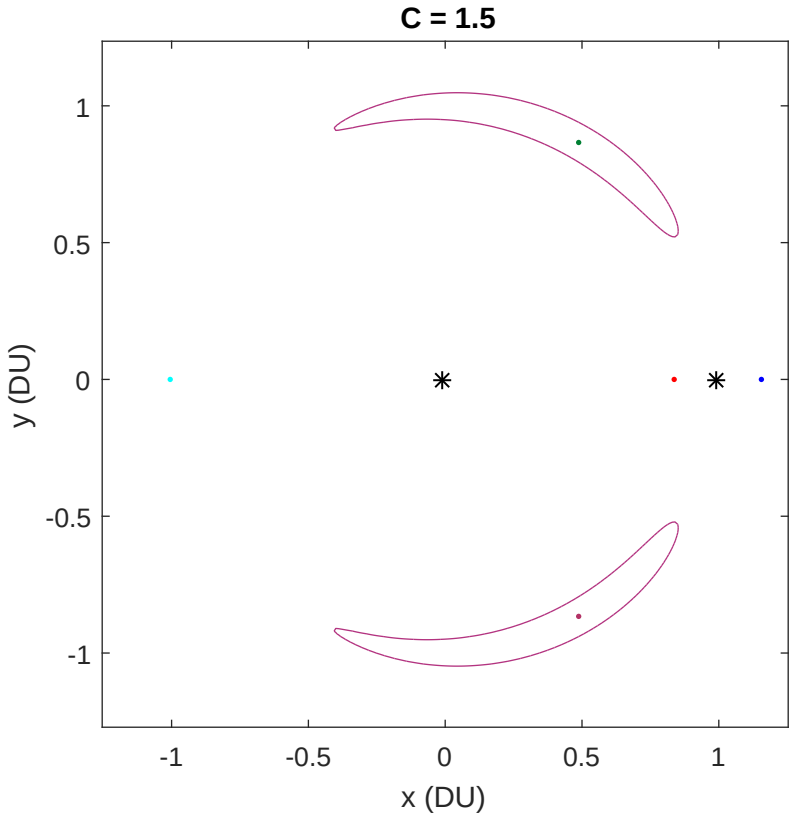

Figure 2.8. Zero Velocity Curves for Jacobi Energy of $C = 1.5$ in the Earth-Moon system

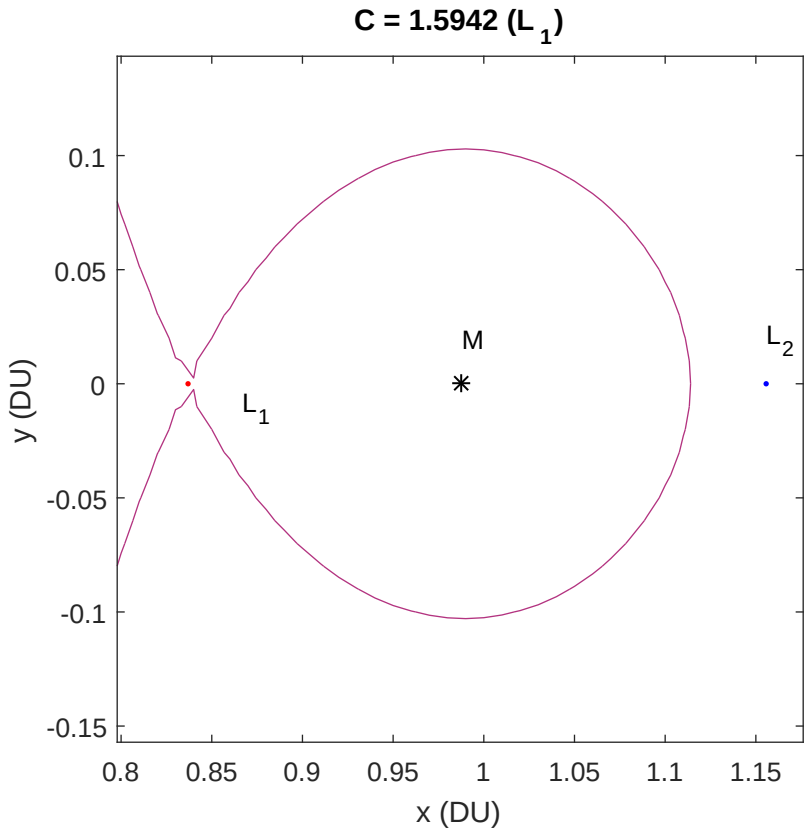

Figure 2.9. Zoomed in Zero Velocity Curves for Jacobi Energy of L_1 point in the Earth-Moon system

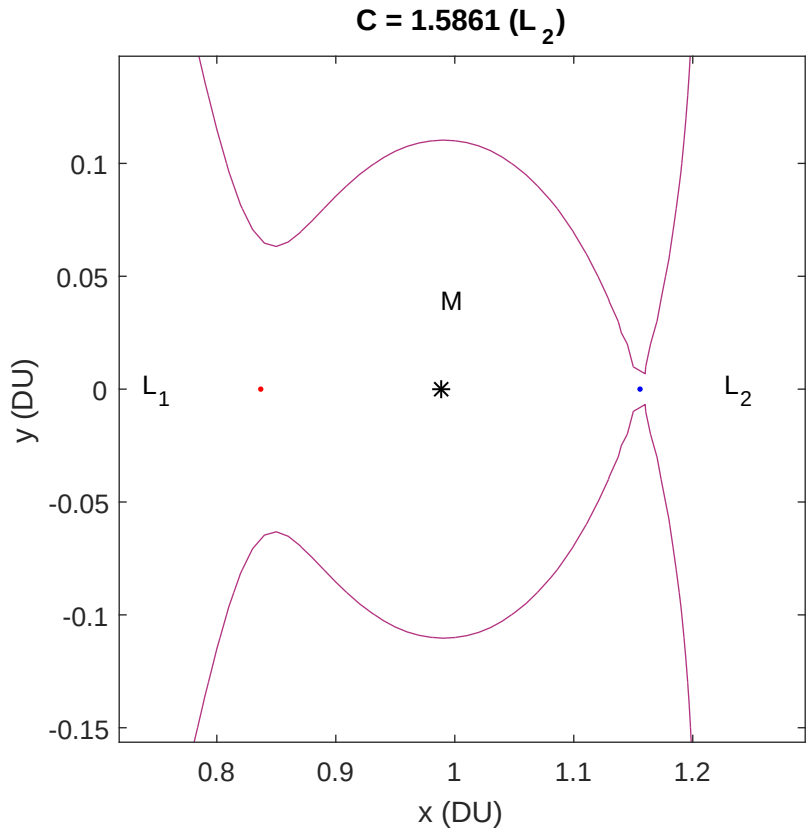

Figure 2.10. Zoomed in Zero Velocity Curves for Jacobi Energy of L_2 point in the Earth-Moon system

2.6 Lagrange Point Orbits

This section will focus on the different kinds of possible Lagrange point orbits. A method of obtaining families of these orbits using differential correction techniques is presented. Finally, the Lagrange point of interest is identified and the desired orbit to be used for transfer is obtained. While it is recognized that LPOs maybe periodic or quasi-periodic orbits close to various Lagrange points, it is important to realize that the Lagrange point themselves do not attract the objects in an LPO. It is the combined dynamics and gravitational interaction of the three-body system that allows for regions of equilibrium. Another fact that is important, is to realize that while the Lagrange points are not stable points in space, i.e. an object placed *at* a Lagrange point will not remain stationary with respect to the two massive bodies, it is possible to place an object in orbit around the point with minimal

orbit correction maneuvers for a longer duration.

Some different types of Lagrange point orbits are :

Lyapunov Orbits : These are planar orbits that lie in the orbital plane of the two massive bodies. These exhibit a characteristic 'kidney bean' shape.

Halo Orbits : These are three-dimensional orbits that, with large z-component, look like a halo around the one of the primaries when viewed from the other one. In an ideal system, these are periodic and are categorized as northern or southern halo orbit, depending on the out-of-plane or z-component of the orbit.

Lissajous Orbits : These are three-dimensional, confined within a certain region of space near a Lagrange point. These are quasi-periodic in nature such that they look like a chaotic orbits in the short term but these do exhibit a certain amount of periodicity when viewed over longer integration times.

Apart from the ones mentioned above, there are a few more LPOs with complex shapes such as axial orbits, vertical orbits, resonant orbits, distant prograde orbits and distant retrograde orbits [10]. These orbits occur in the dynamical system due to specific conditions and each one has its own characteristics. For the purposes of this thesis, the focus will largely remain on Lyapunov and halo orbits. Having established the different types of LPOs, the focus now shifts to the generation of such orbits in the Earth-Moon system to design optimal transfer trajectories from these towards a Earth.

2.7 Generation of Lagrange Point Orbits

One of the most important requirements for designing a transfer trajectory is to start with an initial orbit. Since the orbits around Lagrange points do not conform to conic shapes like a circle or an ellipse, it becomes very difficult to generate initial conditions for an initial orbits. However, certain numerical techniques have been developed, that allows us to obtain orbits which exhibit a certain characteristics. Howell [11] gives a very simple algorithm to generate seed orbits to generate families of orbits using single shooting. Multiple shooting methods are also used for generating the initial conditions [12] [2] [13], if the estimated states around an orbit are available. Multiple shooting is especially useful when a periodic orbit is desired while using the full ephemeris model of the solar system. Continuation

techniques such as pseudo-arclength continuation methods are employed when it is desired to study the families of orbits of a certain type [2], [12], [13], [10], [14]. The differential correction methods utilize the symmetry of the CR3BP to exploit certain characteristics of the LPO. The procedure is fairly simple.

The initial condition of the orbit is defined using some analytic approximations provided by the Richardson or Linstead-Poincaré approximation [15]. The initial state of the orbit is then corrected by integrating the orbit between two intercepts of the x - z axis. The particle lies on the x-axis initially. This implies that y-location is initially zero. The initial velocity along the x-direction is considered to be zero so that the initial y-direction velocity is normal to the x-axis. In case of a Lyapunov orbit, the z-coordinate and hence the z-direction velocity remains zero throughout the orbit due to the planar nature of the orbit. Due to the symmetry of the orbit, the next intercept of the x-z plane is expected at the half orbit point where the y-velocity is normal to the x-axis but in the opposite direction. This provides the state vector conditions at $t = T/2$ given by such that y-location is again zero, the x-direction velocity is expected to be zero as this is the farthest point along the x-axis that the particle is expected to travel i.e. $y_{T/2} = 0$ and $\dot{x}_{T/2} = 0$ where $T/2$ stands for the half-period. Since the expected states at two points along the orbit are established, therefore this problem can be formulated as a two-point boundary value problem (TPBVP). This TPBVP can be solved using the single shooting algorithm using Newton's method. The initial conditions and desired conditions at the half orbit can be written as

$$\vec{X}_{t_0} = \begin{bmatrix} x_{t_0} & 0 & 0 & 0 & \dot{y}_{t_0} & 0 \end{bmatrix}^T \tag{2.68}$$

$$\vec{X}_{T/2} = \begin{bmatrix} x_{T/2} & 0 & 0 & 0 & \dot{y}_{T/2} & 0 \end{bmatrix}^T \tag{2.69}$$

Here, the x_{t_0} and $\dot{y}_{t_0}$ are considered to be the free variables. The free variables are free to change between successive iterations. The desired values of $y_{T/2}$ and $\dot{x}_{T/2}$ are obtained by integrating the equations of motion Eq. (2.31) till the first x axis intersection. This ensures that the $y_{T/2} = 0$ condition is always satisfied. Since the equations are numerically integrated, generally the state vector obtained at $T/2$ is

of the following form

$$\vec{X}_{T/2} = \begin{bmatrix} x_{T/2} & 0 & 0 & \dot{x}_{T/2} & \dot{y}_{T/2} & 0 \end{bmatrix}^T \tag{2.70}$$

Since it is desired to obtain $\dot{x}_{T/2} = 0$, the initial condition for x_{t_0} needs to be adjusted. Such an adjustment will also cause a change in the integration half time $T/2$ therefore the following procedure is is used to make the adjustment

$$\delta\vec{X}(T/2) \approx \Phi(T/2, t_0)\delta\vec{X}(t_0) + \frac{\partial\vec{X}}{\partial t}\delta(T/2) \tag{2.71}$$

where, $\delta\vec{X}(T/2)$ is the change in the final conditions required to obtain the desired final condition at $T/2$. $\delta\vec{X}(t_0)$ is the desired correction to the initial vector to make the $\delta\vec{X}(T/2) = 0$. $\Phi(T/2, t_0)$ is the state transition matrix obtained from Eq. (2.40).$\dfrac{\partial\vec{X}}{\partial t}$ is the time rate of change of the state vector obtained by evaluating the equations of motion at $T/2$. Finally, $\delta(T/2)$ is the change in the half period due to driving $\delta\vec{X}(T/2)$ to zero. The forms of $\delta\vec{X}(T/2)$ and $\delta\vec{X}(t_0)$ are

$$\delta\vec{X}(T/2) = \begin{bmatrix} \delta x_{T/2} & 0 & 0 & -\delta\dot{x}_{T/2} & \delta y_{T/2} & 0 \end{bmatrix}^T \tag{2.72}$$

$$\delta\vec{X}(t_0) = \begin{bmatrix} \delta x_{t_0} & 0 & 0 & 0 & \delta y_{t_0} & 0 \end{bmatrix}^T \tag{2.73}$$

Hence Eq. (2.71) can now be written as

$$\begin{bmatrix} \delta x_{T/2} \\ 0 \\ 0 \\ -\delta\dot{x}_{T/2} \\ \delta y_{T/2} \\ 0 \end{bmatrix} \approx \begin{bmatrix} \phi_{1,1} & \phi_{1,2} & \phi_{1,3} & \phi_{1,4} & \phi_{1,5} & \phi_{1,6} \\ \phi_{2,1} & \phi_{2,2} & \phi_{2,3} & \phi_{2,4} & \phi_{2,5} & \phi_{2,6} \\ \phi_{3,1} & \phi_{3,2} & \phi_{3,3} & \phi_{3,4} & \phi_{3,5} & \phi_{3,6} \\ \phi_{4,1} & \phi_{4,2} & \phi_{4,3} & \phi_{4,4} & \phi_{4,5} & \phi_{4,6} \\ \phi_{5,1} & \phi_{5,2} & \phi_{5,3} & \phi_{5,4} & \phi_{5,5} & \phi_{5,6} \\ \phi_{6,1} & \phi_{6,2} & \phi_{6,3} & \phi_{6,4} & \phi_{6,5} & \phi_{6,6} \end{bmatrix}_{(T/2,t_0)} \begin{bmatrix} \delta x_{t_0} \\ 0 \\ 0 \\ 0 \\ \delta\dot{y}_{t_0} \\ 0 \end{bmatrix} + \begin{bmatrix} \dot{x} \\ \dot{y} \\ \dot{z} \\ \ddot{x} \\ \ddot{y} \\ \ddot{z} \end{bmatrix} \delta(T/2) \tag{2.74}$$

Note that the desired change in $\delta\dot{x}_{T/2}$ has a negative sign. This is the deviation in the desired state vector at the half-period and needs to be driven to zero. $\delta(T/2)$

is obtained by using the fact that $y_{T/2}$ is always zero. This is caused due to the integration termination condition.The term $\delta(T/2)$ is written as follows

$$\delta(T/2) = \frac{-\phi_{2,1}\delta x_{t_0} - \phi_{2,5}\delta\dot{y}_{t_0}}{\dot{y}} \tag{2.75}$$

Finally, the equation for driving $\delta\dot{x}_{T/2}$ is given as

$$-x\dot{}_{T/2} \approx \Big(\phi_{4,1} - \phi_{2,1}\frac{\ddot{x}}{\dot{y}}\Big)\delta x_{t_0} + \Big(\phi_{4,5} - \phi_{2,5}\frac{\ddot{x}}{\dot{y}}\Big)\delta\dot{y}_{t_0} \tag{2.76}$$

Keeping the initial x_{t_0} as a constant, Eq. (2.76) is used solve for the estimated adjustment in the $\dot{y}_{t_0}$ such that the error in $\dot{x}_{T/2}$ is below a desired tolerance ϵ

$$\delta\dot{y}_{t_0} \approx \left[\phi_{4,5} - \phi_{2,5}\frac{\ddot{x}}{\dot{y}}\right]^{-1}\big[-\dot{x}_{T/2}\big] \tag{2.77}$$

Since this is based on the linear model of dynamics, a few iterations are required to achieve the desired convergence. It is important to note that this process is highly sensitive to the initial conditions used in the initial seed state vector. For a three-dimensional halo orbit, a similar process is followed, however, the initial z location is now desired such that such that the initial z velocity is zero i.e. z is at an extremum. Similar to the case with Lyapunov orbit, the half orbit conditions for this case are expected to be $y_{T/2} = 0$, $\dot{x}_{T/2} = 0$ and $\dot{z}_{T/2} = 0$. $\delta\vec{X}(T/2)$ and $\delta\vec{X}(t_0)$ for a halo orbit becomes

$$\delta\vec{X}(T/2) = \begin{bmatrix}\delta x_{T/2} & 0 & \delta z_{T/2} & -\delta\dot{x}_{T/2} & \delta y_{T/2} & -\delta z_{T/2}\end{bmatrix}^T \tag{2.78}$$

$$\delta\vec{X}(t_0) = \begin{bmatrix}\delta x_{t_0} & 0 & \delta z_{t_0} & 0 & \delta y_{t_0} & 0\end{bmatrix}^T \tag{2.79}$$

Substituting these vectors in Eq. (2.74) and following the same process as shown above, the equations become

$$\delta(T/2) = \frac{-\phi_{2,1}\delta x_{t_0} - \phi_{2,3}\delta z_{t_0} - \phi_{2,5}\delta\dot{y}_{t_0}}{\dot{y}} \tag{2.80}$$

The objective in this case is to drive the $\dot{x}_{T/2}$ and $\dot{z}_{T/2}$ to zero. This is done through

the equations

$$
\begin{aligned}
-\dot{x}_{T/2} &\approx \left(\phi_{4,1} - \phi_{2,1}\frac{\ddot{x}}{\dot{y}}\right)\delta x_{t_0} + \left(\phi_{4,3} - \phi_{2,3}\frac{\ddot{x}}{\dot{y}}\right)\delta z_{t_0} + \left(\phi_{4,5} - \phi_{2,5}\frac{\ddot{x}}{\dot{y}}\right)\delta \dot{y}_{t_0} \\
-\dot{z}_{T/2} &\approx \left(\phi_{6,1} - \phi_{2,1}\frac{\ddot{z}}{\dot{y}}\right)\delta x_{t_0} + \left(\phi_{6,3} - \phi_{2,3}\frac{\ddot{z}}{\dot{y}}\right)\delta z_{t_0} + \left(\phi_{6,5} - \phi_{2,5}\frac{\ddot{z}}{\dot{y}}\right)\delta \dot{y}_{t_0}
\end{aligned} \tag{2.81}
$$

The adjustments to the initial conditions are obtained by either keeping x_{t_0} or z_{t_0} as constant and adjusting the other along with $\dot{y}_{t_0}$. Keeping x_{t_0} as constant, the final equations for adjustments to the initial conditions are

$$
\begin{bmatrix} \delta z_{t_0} \\ \delta \dot{y}_{t_0} \end{bmatrix} \approx \begin{bmatrix} \phi_{4,3} - \phi_{2,3}\dfrac{\ddot{x}}{\dot{y}} & \phi_{4,5} - \phi_{2,5}\dfrac{\ddot{x}}{\dot{y}} \\ \phi_{6,3} - \phi_{2,3}\dfrac{\ddot{z}}{\dot{y}} & \phi_{6,5} - \phi_{2,5}\dfrac{\ddot{z}}{\dot{y}} \end{bmatrix}^{-1} \begin{bmatrix} -\dot{x}_{T/2} \\ -\dot{z}_{T/2} \end{bmatrix} \tag{2.82}
$$

This methodology is employed throughout the thesis for generating periodic LPOs. Now that the periodic orbits and the method to obtain them is established, methods used to define trajectories to and from these orbits needs to be discussed. The next chapter presents the analysis techniques and finally, the optimization problem as used in this thesis.

Chapter 3
Analysis

This chapter showcases the techniques used to analyze the orbits and to obtain the final optimized trajectory. First, an introduction to the DST as relevant to this thesis is presented. A brief description of invariant manifold and their application to the trajectory design problem is discussed. Then, a methodology to generate the manifolds is provided.

The basics of optimization theory are presented next. A general optimization problem and some basic methodologies used to solve optimization problems are discussed. Finally, a description of particle swarm optimization procedure to be used in the present work is presented along with a description of the strategy to solve the desired trajectory optimization problem.

3.1 Introduction to Dynamical Systems Theory

DST was developed as a way to study the complex dynamics of non-linear system. A number of books provide detailed description of the basic concepts of dynamical systems such as Strogatz [16], Wiggins [17], Guckenheimer [18]. Essentially it deals with the graphical description of the system in the phase space and recognizing characteristic points in the space that govern the flow of the state of the system when certain condition are met. It helps to study the different states that a system can achieve and allows one to distinguish between desirable and undesirable states. Based on the knowledge, it then becomes possible to change the dynamics of the system by providing appropriate inputs to steer the system to achieve a desired state.

The dynamical system may either be considered as continuous or discrete. The

solution of the system in case of a continuous system is called a flow. For a discrete system, the solution is called a map [16]. Since the system studied in this thesis is represented in the form of a differential equation, it is a continuous system and therefore, the system as presented in this thesis is considered as a flow.

The objective of DST is to characterize the dynamics of the system using graphical tools and methods instead of actually solving the system of equations. The study of the system near the equilibrium points in this greatly helps in this regard. Once the fixed points are recognized, the evolution of the flow near these points are studied. The system is linearized near the fixed points and the eigenvectors of the Jacobian matrix helps characterize the stability of the flow at and near these points. Qualitative changes in the properties of the system due to quantitative changes to the system parameters help characterize the existence of points called bifurcation points. Bifurcation points are interesting because near these points, the system dynamics changes in very significant ways [16]. These could be creation of fixed points, or annihilation of previously existing fixed points. This becomes relevant when studying the flow of a system whose parameters change with time. In case of the CR3BP, the existence of multiple types of Lagrange Point Orbits are due to bifurcation of one family of orbits from another family of orbits. These points and the conditions to achieve them, while interesting, are not the focus of this thesis. Work by Parker [10], Grebow [19] and others have detailed discussion on this topic.

3.2 Monodromy Matrix

Untill now, the STM was used in finding the solution of initial conditions for a periodic orbit given initial estimates. It is able to give us the required changes in the initial conditions because the STM characterizes the sensitivity of the *change* in final state to the *change* in initial state of the system. Since it contains the knowledge of the evolution of the system, it is able to provide the knowledge of the stability of an orbit [10]. The state transition matrix, when integrated for the entire period of a periodic orbit, is called the monodromy matrix. That is,

$$M = \Phi(T, t_0) \tag{3.1}$$

where T is the period of the orbit. Consider a vertical plane at the initial condition of the orbit. This will be a point on the vertical plane with the trajectory of the orbit flowing normal to this plane. For a periodic orbit, integrating the orbit trajectory for exactly one period yields another point exactly coinciding with and initial point. Hence the periodic orbit will be represented as a single fixed point on this map. Such a map is called a Poincaré map. It effectively reduces the dimensionality of the dynamics by one [10]. The monodromy matrix then serves as a linear map that transitions the initial state to the final state (in discrete intervals of the period of the orbit), corresponding to individual points on the Poincaré map [14]. Knowledge of the flow in the phase space of the system in the vicinity of this point on the map can be extracted from the eigenvalues and eigenvectors of the monodromy matrix. Since the selection of the initial point is arbitrary, the can eigenvectors change for each individual initial state along a period orbit but the eigenvalues remain the same for a particular orbit as it is a property of the orbit itself.

Recall that the linearization performed in Chapter 2 of the EOMs was done with the assumption that the system is very close to the equilibrium point. That same analysis can be extended for linearization of motion about an entire LPO, however, now the Jacobian matrix will have explicit time dependence. Details of this analysis are provided in Abraham [2] and Rausch [14], among others. Essentially the analysis uses Floquet's Theorem given in Perko [20] to obtain a solution for the monodromy matrix to get insight into eigenvalues of the monodromy matrix since the eigenvalues characterizes the stability of the orbit.

It is shown in Abraham [2] that for a closed, periodic orbit, at least one eigenvalue of the monodromy matrix is one, i.e. $\Lambda = 1$ where Λ represents one of the eigenvalues of the monodromy matrix. Furthermore, for periodic orbits in the CR3BP, due to the symmetry about the x-z plane and time invariance of the system under $t \rightarrow -t$, it can be shown that eigenvalues of the monodromy matrix occur in reciprocal pairs as shown in [11] [21] [10] [14].

$$\Lambda_i \;=\; \left(\Lambda_1,\;\; \frac{1}{\Lambda_1},\;\; \Lambda_2,\;\; \frac{1}{\Lambda_2},\;\; 1,\;\; 1\right) \tag{3.2}$$

Once the eigenvalues are obtained, eigenvectors can be computationally generated.

3.3 Invariant Manifolds

Having obtained the eigenvalues and eigenvectors of the monodromy matrix, investigations into the stability characteristics can now begin. It is known that each eigenvalue has an associated eigenvector. From basic stability analysis, eigenvalues with negative real part are stable and the corresponding eigenvector spans the stable subspace, while eigenvalues with positive real part are unstable and the corresponding eigenvector spans the unstable subspace. The phase space of the system is the entire set of possible states that an object in the system can achieve. The stable and unstable subspaces are a subset of the entire phase space such that motion along the eigenvectors and in turn their respective subspaces implies motion or trajectories of the system in phase space. The set of trajectories that exponentially diverge due to a perturbation in the initial conditions are defined as the unstable trajectories, conversely, trajectories that exponentially converge to the periodic orbit are called stable trajectories. The set of all unstable trajectories originating from the periodic orbit form a surface in the three-dimensional space. This surface is called the invariant unstable manifold W^U and likewise, the surface formed by the set of all stable trajectories terminating at the periodic orbit is called the invariant stable manifold W^S. Since the trajectories are entirely dependent on the eigenvectors of the periodic orbit and do not vary under the natural dynamics of the system, these are called invariant.

It is important to note that for a neutrally stable orbit (no positive or negative eigenvalues), like in the case of orbits in the two-body dynamics, there are no stable or unstable manifolds as a perturbed initial state results in a new orbit around the final state. In case of a purely stable orbit, there will exist only a stable manifold but no unstable manifolds, hence it is not possible to naturally move away from an orbit as the perturbations will bring the spacecraft back to the initial orbit. Fortunately, the orbits about collinear Lagrange points are unstable in nature, i.e. there exists atleast one stable and one unstable eigenvalue with corresponding eigenvectors [10], therefore it is possible to use the existence of stable and unstable manifolds to design low energy trajectories to and from the LPO.

Another important aspect of manifolds is that apart from the trajectories originating from and terminating at unstable periodic orbits, manifolds are also possible for the Lagrange points themselves. Since the collinear Lagrange points

are unstable, there are trajectories possible to and from these points. Hence there are manifolds possible for periodic orbits as well as for the Lagrange points [10].

3.4 Generation of Manifolds

It is possible to computationally generate these manifolds using the eigenvectors of the monodromy matrix and their associated stable and unstable subspaces. However, while the eigenvectors do specify an orientation in space, they are not specific to a direction and hence multiplying them with a negative number gives a new direction for the vector. Therefore, for each type of manifold, there exist two directions in which the manifold can evolve. These directions are termed as interior manifold for the manifold moving towards the smaller primary and exterior manifold for manifold moving towards the larger primary. The initial state of the periodic orbit is perturbed using the required eigenvectors by either adding to or subtracting the scaled eigenvector from the initial state and then numerically integrated either forwards or backwards in time,

$$\begin{aligned} \vec{X}_{pert} &= \vec{X} \pm \epsilon \frac{\vec{V}}{|V|} \\ \epsilon &= \frac{\eta}{\sqrt{V_x^2 + V_y^2 + V_x^2}} \end{aligned} \tag{3.3}$$

where ϵ is the normalized magnitude of the perturbation and $\vec{V}$ represents the appropriate eigenvector for the desired manifold. The $\pm$ sign represents the interior and exterior directions of the evolution of the manifold. If a stable manifold is desired, then the eigenvector $\vec{V}^S$ associated with the stable eigenvalue is used and then the integration is performed backwards in time since the trajectories on this manifold approaches the periodic orbit. On the other hand, if the unstable manifold is desired, the appropriate eigenvector $\vec{V}^U$ is used and the integration is performed forwards in time since the trajectories on this manifold evolves forwards in time as it moves away from the initial orbit.

The process described above will produce a single trajectory on the manifold as only one state was perturbed. To generate a representation a surface, the periodic orbit is first discretized to have a preselected number of states along the orbit. This

selection will be based on the desired number of trajectories on the manifold. Then each state is perturbed as shown above, integrated forwards in time for one period to generate the monodromy matrix for each state to generate the eigenvectors for each state. Then each state is perturbed using their respective eigenvectors and integrated based on the type on manifold. The procedure as discussed in refrences [2] [10] and [22], is summarized as follows.

- The initial conditions for the periodic Lagrange point orbit is corrected using the single shooting algorithm to ensure that no discontinuities exists between the initial and final states.
- The state is integrated for one period and the monodromy matrix is calculated.
- The eigenvalues and eigenvectors of the monodromy matrix are calculated such that $\vec{V}^S$ is the eigenvector associated with the stable eigenvalue and $\vec{V}^U$ is the eigenvector associated with the unstable eigenvalue.
- A perturbation magnitude ϵ is defined as approximately 100 km [10] in non-dimensional units and is normalized based on the velocity of the orbit state under consideration. A small perturbation will cause the trajectory to remain close to the LPO and will take a long time to move away from the LPO, requiring longer integration times to generate the trajectory until a certain point in space. A large perturbation will cause the linear assumption of the STM to be violated and the produced trajectories will not represent the actual manifold. Parker [10] mentions that for Earth-Moon systems, perturbations are of the order of 100 km and for Sun-Earth system, they are of the order of 1000 km.
- The eigenvectors are normalized. This is done to ensure a commensurate amount of perturbation for each state.
- The perturbation is calculated based on the Eq. (3.3).
- The perturbed states are then integrated forwards for unstable and backwards for stable manifolds.
- The entire process is repeated for each discretized initial state on the periodic orbit.

3.5 General Optimization Problem

Now that the manifolds are defined, it is necessary to discuss how they are used to generate optimal trajectories. The objective of this thesis is to utilize the invariant manifolds of the LPOs to obtain optimal transfers from the LPO to a LEO orbit. This can be done by picking a point on the manifold and calculating the ΔV required to transfer the spacecraft to an orbit around the Earth. The point on the manifold that provides the minimum ΔV is considered to be the optimal point for initiating the transfer. Selection this optimal point is the task of the optimization algorithm.

In general, an optimization problem can be stated as follows,

$$\begin{aligned} min(or\ max) \quad & f(\vec{x}) \\ subject\ to \quad & x \in S \end{aligned} \tag{3.4}$$

where $f(\vec{x})$ (also known as the cost function) is the function that is required to be minimized, $\vec{x}$ is the vector of decision variables and S is the set of all feasible values of $\vec{x}$. For the purposes of this thesis, the decision variable vector $\vec{x}$ is represented by the the state vector $\vec{X}$, since it is desired to find the state of the spacecraft which will result in the minimum transfer cost and S will be the set of all points on the manifold. $f(\vec{X})$ will be a function that calculates the minimum $\Delta\vec{V}$ (or transfer cost) required to transfer to LEO.

3.6 Optimization Techniques

Optimization problems can be various types such as linear programming, non-linear programming, convex optimization, discrete optimization, constrained optimization, unconstrained optimization among others. There are a multitude of optimization techniques available, each designed to optimize a specific type of problem. It is very difficult to find a single technique capable of optimizing all kinds of problems. The most common types of optimization techniques are gradient-based methods covered in a variety of texts such as Sergiy and Panos [23] and Nocedal and Wright [24]. These, as the name suggests, uses the gradients of the cost functions to determine the extremum of the function at a particular value of the decision variable until

the function value converges to a pre-defined tolerance. The first- and second-order optimality conditions provide the necessary and sufficient conditions for investigation of an optimal solution [23].

While gradient based methods are widely used, there are a number of difficulties with using such methods. First, these require an initial estimate of the solution to be accurate to a certain degree to be able to reach a solution within finite time. While for simple problems this can be easily accomplished, for problems with higher complexities, generation of said initial guesses can be very tedious if not impossible. Second, while it is possible to obtain the gradients and Hessian of the cost functions used in the evaluation of the optimality conditions for fairly complex problems, for problems where the cost functions are not defined as simple equations, obtaining analytical expressions for the gradient and Hessian can be very computationally expensive and in many cases, impossible. For such problems, multiple heuristic based optimization methods have been developed such as Evolutionary algorithms which includes algorithms like Bacteria Foraging, Genetic algorithms among others. These are designed on the patterns of evolution of organisms. Swarm algorithms which includes techniques like Particle Swarm, Ant colony optimization etc. are based on the social interactions within a group of organisms and Physical algorithms with methods like Simulated Annealing, Ray optimization among others. These are based on the physical systems that occur in nature [25]. These techniques are based on heuristic techniques which circumvent the need to calculate the gradients.

3.7 Particle Swarm Optimization

Particle swarm is a swarm intelligence algorithm first introduced by Kennedy and Eberhart in 1995 [26]. It is based on the social interaction and swarming behavior of a flock of birds. The basic idea behind the algorithm is based on social interaction between particles (birds) in a swarm to reach a desired location (food). It is robust technique and has been widely used in a variety of applications [27]. The most attractive part is that the algorithm comprises of just two simple equations to model the swarm behavior

$$v^{i+1} = C_I\, v^i + C_C\, rand(0,1)\, [X_P^{Best} - X^i]$$

$$+C_S\ rand(0,1)\ [X_G^{Best} - X^i] \tag{3.5}$$

$$X^{i+1} = X^i + v^{i+1} \tag{3.6}$$

where X^i is the decision variable at the i^{th} iteration. The term, v, is generally called the velocity but is technically a ΔX update to the current position calculated at then end of the iteration. X_P^{Best} and X_G^{Best} are value of the decision variable that yields the best value of cost function till the i^{th} iteration for each individual particle in the swarm and any particle in the swarm respectively. The variables C_I, C_C and C_S are the inertial, cognitive and social components of the velocity. C_I represents the tendency of the particle to follow the current path i.e. the Newtonian motion. Each particle 'remembers' its best known location (location of minimum cost) and this is represented by C_C which is the cognitive component and it directs the motion of the particle towards a previously known best location. Finally, C_S represents the component that is gained through the social interaction of the swarm. The swarm is able to communicate the best known location untill the current iteration and thus the particle will attempt to reorient its position based on this global best location [2] [26]. The values for C_I, C_C and C_S are based on the works by Abraham [2] and Conway [28], [29] and are listed below.

$$C_I = 0.15 \tag{3.7}$$

$$C_C = 1 \tag{3.8}$$

$$C_S = 1 \tag{3.9}$$

3.8 Search Space

Since the search space for the problem under consideration consists of all points *on* each individual trajectory of the manifold, it is convenient to parameterize the space space based on the trajectory number k and the location of the point from the LPO defined by the value τ such that

$$\mathbf{X}_{manifold}(k,\tau) \in W^{S/U} \tag{3.10}$$

where $W^{S/U}$ represents the stable and unstable manifold sets. The value τ is normalized over the entire TOF of a particular trajectory and lies between $(0,1)$.

The trajectory number k is also calculated as the **mod** N, i.e $k = \mathbf{mod}\,(k, N)$. This ensures that if the trajectory number is exceeded greater than N, it will still remain a valid trajectory in the search space. This allows for a convenient and standard update of the position of every particle throughout all trajectories in terms of k and τ.

3.9 Boundary Conditions

Now that the search space is parameterized, the velocity update for each particle is defined based on the two parameters introduced above namely, trajectory number k, and the time since departure from the LPO called τ, normalized between 0 and 1. However, since each position update adds to the previous known location, there is a possibility that the particle might end up outside the allowable space. Therefore, certain boundary conditions need to be imposed to maintain a particle within the search space. The limits of the search space has been defined above, it also helps to limit the maximum change in the trajectory number (i.e. velocity in the parameter δk) and the maximum jump in the location based on time $\delta\tau$. The following limits are imposed.

$$\delta\tau_{max} = \pm\frac{1}{2} \tag{3.11}$$

$$\delta k_{max} = \frac{1}{2}\,N \tag{3.12}$$

$$v_{max}^{i+1} = \begin{bmatrix}\delta k_{max} & \delta\tau\end{bmatrix} \tag{3.13}$$

where N is the total number of trajectories in the manifold. Additionally, in case the particle is found to leave the search space, the particle location and the velocity for the next iteration is changed as follows.

$$X_k^{i+1} = \mathbf{mod}(k, N) \tag{3.14}$$

$$X_\tau^{i+1} = 1.0 \;\; (if\, \tau > 1)$$

$$X_\tau^{i+1} = 0.0 \;\; (if\, \tau < 0) \tag{3.15}$$

$$\delta\tau^{i+1} = 0 \tag{3.16}$$

where i is the iteration number, X^{i+1} is the updated state of the particle, $\delta\tau$ is the change in τ of the particle for the next iteration. Notice that δk is not changed as it can loop back upon itself based on the **mod** function.

3.10 Cost Function

The most important element of the optimization problem is the cost function. It determines the complexity of the problem and is a major concern when selecting an appropriate method for optimization. This work focuses on the two-burn impulsive transfer from the manifold to an LEO orbit. This is achieved using the solution to Lambert's problem where the method exploits the natural geometry of orbits in the two-body dynamics to determine the initial and final velocity vectors and therefore the trajectory in the two-body system. The procedure is simple and is well studied in the literature ([30], [31], [9]). Given the initial and final position vectors, it is possible to obtain the velocity vectors by solving a TPBVP. The selection of this methods was driven by the fact that computations involving numerical integration methods tend to be very expensive and time consuming. Using this method, one can obtain the quick initial estimates of the impulses required to transfer from the manifold to the desired Earth orbit in a very time efficient manner. It also allows quick variation of the parameters of the PSO algorithm and allows for experimentation with different types of cost functions by adding the TOF constraint along with velocity change ΔV.

The Lambert's solution is utilized here to obtain the velocity vectors and the magnitude of the total ΔV required for the complete transfer from the manifold to an LEO orbit. The objective is to find the transfer scheme which minimizes this ΔV. It must be noted that Lambert's solution works for a single gravitational center of attraction and as such will provide incorrect values for the velocities. However, this method is primarily used to facilitate quick analysis of the transfers and the expected orders of magnitudes for the ΔV requirements.

The difference in the gravitational potentials of the Earth system compared to the combined Earth-Moon system yields a 1.2% difference, hence the velocity values obtained via this method can provide good initial estimates for gradient-based optimization techniques. To minimize the impact of using two different systems, the search space boundary close to the LPO is defined by the plane normal to the

x-y plane located at a distance equal to of radius of the Sphere-of-Influence (SOI) of the Moon along the x-axis. This is done because transfers originating closer to the Moon will result in higher deviation in the final result.

3.11 Particle Swarm Optimization Procedure

Having defined the cost function, the entire solution process can now be summarized as follows:

- The particles for the procedure are randomly initialized based on τ and k values. The values of initial velocity v and global best X_G^{Best} are also initialized for use during the first iteration.
- For each particle, the τ and k values are converted to the state vector and lies on the search space defined within the specified boundaries.
- The final state vector on the LEO is defined as this will form the final condition (second radius vector) for the Lambert's problem solver.
- The initial state on the manifold is converted to the dimensional, Earth-Centered Inertial (ECI) system from the canonical, CR3BP system.
- The initial state (of the particle) and final state (of the LEO) are now passed to the Lambert's solver and the value for ΔV is obtained and stored. This process is repeated for every particle in the swarm.
- The value of ΔV (cost function) is now compared to the personal best X_P^{Best} and the global best X_G^{Best} to determine the best transfer location in the current iteration.
- The velocity update v^{i+1} is calculated based on the X^i, X_P^{Best}, X_G^{Best} and the previous velocity v^i.
- The boundary conditions on the particle position X^{i+1} and the velocity v^{i+1} are imposed as required.
- A convergence criteria is defined as a predefined percentage of particle in the vicinity of the X_G^{Best}.

- The states of the particles are updated with the calculated velocities and the entire process is repeated till either convergence is achieved or till the maximum loop iterations have been completed.

The global best obtained from the above procedure is the closest point to the global optimal location on the search space found by the PSO algorithm.

3.12 Lambert's Solver

The method of solution for the transfer ΔV in this thesis is based on the Lambert's Problem solver. The method uses two-body assumption to find the initial and final velocity requirements, given the initial and final radius. Additionally it also requires the transfer time to be provided to the solver to obtain the required velocity changes. The procedure to find the solution to the Lambert's problem is well established and studied in astrodynamics. The basic algorithm is taken from Curtis [30] and the transfer time of flight between the two radii is obtained from Prussing and Conway [31] as the transfer time for the minimum energy semi-major axis between the two radii. The initial radius vector is taken as the initial point from which the transfer is initiated. The second and final radius vector is the desired vector in the final orbit. Since this method requires a final vector to be given, the final orbit must be known and well defined and a state on the final is then selected as the target to be achieved. The procedure as presented in [30] is summarized as follows.

Let $\vec{r}_1$ and $\vec{r}_2$ be the initial and final radius vectors respectively. Then the transfer angle between the two radii can be calculated using the equation

$$\cos \Delta\theta = \frac{\vec{r}_1 \cdot \vec{r}_2}{r_1 \, r_2} \tag{3.17}$$

$$r_1 = \sqrt{\vec{r}_1 \cdot \vec{r}_1} \;\; and \;\; r_2 = \sqrt{\vec{r}_2 \cdot \vec{r}_2} \tag{3.18}$$

where $\Delta\theta$ is the transfer angle between the two radii. Since there is a quadrant ambiguity associated with the $\cos^{-1}$ function, the following equation is used

$$(\vec{r}_1 \times \vec{r}_2)_Z = r_1 r_2 \sin(\Delta\theta) \cos i \tag{3.19}$$

where $(\vec{r}_1 \times \vec{r}_2)_Z$ represents the normal component of the cross product of $\vec{r}_1$ and $\vec{r}_2$. The sign of $(\vec{r}_1 \times \vec{r}_2)_Z$ is used to determine the required quadrant of the

transfer angle. For prograde trajectories this is done as

$$\Delta\theta = \begin{array}{l} \cos^{-1}\left(\dfrac{\vec{r}_1 \cdot \vec{r}_2}{r_1\, r_2}\right) \quad if(\vec{r}_1 \times \vec{r}_2)_Z \geq 0 \\ 2\pi - \cos^{-1}\left(\dfrac{\vec{r}_1 \cdot \vec{r}_2}{r_1\, r_2}\right) \quad if(\vec{r}_1 \times \vec{r}_2)_Z < 0 \end{array}$$

The method presented in Curtis [30] uses Lagrange coefficients $f, g, \dot{f}$ *and* $\dot{g}$ and the universal variable χ to simplify the analysis. The Lagrange coefficients are presented as follows

$$f = 1 - \frac{\mu r_2}{h^2}(1 - \cos\Delta\theta) \tag{3.20}$$

$$g = \frac{r_1 r_2}{h}\sin\Delta\theta \tag{3.21}$$

$$\dot{f} = \frac{\mu}{h}\frac{1-\cos\Delta\theta}{\sin\Delta\theta}\left[\frac{\mu}{h^2}(1-\cos\Delta\theta) - \frac{1}{r_1} - \frac{1}{r_2}\right] \tag{3.22}$$

$$\dot{g} = 1 - \frac{\mu r_1}{h^2}(1 - \cos\Delta\theta) \tag{3.23}$$

In terms of the universal variable χ, the Lagrange coefficients can be re-written as

$$f = 1 - \frac{\chi^2}{r_1}C(z) \tag{3.24}$$

$$g = \Delta t - \frac{1}{\sqrt{\mu}}\chi^3 S(z) \tag{3.25}$$

$$\dot{f} = \frac{\sqrt{\mu}}{r_1 r_2}\chi\big[zS(z) - 1\big] \tag{3.26}$$

$$\dot{g} = 1 - \frac{\chi^2}{r_2}C(z) \tag{3.27}$$

where $z = \alpha\chi^2$ and α is the reciprocal of the semimajor axis of the transfer trajectory and Δt is the transfer time-of-flight. $S(z)$ *and* $C(z)$ are Stumpff functions. h is the specific angular momentum of the associated transfer trajectory. Upon equating

and simplifying (3.21) and (3.25), a relation between Δt and $\Delta\theta$ can be obtained as

$$\sqrt{\mu}\Delta t = \chi^3 S(z) + A\chi\sqrt{C(z)} \tag{3.28}$$

$$A = \sin\Delta\theta\sqrt{\frac{r_1 r_2}{1-\cos\Delta\theta}} \tag{3.29}$$

Simplifying the Eq. (3.28) further, we can write

$$\sqrt{\mu}\Delta t = \left[\frac{y(z)}{C(z)}\right]^{3/2} S(z) + A\sqrt{y(z)} \tag{3.30}$$

$$y(z) = r_1 + r_2 + A\frac{zS(z)-1}{\sqrt{C(z)}} \tag{3.31}$$

Equation (3.30) can be used to solve for z using Newton's method iteratively by making use of the following equation

$$z_{i+1} = z_i - \frac{F(z_i)}{F'(z_i)} \tag{3.32}$$

where $F(z_i)$ and $F'(z_i)$, in simplified form, are defined as follows

$$F(z) = \left[\frac{y(z)}{C(z)}\right]^{3/2} S(z) + A\sqrt{y(z)} - \sqrt{\mu}\Delta t \tag{3.33}$$

$$F'(z_i) = \left[\frac{y(z)}{C(z)}\right]^{3/2}\left\{\frac{1}{2z}\left[C(z) - \frac{3S(z)}{2C(z)}\right] + \frac{3S(z)^2}{4C(z)}\right\} + \frac{A}{8}\left[3\frac{S(z)}{C(z)}\sqrt{y(z)} + A\sqrt{\frac{C(z)}{y(z)}}\right] \qquad (z \neq 0) \tag{3.34}$$

$$F'(z_i) = \frac{\sqrt{2}}{40}y(0)^{3/2} + \frac{A}{8}\left[\sqrt{y(0)} + A\sqrt{\frac{1}{2y(0)}}\right] \qquad (z = 0) \tag{3.35}$$

The z obtained from the Newton's method is then substituted in to the Lagrange

coefficients to obtain the values of $f, g, \dot{f}$ *and* $\dot{g}$. For this, one last simplification is performed on the Eq. (3.30) such that the Lagrange coefficients are dependent on $y(z)$ and Stumpff functions $S(z)$ and $C(z)$.

$$f = 1 - \frac{y(z)}{r_1} \tag{3.36}$$

$$g = A\sqrt{\frac{y(z)}{\mu}} \tag{3.37}$$

$$\dot{f} = \frac{\sqrt{\mu}}{r_1 r_2}\sqrt{\frac{y(z)}{C(z)}}\Big[zS(z) - 1\Big] \tag{3.38}$$

$$\dot{g} = 1 - \frac{y(z)}{r_2} \tag{3.39}$$

The values of the initial and final velocities on the transfer trajectory are obtained as,

$$\vec{v}_1 = \frac{1}{g}(\vec{r}_2 - f\vec{r}_1) \tag{3.40}$$

$$\vec{v}_2 = \frac{1}{g}(\dot{g}\vec{r}_2 - \vec{r}_1) \tag{3.41}$$

Finally, to be able to use this method, the procedure requires the transfer time between the two radii. This is obtained from the methodology described in the Prussing and Conway [31] for the minimum energy transfer.

Let the two position vectors $\vec{r}_1$ and $\vec{r}_2$ be joined by a chord c. These three lines then form a triangle. It is found that for a minimum energy transfer, the semimajor axis is given as

$$a_m = \frac{s}{2} \tag{3.42}$$

$$s = \frac{r_1 + r_2 + c}{2} \tag{3.43}$$

where, a_m is the semimajor axis associated with the minimum energy transfer trajectory. s is the semiperimeter of the triangle which can be obtained by applying

the law of cosines using $\Delta\theta$ as the angle between the radii. Then, the minimum energy time-of-flight is obtained from

$$\sqrt{\mu}t_m = \left[\frac{s^3}{8}\right]^{1/2} (\pi - \beta_m + \sin\beta_m) \tag{3.44}$$

where β_m for the minimum energy transfer is obtained from

$$\sin(\beta_m/2) = \left[\frac{s-c}{s}\right]^{1/2} \tag{3.45}$$

The time-of-flight, t_m obtained from this method is used as the desired time of flight from the manifold to the LEO. Since the objective is to obtain the lowest ΔV, this choice for the time-of-flight seems reasonable.

Now that the description of the problem and the various individual methods to be used have been completely defined, the results obtained by employing the above mentioned methodology will be presented next, followed by the discussions and concluding remarks in Chapter 5.

Chapter 4
Methodology and Results

Having described the various techniques and procedures to be followed for the treatment of orbits, the procedures are now used for the desired orbit. The methodology to be followed is showcased in detail and the results of each of the previous steps are presented. The first step in finding valid solutions to the desired problem is to validate the procedures and algorithms developed for this thesis. For the work presented in this chapter, initially, it is attempted to recreate the results of the work presented by Abraham et al. [1], [2]. The idea is to use the same initial conditions to create the manifold as close as possible to the one used by Abraham [1] and obtain an optimized trajectory for the same transfer using the techniques developed in this thesis. Abraham et al. used a single shooting differential corrections solver to optimize a transfer from an initial LEO to a desired LPO using the invariant manifold and particle swarm optimization. The mission profile in [1] are the same as the one presented in reference [2], the latter also uses low-thrust model to find the optimal low-thrust trajectory along with a PSO/single shooting technique.

4.1 Validation

The initial conditions used by Abraham et al. were found to be non-periodic, possibly due to numerical error and had to be corrected through differential corrections algorithm. For this purpose, the x-z plane intersection was first obtained by integrating the initial conditions used by Abraham et al. (column 2 in Table 4.1) backwards in time to obtain the state vector at positive z intersection (column 3 in Table 4.1). The conditions so obtained were corrected using the differential

corrections algorithm as discussed previously and are presented in column 4 in Table 4.1.

Table 4.1. Initial Conditions for the Validation Orbit ($\mu = 0.012150515$)

States	Initial Condition	Initial x-z State	Corrected x-z State
x (DU)	0.86622405	0.86589479	0.86589479
y (DU)	0.01167019	-7.58941520e-19	0
z (DU)	0.18691218	0.18742934	0.18740607
$\dot{x}$ (DU/TU)	0.01387055	2.16420739e-06	0
$\dot{y}$ (DU/TU)	0.24527016	0.24633128	0.24632922
$\dot{z}$ (DU/TU)	-0.02179277	-2.54628854e-06	0

The period for the initial orbit as given in reference [2] is $P = 2.31339$ [TU].The y-coordinate, $\dot{x}$-coordinate and the $\dot{z}$-coordinate of the corrected state was considered as zero due to their small magnitudes. The algorithm took only two iterations to reach the final state with a period of $T = 2.313613$. The difference in the initial and final states after the correction was of the order 10^{-8} or smaller. The resulting orbit is shown in Figure 4.1.

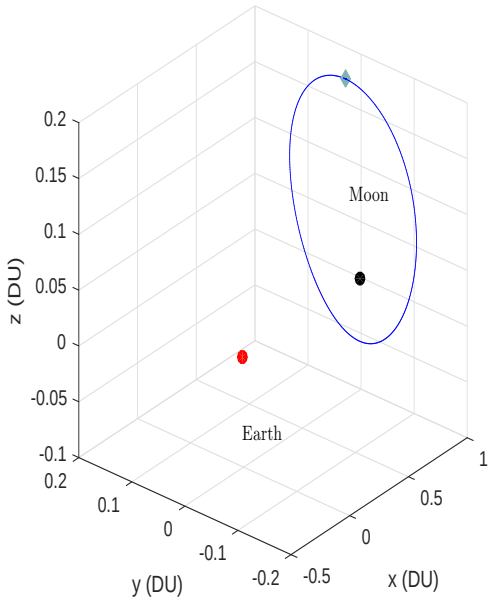

Figure 4.1. Initial Orbit used for Validation in canonical units

Finally, as a last step, the initial conditions so obtained were integrated and the point on this corrected orbit, which was closest to the initial point presented by Abraham is shown in Table 4.2.

Table 4.2. Corrected Initial Conditions for L_1 Halo orbit used by Abraham

States	**Initial Conditions**
x (DU)	0.866224082613834
y (DU)	0.0116722218230222
z (DU)	0.186888845428483
$\dot{x}$ (DU/TU)	0.0138714392076127
$\dot{y}$ (DU/TU)	0.245267826404146
$\dot{z}$ (DU/TU)	-0.0217942137764217

Now that the initial conditions are established, the next step is the generation of manifolds. The stable manifold of the orbit is shown in Figure 4.2. The number of desired trajectories for the manifold is $N = 791$. The author has recreated the orbit and manifold used in [1] with a similar color scheme.

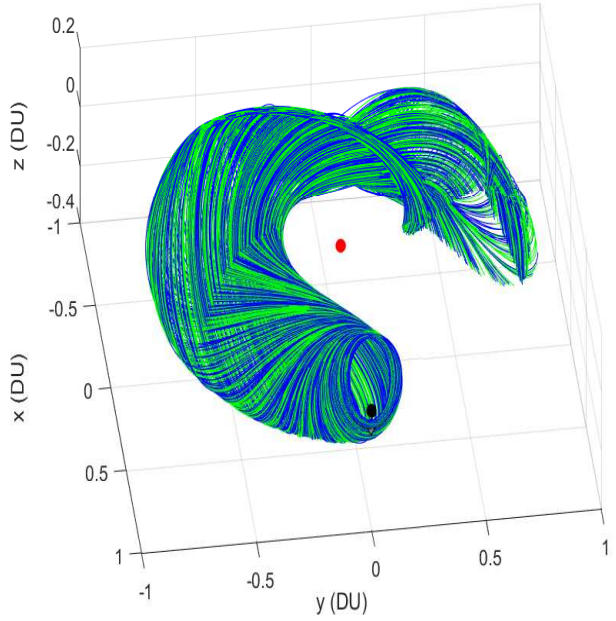

Figure 4.2. Manifold of the LPO as used in [1]

Having obtained the manifold, the PSO algorithm along with the Lambert's solver were used to optimize the slow and fast transfers to the LPO. While the initial orbit (LEO) used in [2] was defined based on the radius and inclination, the solver used in this thesis requires the state vector at the final condition. For this reason, a specific final point on orbit was defined. This was done using the six classical orbital elements. The final orbit used by Abraham ensured a circular orbit based on the terminating condition when shooting to achieve the required initial orbit from the manifold. Similarly, the final state vector used for the Lambert's solver assumed a circular orbit with a radius of 400 km, the right ascension Ω, argument of perigee ω, and eccentricity e were taken to be zero at the final state. The transfers in [2] were optimized for two cases, one for inclination, $i_{LEO} = 28°$ and one for any inclination. For the Lambert's solver, the cases with $i_{LEO} = 28°$ and $i_{LEO} = 0°$ were optimized for minimum ΔV. Since an inclination change is one of the most expensive maneuvers, an $i_{LEO} = 0°$ was selected in hopes to achieve the lowest ΔV to closely represent the any inclination scenario used by Abraham. Finally, for the single shooting method used by Abraham, the true anomaly, θ_{LEO}, at the point of insertion into the LEO ('departure' since the objective is to transfer from LEO to LPO) was not a concern since the method automatically finds the

best point of insertion based on least ΔV. However, for the Lambert's solver used in this thesis, the true anomaly of the desired LEO orbit had to be provided as it would rigidly enforce the final radius vector and its spacial location with respect to the primaries. For this reason, multiple trials were conducted to obtain the true anomaly that gave the lowest ΔV for a particular transfer. The two kinds of transfers as defined by Abraham [1] are as follows.

- **Slow Transfer**: The search space for this transfer ranges from the L_1 Lagrange point until the end of the trajectory at the y-z axis crossing crossing from the negative side, i.e. when the x-coordinate changes from negative to positive. This transfer involves a longer coast time on the manifold, as the spacecraft is allowed to jump on to the manifold near the Earth.

- **Fast Transfer**: This transfer requires the spacecraft to travel directly to the LPO and jump on to the manifold in the vicinity of the LPO. For this, the allowable search space for the PSO algorithm is the trajectory segments between the initial point of the trajectory ($t = 0$) *on* the LPO and the L_1 Lagrange point.

It was observed that for the slow transfer, a true anomaly, $\theta_{LEO} = 0^\circ$ gave the most suitable result in comparison to that by Abraham and for the fast transfer, $\theta_{LEO} = 180^\circ$ resulted in the lowest total ΔV cost. A comparison of the results obtained by the two techniques are presented in the Table 4.3. The results for the single shooting Method (SS) are taken directly from [1].

Table 4.3. Comparison of the Lambert Solver and single shooting Solver

Solver	Type	i (deg)	ΔV_1 (km/s)	ΔV_2 (km/s)	TOF_1 (days)	TOF_2 (days)	ΔV_T (km/s)	TOF_T (days)
SS	Slow	any	3.040	0.507	3.89	150.84	3.548	154.73
Lambert	Slow	0	3.063	0.80	3.60	157.76	3.863	161.37
SS	Slow	28	3.047	0.629	3.76	133.38	3.676	137.14
Lambert	Slow	28	3.12	0.68	3.88	177.28	3.810	181.17
SS	Fast	any	3.070	0.373	4.98	90	3.443	94.98
Lambert	Fast	0	3.097	0.643	4.94	172.55	3.740	177.50
SS	Fast	28	3.069	0.444	4.89	60.94	3.513	65.83
Lambert	Fast	28	3.094	0.405	4.99	173.04	3.499	178.04

Table 4.3 shows that the ΔV for both the slow and fast transfer schemes closely follow that obtained in [2]. The values obtained for $i = 28°$ for both slow and fast solutions of Lambert's method are very close to the values obtained by the single shooting method for the corresponding transfers. The difference is larger between the any inclination scenario for single shooting solver and the $i_{LEO} = 0°$ assumption of the Lambert's Solver as is reasonable since it is not possible to find the most optimal inclination using Lambert's solver without investigating the final orbit condition in small increments of inclination. ΔV_1, which is the energy change required to leave the parking LEO are very close in magnitude in all cases. The ΔV_2, which is the energy change required to insert the spacecraft into the stable manifold has a slightly higher difference. This could be due to the fact that ΔV_2 occurs further away from the Earth as compared to ΔV_1 and the differences between the two-body approximation from the Lambert's Solver and the three-body single shooting solver used by Abraham starts to take effect. Another reason for this difference could be due to the slight differences in the generation of the manifold. In spite of trying to achieve a close approximation of the manifold, it is possible that numerical error, accuracy of the integration, changes in the 'ode113' integration algorithm provided by Mathworks might have contributed to the differences seen above. Differences in the magnitude of initial perturbation used when generating the manifold would have contributed to the difference. Since

integration is performed for long periods of time to obtain the trajectories, small initial differences can cause larger differences in the final location of the optimal point along the trajectory.

The total TOF for both types of transfers have strong differences for the single shooting and the Lambert solver. But, since the majority of the difference is in the time of coast on the manifold, this could be attributed to the fact that a small perturbation at the time of generating the manifold may cause the spacecraft to experience multiple revolutions before leaving the LPO.

Despite the difference in the kinds of systems assumed in each case, i.e. three-body system in single shooting and two-body system in Lambert's Solver, the difference in the magnitudes in the ΔV_T are fairly small. This implies that the two-body assumption in the Earth-Moon system is still valid for preliminary mission planning. The computational time to achieve this result using the Lambert's solver was a fraction of the time required to solve using the single shooting technique. This method, therefore, allows the mission planner to make quick adjustments to the mission profile and study the changes in the overall mission ΔV costs. Additionally, the performance of the optimization algorithm can be studied by making adjustments to the particle swarm algorithm and studying the results can be without being prohibited by the computation time requirements.

The solutions from Lambert's method resulted in significant time savings compared to the single shooting method. Since the Lambert's method doesn't require any numerical integrations, the solutions so obtained are very quick. On average, a single case ran for 30 seconds. This value varied in case when the maximum number of iterations were changed or when the number of particles were changed. Therefore, there was approximately 1400 fold decrease in time required to solve for the lowest ΔV transfer which is a reduction by 3 orders of magnitude compared to the single shooting technique. These time savings are significant because it the user to change the parameters of the algorithm and study the variations very quickly. In cases when the mission designer needs to change the number of trajectories in the manifold or change the LPO, the results from these changes can be obtained very quickly allowing the mission designer to explore many mission designs without the computational expense.

An important observation that is made in accordance with the findings of Abraham in [1] is that even with the solutions using the Lambert's solver, the

ΔV_T for fast transfers is less than that for slow transfers. This observation is counterintuitive and lends further credibility to the solutions obtained via this method.

It is important to mention a significant limitation of the Lambert's solver. Since the solver uses mathematical formulas for obtaining the solution, it is subject to singularities that occur when the transfer angle between the initial and final radius vector is 180°. This is depicted in Figure 4.3. It can be clearly seen that the singularity causes the results to vary by a large value and has a potential to give invalid results in the vicinity of 180° *or* 0° transfer angle.

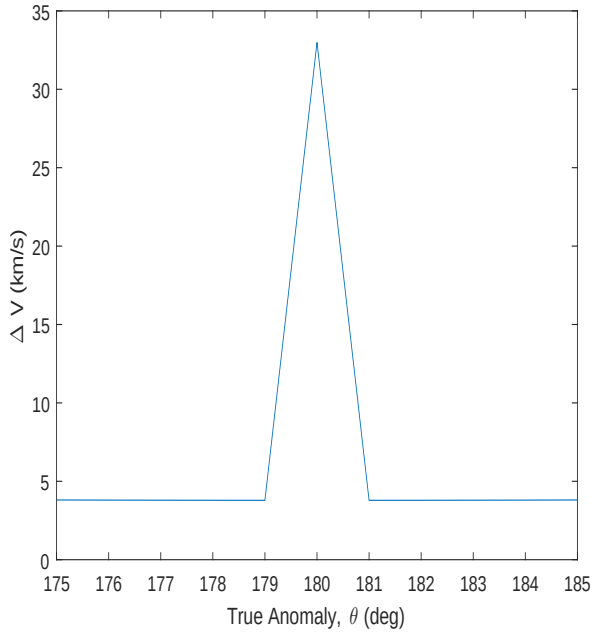

Figure 4.3. Results of transfer from GEO to LEO and singularity at $\theta_{LEO} = 180°$

4.2 Final Orbit

For the remainder of the thesis, an arbitrary circular orbit with the following classical orbital elements was selected as the desired LEO to be achieved.

Table 4.4. Classical Elements for the final LEO

Classical Elements	**Value**
Altitude of Periapse R_p (km)	400
Altitude of Apoapse R_a (km)	400
Eccentricity	0
Argument of periapse ω (deg)	0°
RAAN Ω (deg)	0°

This orbit is similar to that of the International Space Station (ISS) which on 1 August 2016, $17:04:35$[1] was at a perigee altitude of $R_p = 401$ km and apogee altitude of $R_a = 404$ km above the Earth's surface, with an inclination of $i_{ISS} = 51.6417°$, right ascension of $\Omega = 190.8898°$, eccentricity of $e = 0.0001972$ and argument of perigee of $\omega = 85.0276°$. It needs to be stated that the objective here is *not* to rendezvous with the ISS, but instead to simply attain a similar orbit as the final LEO orbit.

The primary reason for this selection is to show ΔV requirements to reach an LEO from the manifold. Selection of an LEO orbit makes sense because for a sample return mission or for a mission where supplies are brought from an asteroid, Sending the supplies to a GEO would be counter productive as to retrieve the payload from a high altitude orbit would effectively negate any cost savings achieved from using the invariant manifolds in the mission design. The reason for selection of an orbit at the same altitude as the ISS is due to the fact that there has a been a constant human presence in the selected orbit and the orbit and its environment are well understood and modeled and hence will eliminate the need for additional mission design associated with the parking orbit. Another reason for selecting a LEO is that it allows for a ballistic descent for example in the case of cargo drop scenario to the Earth's surface further opening up the possibility of saving ΔV costs, which would be almost impossible with a higher orbit within a limited time frame.

[1] http://heavens-above.com/orbit.aspx?satid=25544, 08/1/2016 17:04:35 UTC

4.3 Local PSO

The optimization was performed with 200 particles with a maximum of 30 iterations, using the inertial, social and cognitive constants as mentioned earlier. A local version of the particle swarm optimization algorithm was used to ensure that the algorithm is not stuck in a local minima. Since the local scheme allows each particle a limited view of the swarm, the particle will only recognize the global optimum point achieved by another particle within its field of view. Therefore a convergence criteria of 75% was defined for particles having converged at *their* global optimum and simultaneously being within a predefined radius and cost tolerance.

For the local radius conditions, each particle can observe particles within a '*radius*' of 100 nearby trajectories, 50 trajecrtories in either direction. This implies that for each particle, the global minimum point achieved by *any* another particle *within* 100 trajectories of its current location becomes the global point. The local radius is defined based on the trajectory number *only* and is not restricted by τ, therefore a point located at the beginning of the trajectory near the LPO can view another point at the end of the trajectory near the Earth. So, in this sense, it would be unfair to call it a 'Local' PSO or even a 'radius', but since this is the conventionally accepted terminology [2], the author decided to follow it. Additionally, unlike in [2], the particle is bounded by the trajectory number *only*, hence it would make more sense to call this version of PSO a 'partial' local PSO.

The radius for convergence at the globally optimal point in the vicinity of each particle is arbitrarily defined as being within a physical radius of 0.05 DU which corresponds to a spacial radius of 19220 km with a maximum allowable ΔV cost difference of 10^{-4} km/s. This can be considered as a very strict constraint but the intention of the author behind such a constraint is to allow time for the algorithm to find multiple local minima and then selecting the particle with the lowest cost as the best cost and best location for that iteration. While the algorithm records the globally lowest cost on the search space, the particles themselves are updated based only on the locally available best location.

4.4 Results

Since the objective of this thesis is to find the optimal return trajectories from a LPO, this section presents results for trajectories from the collinear Lagrange points. The particle swarm optimization algorithm was run on multiple LPO about each point. The initial conditions, manifolds and the results are presented in this section.

It was desired to study the variations in the ΔV requirements based on the inclination changes, to that end, inclination was varied from 0° to 90° in 10° increments for transfers from each LPO to observe the ΔV variations. Additionally, due to the restriction imposed on the final orbit conditions by the Lambert's solver, it was decided to present the total ΔV required for multiple true anomaly cases along the final orbit. The true anomaly was varied from 0° to 360° in 15° increments to obtain an understanding of the energy change required along an orbit. Finally, to obtain closest solution to an optimal point on the manifold, each true anomaly case was solved for five trials and then the best solutions were presented.

Since the solutions using Lambert's method did not require integration, the results obtained using this method was very quick. The solutions for a single true anomaly case usually took about a minute to complete. This value changed when the number of particles, maximum number of iterations or the convergence criterion was changed. To obtain the final results, the solutions were run for all the mentioned true anomaly cases with 5 trials for each case, then the solution with the lowest ΔV was selected as the final solution for that true anomaly.

4.4.1 L_1 Halo Orbit

The initial conditions for this halo orbit were obtained from reference [19] and then corrected to ensure that the orbit was periodic. The corrected initial conditions in canonical units are found in Table 4.5 with a period, $T = 2.721490$ [TU].

Table 4.5. L_1 Halo Orbit Initial Conditions, ($\mu = 0.01215051$)

States	Initial Conditions
x (DU)	0.8389
y (DU)	0
z (DU)	0.15437599
$\dot{x}$ (DU/TU)	0
$\dot{y}$ (DU/TU)	0.25985324
$\dot{z}$ (DU/TU)	0

The orbit is shown in Figure 4.4 and the associated manifold is shown in Figure 4.5 with 800 trajectories.

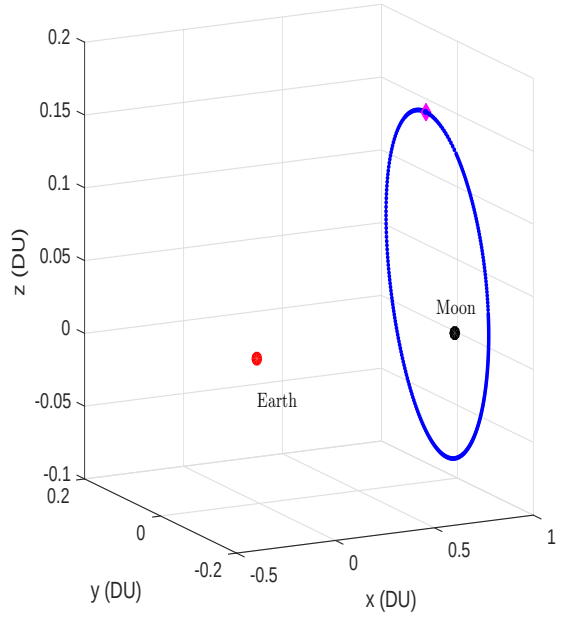

Figure 4.4. L_1 Halo Orbit

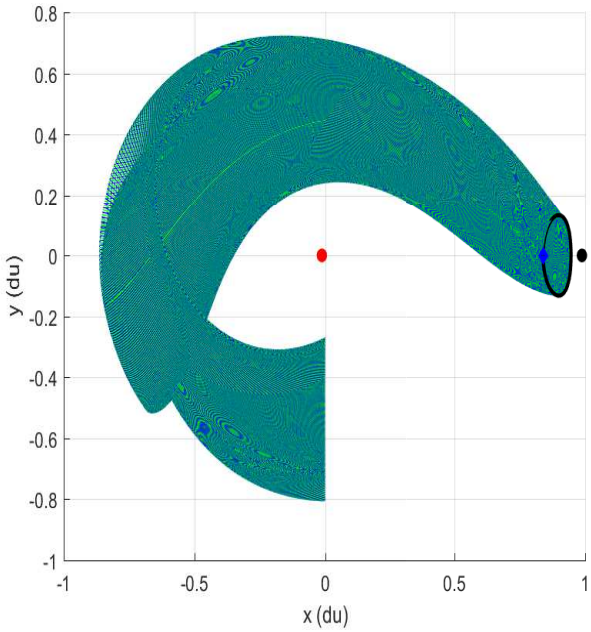

Figure 4.5. Manifold of the L_1 Halo LPO

Figure 4.6 shows the total ΔV for the selected orbit in 10° increments of the inclination of the final orbit. The data used to create this plot is presented in the Appendix A.1. It can be seen in Figure 4.6 that the ΔV_T for $\theta_{LEO} = 90°$ and $\theta_{LEO} = 270°$ increases as the inclination is increased. This is easy to understand as a true anomaly of 90° or 270° corresponds to the point on the final orbit at the extremum of z-component for the orbit and plane change at these locations are known to be very expensive. Whereas, $\theta_{LEO} = 0°$ and $\theta_{LEO} = 180°$ corresponds to the point at the intersection of the orbit and the apse line. A plane change at this location results in least ΔV. In spite of changing the inclination of the final orbit, the ΔV_T requirements for $\theta_{LEO} = 0°$ and $\theta_{LEO} = 180°$ remain confined to a small range suggesting that it is possible to achieve any inclination LEO due to the natural flow of trajectories on the manifold. Such a case will be helpful in case it is required to rendezvous with a spacecraft in the final LEO, then the mission can be planned such that the time of arrival of the spacecraft from the manifold and the location of in-orbit spacecraft is synchronized. This will reduce the ΔV requirements for such a maneuver.

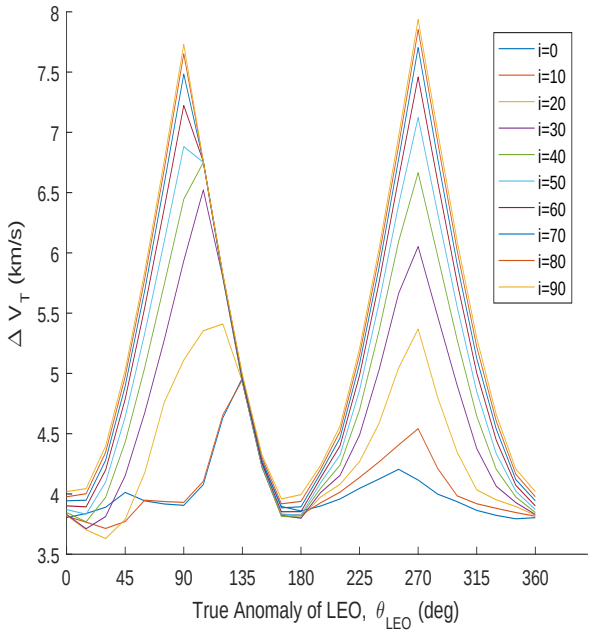

Figure 4.6. Variation of Transfer Costs for L_1 Halo LPO with True Anomaly

Additionally, if it is required to descend on to the surface of the Earth in a particular location (for example to drop cargo) which might exist at inclination with respect to the equator, it might be possible to reach such location when returning from a manifold since it is possible to achieve LEOs of different inclinations. Similar trends were seen for different halo orbits around the L_1 Lagrange point.

It remains to be seen whether this trend also holds for trajectories going towards LPOs using a stable manifold. Since it follows a similar analysis and due to the symmetry of the manifold in the CR3BP system, it may be possible to launch a spacecraft from an LEO towards a manifold patch point with any inclination. This will result in saving ΔV, as the spacecraft need not be brought to a 0° inclination before launching the spacecraft toward the manifold. This will also relax the requirement on the location of the launch site. It may also be possible to design trajectories to and from manifolds with launch site being at different latitudes without incurring huge ΔV cost. However, since sites at higher latitudes fail to make full use of the rotational velocity of the Earth, it is hard to say how this will impact actual mission feasibility while traveling from the Earth to an LPO without detailed analysis of mission requirements and constraints.

4.4.2 L_1 Lyapunov Orbit

The results for a Lyapunov orbit about the L_1 Lagrange point are presented in this subsection. It is desired to study the changes in the ΔV requirements based on the changes in the trajectories originating from an initial LPO. These results help develop reasoning for the selection of the type of initial LPO for a mission designed to return to the Earth using the invariant manifolds. The initial conditions for the selected orbit are taken from reference [19] and the same methodology is followed to first correct the initial conditions, generate the unstable manifolds and finally generate the results for a two-impulse transfer to a LEO. The corrected conditions are given in Table 4.6 with a time period of $T = 2.794929$ TU.

Table 4.6. L_1 Lyapunov Orbit Initial Conditions, ($\mu = 0.01215051$)

States	**Initial Conditions**
x (DU)	0.81892874
y (DU)	0
z (DU)	0
$\dot{x}$ (DU/TU)	0
$\dot{y}$ (DU/TU)	0.17422664
$\dot{z}$ (DU/TU)	0

The orbit and the associated manifold are shown in Figures 4.7 and 4.8, respectively. The number of trajectories generated in the manifold are 800.

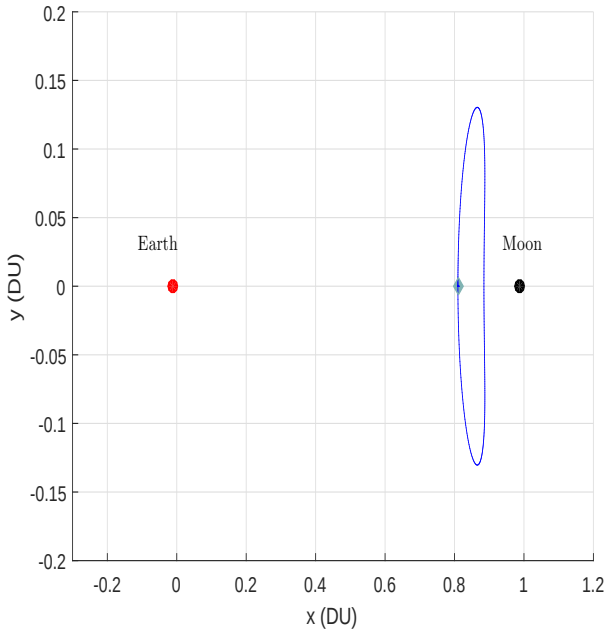

Figure 4.7. L_1 Lyapunov Orbit

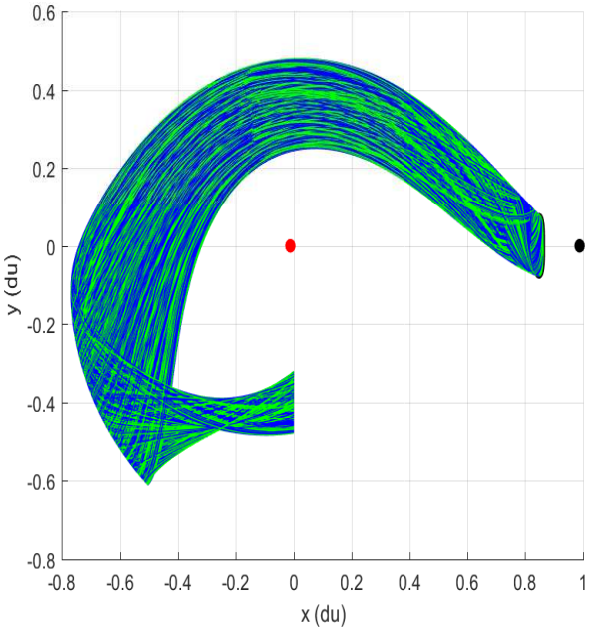

Figure 4.8. Manifold of the L_1 Halo LPO

The manifold shown in Figure 4.8 clearly shows trajectories originating close

to the Moon (represented by a black dot) and terminating at the intersection of the trajectories with the y-z plane from the negative x-direction. It can be clearly seen that none of the trajectories approach a LEO and hence, as in the case of a halo orbit, the objective is to find the best possible location from the best possible trajectory that minimizes the total ΔV cost to achieve the desired LEO. It is noted that in this entire analysis, only trajectories flowing towards the Earth were analyzed. Trajectories that approach the smaller primary (i.e. on the interior manifold), in this case the Moon, tend to interact with the Moon in complicated ways, at times even going through the surface of the Moon since the primaries are modeled as a point mass. Such trajectories further complicate the analysis and have been excluded from the analysis for convenience. Furthermore, all the transfers originate outside the SOI of the Moon to reduce deviation in the final result due to lunar gravitational influence. The results of the Lambert's solution for a Lyapunov orbit about the L_1 Lagrange point in the Earth-Moon system are summarized in the tables in the Appendix A.2 and are plotted in Figure 4.9 for convenience.

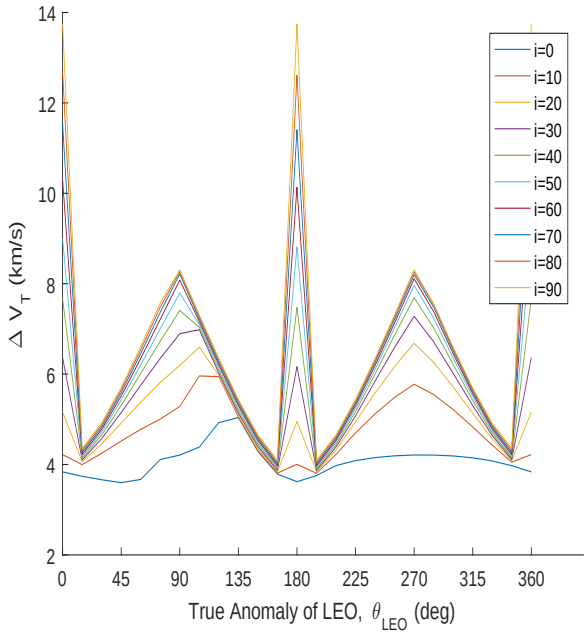

Figure 4.9. Variation of Transfer Costs for L_1 Lyapunov LPO with True Anomaly

Since the Lyapunov orbit lies entirely in the x-y plane, the manifold as well remains confined to the plane. The results obtained for a Lyapunov seems to differ

drastically at the first glance due to the large peaks in the final plot. However, closer inspection shows that the peaks are due to a singularity experienced at 0 (*or* 360)° and 180°. Repeating the analysis in the vicinity of the $\theta_{LEO} = 180°$ shows that the peak is obtained at exactly 180°. The results for this are presented in Figure 4.10. Therefore, if the peaks are ignored, then the results seem similar to the ones obtained for the halo orbit. Here, too, the maximum ΔV is required at points close to $\theta_{LEO} = 90°$ *and* 270°. The is obtained primarily due to the selected final orbit. It was found that changing the argument of periapse for the final LEO changes the true anomalies for which the peaks occur irrespective of the type of LPO orbit.

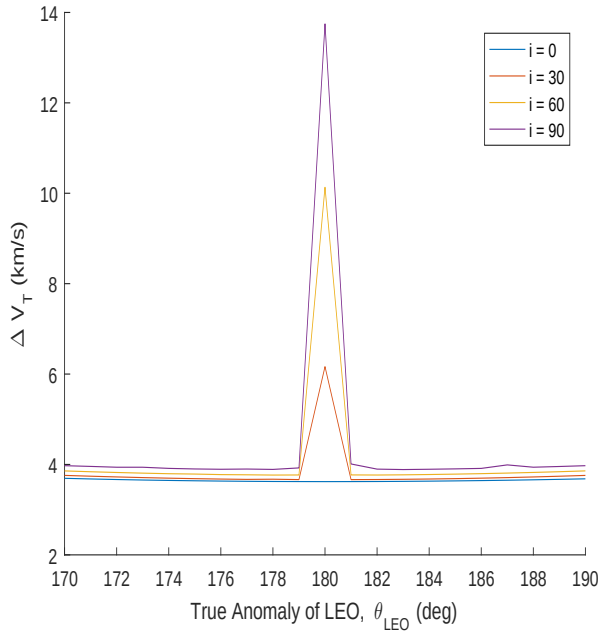

Figure 4.10. Variation of Transfer Costs for L_1 Lyapunov LPO near $\theta_{LEO} = 180°$

In both halo and Lyapunov orbits, the initial ΔV on the manifold departure point is minimal, but to achieve the desired inclination of the LEO, the final ΔV at the LEO includes the plane change maneuvers as well. This increases the ΔV requirements as plane change maneuvers are very costly in terms of ΔV requirements. An important conclusion from the obtained results is that it is more ΔV efficient to aim for LEO insertion points at the intersection of the apse line with the orbit i.e. points where the spacecraft changes the z-axis sign (ascending or

descending node). Finally, to ensure least ΔV requirement, it is desired to insert into a 0° inclination LEO with the insertion points being at various locations around the orbit. The geometry of the manifold will determine the ΔV trend in this case since RAAN, Ω, is undefined and hence there is no ascending or descending node in this case.

Untill now, the analysis was confined to orbits around the L_1 Lagrange point. It is desired to investigate ΔV requirements when the initial LPO is around a different Lagrange point. The following subsections present transfers from L_2 halo and Lyapunov orbits.

4.4.3 L_2 Halo Orbit

To develop a more detailed understanding of the transfers in the CR3BP system, focus now shifts to the L_2 Lagrange point. The analysis now becomes slightly more complicated as the LPO will now lie further away from Earth. Additionally, care must be taken in selecting the manifold about which the analysis is performed. As noted earlier in Section 4.4.2, trajectories traveling directly towards the Earth will now encounter the Moon first. The trajectories on the interior manifold are created as a result of complicated interaction with the Moon's gravitational field and therefore cannot be relied upon for reasons mentioned earlier. For this reason, again, we focus on the exterior manifold as initially flow away from the Earth but eventually circle back and travel towards the Earth albeit after a long time. As was the case with previous orbits, the initial conditions taken from reference [19] are first corrected, manifolds are generated for 800 trajectories and then the analysis is performed and the resulting tables are presented in Appendix B.1. The corrected initial conditions for this orbit are given in Table 4.7 with a time period of $T = 3.409809$ TU.

Table 4.7. L_2 Halo Orbit Initial Conditions, ($\mu = 0.01215051$)

States	**Initial Conditions**
x (DU)	1.1802
y (DU)	0
z (DU)	0.02642143
$\dot{x}$ (DU/TU)	0
$\dot{y}$ (DU/TU)	-0.15977637
$\dot{z}$ (DU/TU)	0

The orbit is shown in Figure 4.11. The exterior manifold is shown in Figure 4.12. It can be seen that the trajectories initially flow away from the Earth but finally terminate closer towards the Earth upon intersection with the y-z plane. The integration times to generate these manifolds were longer to allow the trajectories to terminate at the y-z plane. It can seen in the Figure 4.12 that the trajectories are further away from the Earth and they do not approach the Earth or Earth orbits directly.

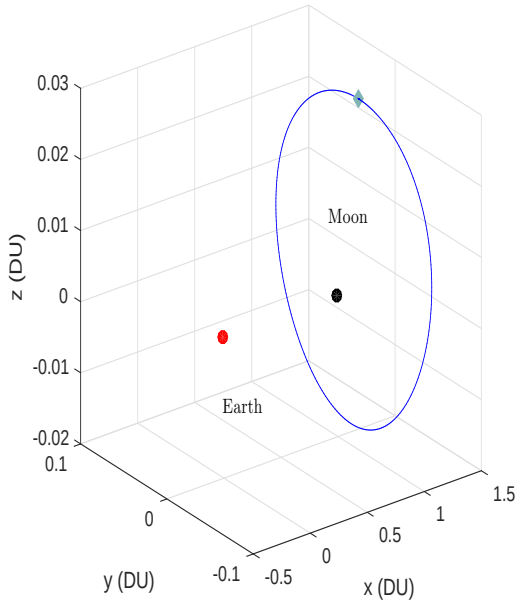

Figure 4.11. L_2 Halo Orbit

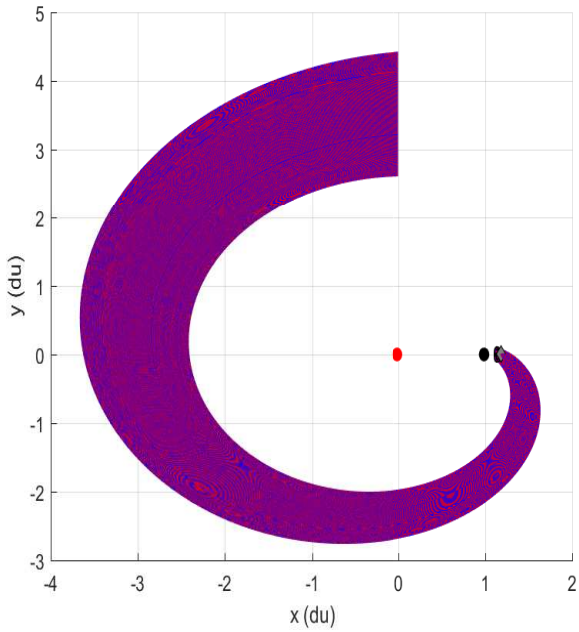

Figure 4.12. Manifold of the L_2 Halo LPO

The results of the Lambert's Solution for a Halo orbit about the L_2 Lagrange point in the Earth-Moon system are summarized in Figure 4.13

Figure 4.13 shows that the trends for ΔV follow the ones obtained for L_1 halo orbit. They are largely a function of the desired final location on the LEO rather than the inclination. For each inclination, there exists points on the manifold that allows ΔV_T in similar range. Minimum ΔV_T can be achieved at $\theta_{LEO} = 0°$. Since the shape of the manifold is such that it flows around the Earth and is not confined to the x-y plane, there exists points on the manifold that allow least ΔV for any inclination. Hence when returning to LEO from an Earth-Moon LPO, it is possible to attain almost any desirable inclination since ΔV_T is not a constraint.

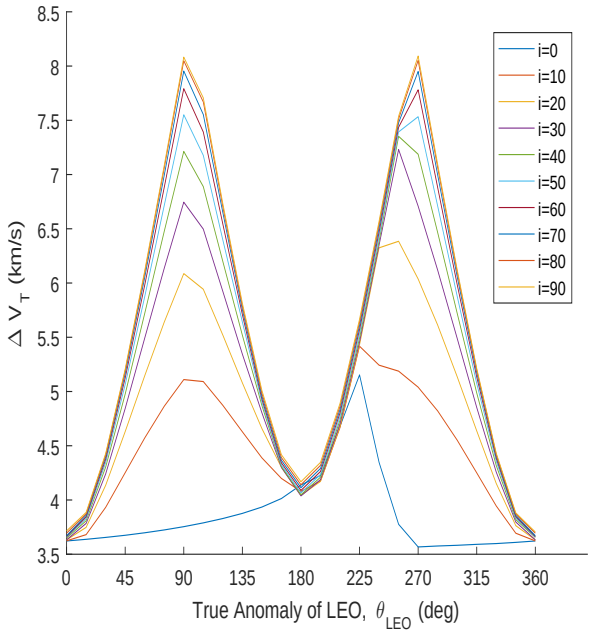

Figure 4.13. Variation of Transfer Costs for L_2 Halo LPO with True Anomaly

It is possible that this behavior is common among manifold going towards the larger primary irrespective of the three-body system under study. Similar studies can by conducted for different systems where the two-body assumption is valid such as Jupiter's system with its natural satellites.

4.4.4 L_2 Lyapunov Orbit

This section presents the results of the transfers from the manifold of an L_2 Lyapunov orbit. The analysis is presented to study if the results observed earlier follow a trend. The initial condition for the selected orbit is taken from reference [19] and then corrected to obtain a closed orbit. For reasons mentioned earlier in subsection 4.4.3, the exterior manifold is selected. The initial conditions, the orbit and the manifold are presented in Table 4.8, Figures 4.14 and 4.15.

Table 4.8. L_2 Lyapunov Orbit Initial Conditions, ($\mu = 0.01215051$)

States	**Initial Conditions**
x (DU)	1.17628287
y (DU)	0
z (DU)	0
$\dot{x}$ (DU/TU)	0
$\dot{y}$ (DU/TU)	-0.12341633
$\dot{z}$ (DU/TU)	0

For this orbit, the time period is $T = 3.398196$ TU. The orbit is shown in the Figure 4.14 and the corresponding manifold can be seen in Figure 4.15.

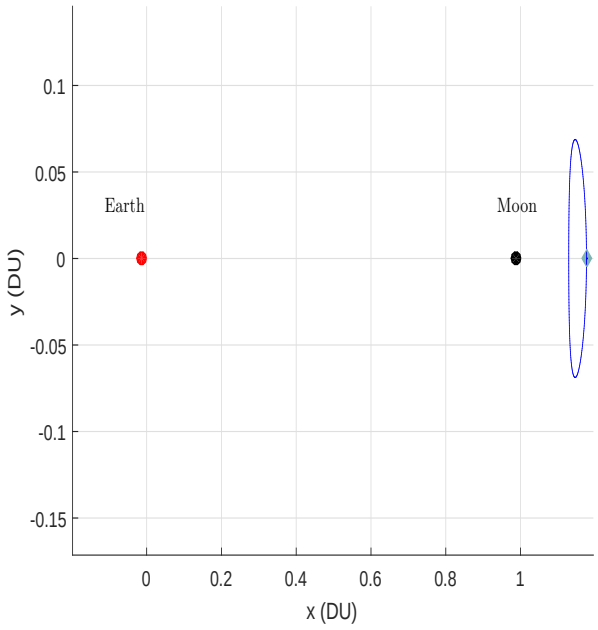

Figure 4.14. L_2 Lyapunov Orbit

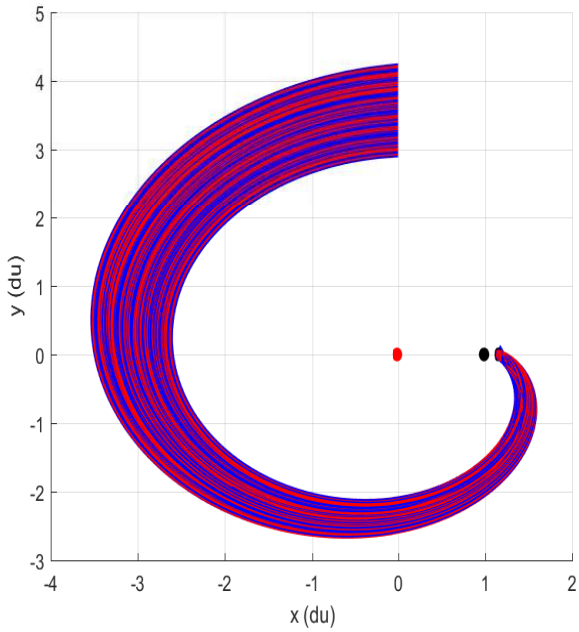

Figure 4.15. Manifold of the L_2 Lyapunov LPO

The results of the Lambert's Solution for the Lyapunov orbit about the L_2 Lagrange point in the Earth-Moon system are summarized in Figure 4.16.

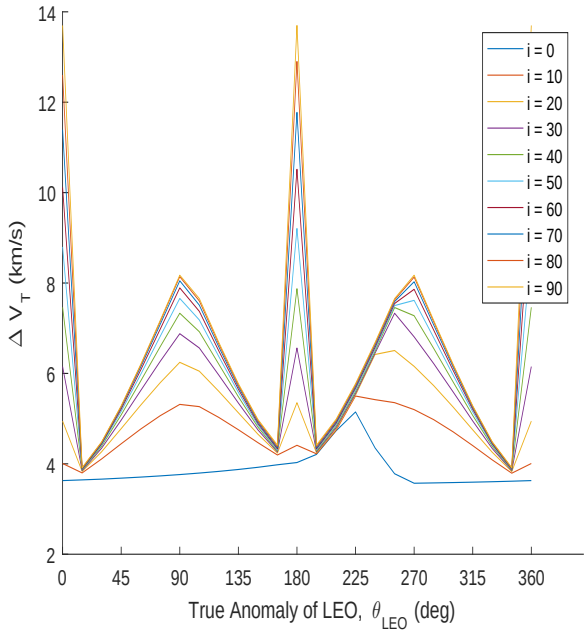

Figure 4.16. Variation of Transfer Costs for L_2 Lyapunov LPO with True Anomaly

The peaks at $\theta_{LEO} = 0°$ *and* 180° are clearly seen in the Figure 4.16. As was the case in the previous result with the Lyapunov orbits, here too the peaks are localized near two specific points. Figure 4.17 provides a closer look at the peaks near the $\theta_{LEO} = 180°$. Similar to the previous case, the values jump considerably at 180° suggesting an anomaly caused due to the geometries of the position vectors used by the Lambert's solver.

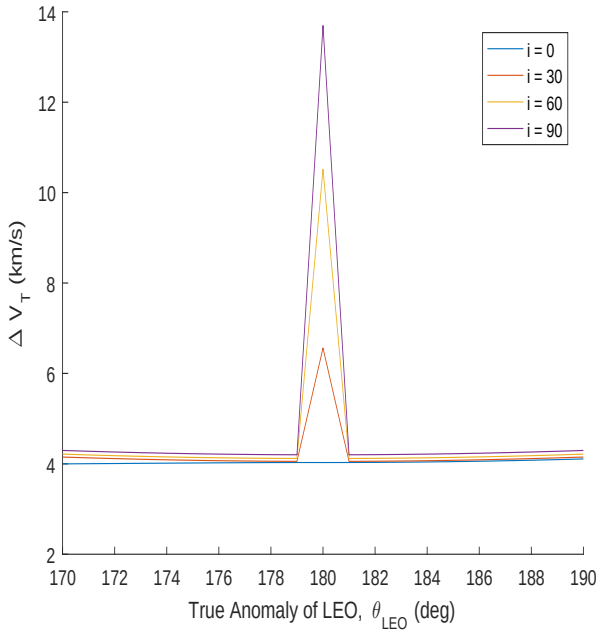

Figure 4.17. Variation of Transfer Costs for L_2 Lyapunov LPO near $\theta_{LEO} = 180°$

Since these peaks are not observed for halo orbits about either of the two Lagrange points under consideration, it seems that the geometries of the position vectors of the particle and the insertion point on the LEO may be causing mathematical anomalies. To better understand these, the same analysis was again conducted on a different final orbit arbitrarily defined.

4.5 Variation with Final Orbit

It was desired to check the variation of the results with a change in the final orbit. This was done primarily to check if the orbit geometries had a role to play in the results. An arbitrary elliptical orbit was defined with the parameters given in Table 4.9.

Table 4.9. Classical Elements for an Arbitrary elliptic LEO

Classical Elements	**Value**
Altitude of Periapse R_p (km)	400
Altitude of Apoapse R_a (km)	500
Eccentricity	0.0073
Argument of periapse ω (deg)	20°
RAAN Ω (deg)	40°

The results for the same Lagrange point orbits as used before are presented in this section. The results are generated for 15° increments of the true anomaly and for inclinations of $0°\,, 20°\,, 40°\,, 60°\,, 80°$ *and* $90°$. Just as in earlier cases, the results are summarized in the from of a plot. For convenience, the tables for the solutions are not included.

Figure 4.18 shows the ΔV costs for the L_1 halo LPO using the classical elements from Table 4.9 for the final LEO orbit.

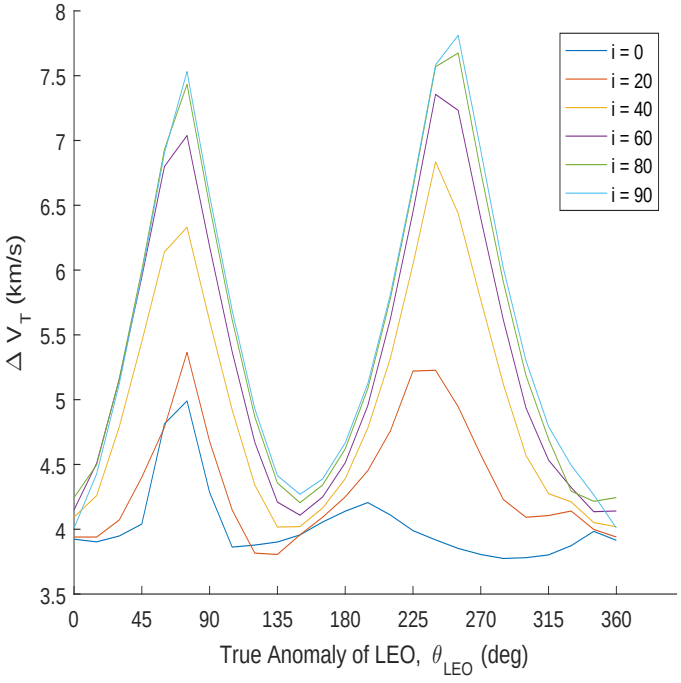

Figure 4.18. Transfer Costs for L_1 halo LPO for elliptic LEO

The results shown in Figure 4.18 are similar to the ones obtained previously

however, there is a shift in the location of the peaks corresponding to the maximum and minimum z-coordinate along the orbit. The troughs are the point corresponding to the ascending and descending nodes. These seem to occur at approximately 160° and 340°. This result again suggests that there are two locations along the orbit where it is possible to insert a spacecraft into an orbit of any inclination with modest increment in ΔV. There is a general increase in the ΔV requirements as the inclination is increased.

Figure 4.19 shows the ΔV costs for the L_1 Lyapunov LPO using the classical elements from Table 4.9 for the final LEO orbit.

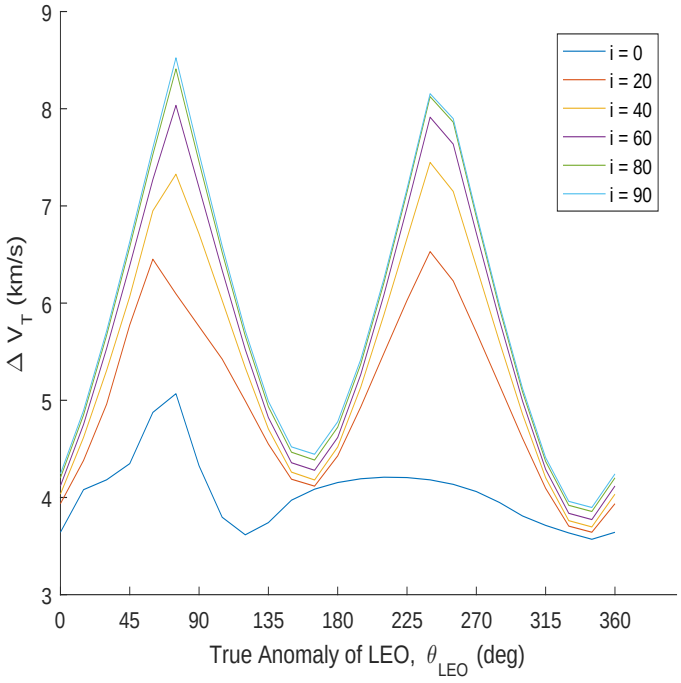

Figure 4.19. Transfer Costs for L_1 Lyapunov LPO for elliptic LPO

The result in Figure 4.19 is slightly different from the one presented in Figure 4.9. The first observation is that unlike the previous case, there are no singularity peaks in the solution. This lends credibility to the assumption that the peaks are caused due the geometry of the selected final orbit. The results show two peaks that correspond to points at the extreme ends with maximum z-component. This result also shows two troughs what corresponds to the ascending and descending nodes. The results seem to follow the results of the halo orbit and seem to suggest that it may be possible to reach final orbits of different inclinations.

Figure 4.20 shows the ΔV costs for the L_2 halo LPO using the classical elements from Table 4.9 for the final LEO orbit.

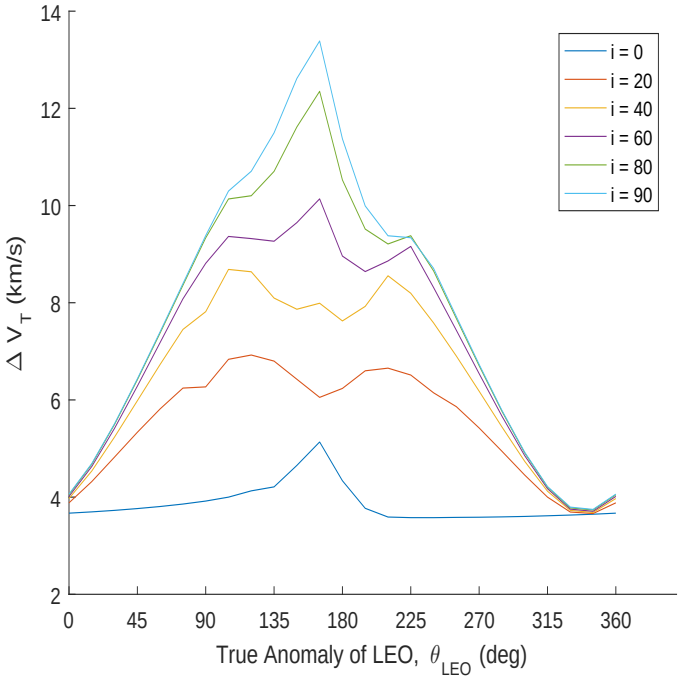

Figure 4.20. Transfer Costs for L_2 Halo LPO for elliptic LEO

The results in Figure 4.20 are quite different than the ones shown in Figure 4.13. There seems to be a gradual increase in the ΔV requirements along the orbit. While the values of ΔV seem to be large, they do not seem to be a result of a singularity. Also, there seems to be a region along the final orbit where it may be possible to achieve an LEO of various inclinations. The locations of the minimum ΔV insertion points seem to be highly sensitive to the type of LEO being achieved.

Figure 4.21 shows the ΔV costs for the L_2 Lyapunov LPO using the classical elements from Table 4.9 for the final LEO orbit.

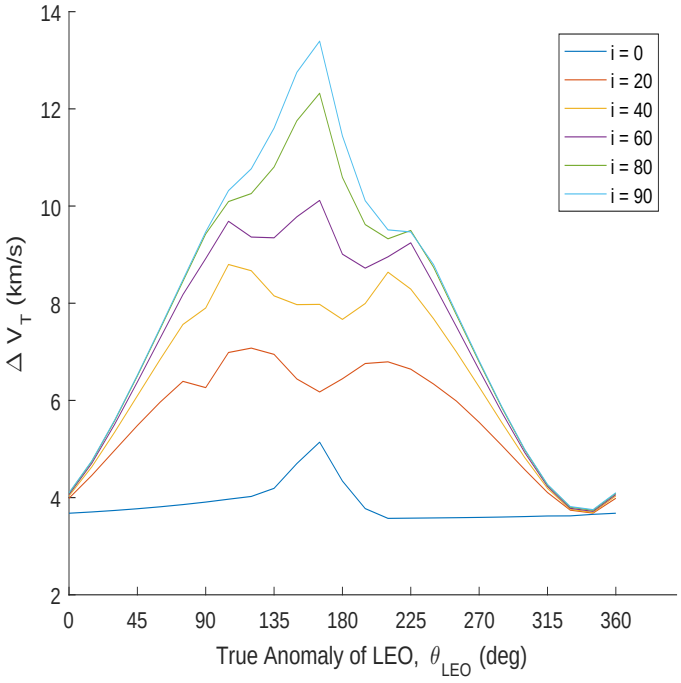

Figure 4.21. Transfer Costs for L_2 Lyapunov LPO for elliptic LEO

The results in Figure 4.21 follow the results in Figure 4.20 closely. Unlike the case with L_1 Lyapunov orbit in Figure 4.16, the variation in ΔV requirements with inclination follows a very different trend. This suggest that the kind of orbit does not dictate the cost of transfer. Instead, it seems that Lagrange points and the direction of their associated manifolds contribute to the final solution along with the selection of the final LEO.

The results seem very sensitive to the type of manifold being used as well as the type of orbit to be achieved. It seems reasonable that such dependence exists, as the energy requirements and the direction of flow of trajectories on the manifold would intuitively have an influence on the ΔV required for transfers. Multiple iterations need to be performed to be able to establish with confidence the least ΔV consumption as that would require the mission designer to check various combinations of the Lagrange point and the final orbit conditions. Hence while this method is capable of doing quick analysis of the search space, it needs to be combined with other techniques to provide complete solutions.

The next chapter will summarize the results and draw conclusions from the analysis that is performed. Additionally, the future scope of work will be established that will serve as a natural extension of the current work.

Chapter 5
Summary, Conclusions and Future Work

This chapter focuses on summarizing the results obtained in Chapter 4, the conclusion that can be drawn from them and the ways the current analysis can be improved to obtain better more accurate results.

5.1 Summary and Conclusions

In Chapter 4, it was shown that the results of the two-body Lambert's solver approached the ones obtained from the single shooting method used by Abraham [1]. It was seen that despite the two-body assumption used in the Lambert's solver, the results closely matched those obtained by Abraham. The slow and fast transfers were approximated by limiting the search space. To obtain the minimum ΔV, the true anomaly, θ, of the final orbit was changed multiple times to finally obtain $\theta = 0^\circ$ for slow transfers and $\theta = 180^\circ$ for fast transfers. The inclination was adjusted manually and was assumed as $i = 0^\circ$ for the 'any inclination' case as presented in [1]. The transfer time from the LEO to manifold point (recall that the analysis is performed backwards in time from manifold point to LEO for stable manifolds) was assumed as the minimum energy TOF as detailed in Chapter 3.

The results obtained from the Lambert's solver were very quick. The solutions for a single true anomaly took in general less than a minute. Compared to the single shooting algorithm used by Abraham, the computational time is reduced by a factor of approximately 1400 or by 3 orders of magnitude. The time savings are primarily due to the fact that unlike in single shooting, there is no requirement

for integrating the trajectory of the spacecraft from a point on the manifold in Lambert's solver. This allows the Particle Swarm Optimization algorithm to scan the search space very quickly and obtain the transfers with the lowest ΔV. This allows the mission designer the freedom to plan missions from various Lagrange point orbits and make adjustments to suit the requirements.

Additionally, it is possible to conduct detailed analysis based on the results of the Lambert's solution as the ΔV_1 and ΔV_2 vectors are obtained from this method and these can then be used with single shooting methods as the initial guess. Furthermore, it is possible to obtain the coordinates of the particle with the minimum ΔV_T as obtained from the PSO algorithm. Therefore, it is possible to run the single shooting algorithm in a reduced search space to find the closest point to optimum solution. This also results in reduced time as less points need to be tested to find the solution.

Since it was shown that the Lambert solver provides close approximations for the stable manifolds, i.e. for missions leaving Earth and going towards an LPO, it was assumed that the analysis could be reliably extended to missions returning to Earth from LPOs, i.e. unstable manifold due to the symmetry of the manifolds as shown in the Chapter 4. The reason for this is because that the transfers take place in the sphere-of-influence of the Earth. However, the solutions presented in this thesis would need to be confirmed with other methods to be considered valid.

The objective of this thesis is to provide a method to reduce the computational requirement associated with mission design in the Earth-Moon system and to analyze the approximate ΔV_T requirements for Earth return missions from different LPOs and how these vary due to the type and location of the LPOs. The former has been validated using work from the literature, the latter formed the second half of Chapter 4. Analysis was conducted from multiple LPOs of two kinds, three-dimensional halo orbits and two-dimensional Lyapunov orbits. The analysis was restricted to L_1 and L_2 Lagrange points due to difficulties in obtaining the manifolds from the L_3 orbits.

To present a more complete analysis, the true anomaly of the location of the final point on the desired final orbit was varied from $\theta = 0°$ to $\theta = 360°$ in increments of 15°. The inclination of the final orbit was also varied from $i = 0°$ to $i = 90°$ in increments of 10°. It was observed that for halo orbits, the lowest ΔV was obtained for $\theta = 0°$, $\theta = 180°$ and $\theta = 360°$ for all inclinations. Additionally, it was observed

that ΔV_T around the final orbit was not sensitive to the inclination of the final orbit. Generally, the ΔV_T increased with inclination however, the ΔV_T requirements for the above mentioned locations for all inclinations remained confined to a small range. This suggests that if the final point on the desired orbit is selected as either $\theta = 0°$ or $\theta = 180°$, then it is possible to reach an orbit of any inclination from the unstable manifold without high ΔV costs. It was found that this result is not specific to the kind of halo orbit. A halo orbit around the L_2 Lagrange point also exhibits similar results. Due to the three-dimensional nature of the LPO, it becomes possible to reach different inclinations of the final orbit. Conversely, based on this result, it is reasonable to assume that it is possible to leave an Earth orbit and approach a manifold point from any inclination therefore, the constraints on the location of the launch site is relaxed.

The Lyapunov orbit, similar to the halo orbits, did not exhibit sensitivity to the inclination of the final orbit. The results, however, show large peaks at $0°\,, 180°$ *and* $360°$ which were not exhibited by the halo orbit transfers. Since the Lyapunov orbit lies entirely in the x-y plane, the geometry of the initial and final radius in the ECI system seemed to be the reason for these peaks causing the solution to approach singularities. The particle swarm algorithm is able to find the patch point with minimum possible ΔV which results in the solution moving away from the optimal configuration of a Hohmann transfer which happens at $180°$ transfer angle. Despite moving away from $180°$ transfer angle configuration, the resulting values for ΔV is very high. Further proof of these values being a result of singularities is provided by the fact that the ΔV at $\pm 0.1°$ away from $0°$ (*or* $360°$) *and* $180°$ gives much smaller values of ΔV.

The above results were obtained by using a very basic orbit. To establish trends and further study the solutions, another orbit with arbitrary classical orbital elements was selected and the analysis was repeated. It was found that while it was true that it is possible to achieve final LEOs of many inclinations from both halo and Lyapunov orbits, the point of insertion on the LEO to achieve this was dependent on the kind of LEO and its classical orbital elements. Specifically, it seems that argument of periapse, ω, and right ascension of the ascending node, Ω, have a strong influence on the final results. While the kind of orbit, either halo or Lyapunov did not affect the result, the Lagrange point under consideration and the direction of the associated manifold of the LPO had an affect on the final

solution. Changing the kind of LEO that was being targeted seemed to eliminate issues related to singularities due the mathematics used in the Lambert solver. It is assumed that due to $\omega = 0°$, $\Omega = 0°$ along with a circular orbit may have caused mathematical singularities with the position vector of the manifold point and that of the LEO insertion point.

Finally, this methods allows one to study the kinds of transfers that are possible and the conditions that are needed for such transfers. This kind insight may prove to be very computationally expensive with a more involved technique.

5.2 Limitations

While the method used has some advantages like reduced computational requirements, algorithmic simplicity, ability to study the variations in ΔV due to different final orbit conditions, it also suffers from some limitations. The analysis is performed with a two-body approximation, this results in some fundamental inaccuracies in the solutions process. Due to the setup of the problem, it is required to provide the algorithm with a specific location in the final orbit. While it may help the mission designer to study feasible final orbits, many times it may not be possible to target a specific point on the final orbit. Care needs to be taken to ensure that the transfers begin outside the SOI of the Moon. Since perturbations from the other bodies are neglected, the final solutions will deviate from the reality even if the manifolds are generated with an ephemeris model since the solver does not require integration of the trajectory to obtain the solution. While it is possible to repeat the analysis multiple times, it becomes very hard to select the best LEO as it is not possible to work through all combinations of the Lagrange point orbits and final LEO configurations. A technique which doesn't require one to specify the exact kind of orbit to be achieved and the location of the point of insertion is versatile and robust.

5.3 Future Scope

The current analysis can be expanded upon in multiple ways. First, in this analysis, the manifolds were generated without considering the planetary and solar perturbations. These can be incorporated using an ephemeris model in the solution

process to approach a more realistic result. Different kinds of LPOs can be examined around the collinear Lagrange points. Also, orbits around the equilateral Lagrange points can be studied to perform a complete study of the Lagrange point orbits in the Earth-Moon system. The same analysis can be performed in a different three-body system to quickly study the mission requirements. It is possible to combine this technique with a gradient based method like the single shooting among others which may allow a quicker, accurate solutions due to an available initial guess and by reducing the size of the search space. A study can be performed documenting the computational time savings obtained from a combined Lambert's, gradient based solution and PSO as compared to simple gradient based solution. A comparision study may be performed using different optimization algorithms and their performance can be compared. Variations of the particle swarm algorithm can be implemented and studied for accuracy and computational performance. A complete mission design study can be performed using this method as a preliminary analysis and then proceeding to detailed analysis using the results of this method as the initial guess. Transfers between two or more Lagrange point orbits using this method can be performed. A different solution method using low-thrust propulsion to LEO from equilateral Lagrange points, or multiple optimal burn transfer scenario may be used to explore the three-body systems and possible mission design space.

Appendix A
L_1 LPO Solutions

The results obtained by solving the Lambert's problem on the manifold of L_1 LPO are presented. The tables are generated as a result of variations in true anomaly θ_{LEO} and inclination i_{LEO}. Each table includes the ΔV_1 for the departure from manifold, ΔV_2 injection into parking orbit, the TOF_1 as the time-of-flight for the transfer trajectory to LEO, TOF_2 as the time of flight required for manifold coast till the optimal patch point, ΔV_T as the total coast for the trajectory and TOF_T as the total time of flight taken for the entire transfer.

A.1 L_1 Halo Orbit

Results for L_1 halo orbit with initial conditions given in Table 4.5 are presented in Tables A.1 - A.10

Table A.1. L_1 Halo orbit results for $i = 0°$ inclination of the LEO

θ (deg)	ΔV_1 (km/s)	ΔV_2 (km/s)	TOF_1 (days)	TOF_2 (days)	ΔV_T (km/s)	TOF_T (days)
0	0.741	3.062	3.515	30.102	3.803	33.618
15	0.775	3.063	3.447	28.707	3.838	32.154
30	0.819	3.072	3.155	27.231	3.890	30.385
45	0.947	3.066	3.147	46.799	4.013	49.946
60	0.887	3.056	3.427	47.859	3.943	51.285
75	0.846	3.071	3.559	47.703	3.917	51.262
90	0.833	3.073	3.596	47.423	3.906	51.019
105	0.825	3.252	3.611	47.188	4.078	50.799
120	0.831	3.800	3.605	47.188	4.631	50.793
135	0.745	4.218	3.713	16.729	4.964	20.442
150	0.742	3.524	3.720	16.719	4.266	20.439
165	0.775	3.122	3.475	17.318	3.896	20.793
180	0.741	3.118	3.714	16.734	3.859	20.448
195	0.824	3.076	3.866	17.226	3.900	21.093
210	0.895	3.063	3.443	19.062	3.958	22.504
225	0.991	3.055	2.910	21.627	4.047	24.537
240	1.096	3.028	2.393	22.265	4.124	24.658
255	1.203	3.002	1.961	22.257	4.205	24.218
270	1.052	3.064	2.598	26.953	4.116	29.551
285	0.926	3.073	3.229	29.630	3.999	32.859
300	0.840	3.096	3.629	30.430	3.936	34.059
315	0.794	3.070	3.783	30.488	3.864	34.271
330	0.749	3.073	3.849	30.352	3.822	34.201
345	0.726	3.068	3.771	30.196	3.794	33.967
360	0.741	3.062	3.515	30.102	3.803	33.618

Table A.2. L_1 Halo orbit results for $i = 10°$ inclination of the LEO

θ (deg)	ΔV_1 (km/s)	ΔV_2 (km/s)	TOF_1 (days)	TOF_2 (days)	ΔV_T (km/s)	TOF_T (days)
0	0.745	3.070	3.539	29.958	3.815	33.497
15	0.700	3.065	3.766	29.920	3.766	33.686
30	0.646	3.068	3.701	27.886	3.714	31.587
45	0.661	3.110	3.522	26.558	3.771	30.080
60	0.884	3.064	3.410	45.125	3.949	48.534
75	0.875	3.062	3.399	44.530	3.937	47.929
90	0.863	3.067	3.388	43.841	3.930	47.228
105	0.861	3.244	3.385	43.654	4.105	47.039
120	0.861	3.796	3.420	43.908	4.656	47.328
135	0.713	4.232	3.707	16.858	4.945	20.565
150	0.715	3.529	3.718	16.805	4.243	20.523
165	0.711	3.119	3.722	16.805	3.830	20.526
180	0.711	3.114	3.722	16.805	3.825	20.527
195	0.859	3.067	3.852	16.442	3.926	20.294
210	0.948	3.067	3.258	19.289	4.015	22.547
225	1.092	3.045	2.468	21.162	4.137	23.630
240	1.256	3.011	1.797	21.271	4.267	23.068
255	1.431	2.975	1.297	21.217	4.406	22.514
270	1.654	2.888	0.866	21.228	4.542	22.094
285	1.005	3.208	2.853	29.312	4.212	32.166
300	0.912	3.072	3.334	31.995	3.984	35.329
315	0.849	3.070	3.589	32.462	3.919	36.051
330	0.816	3.065	3.617	31.799	3.881	35.416
345	0.782	3.064	3.600	30.871	3.846	34.471
360	0.745	3.070	3.539	29.958	3.815	33.497

Table A.3. L_1 Halo orbit results for $i = 20°$ inclination of the LEO

θ (deg)	ΔV_1 (km/s)	ΔV_2 (km/s)	TOF_1 (days)	TOF_2 (days)	ΔV_T (km/s)	TOF_T (days)
0	0.746	3.077	3.620	29.697	3.823	33.317
15	0.622	3.080	3.865	28.216	3.702	32.081
30	0.561	3.069	3.934	26.729	3.630	30.664
45	0.605	3.184	3.761	29.851	3.789	33.612
60	0.542	3.634	3.907	28.382	4.175	32.289
75	0.963	3.797	3.117	43.052	4.759	46.170
90	0.971	4.140	3.040	42.598	5.111	45.639
105	0.973	4.381	2.974	42.094	5.354	45.067
120	0.973	4.438	2.892	41.386	5.410	44.278
135	0.693	4.237	3.715	16.942	4.930	20.658
150	0.694	3.536	3.714	16.932	4.229	20.645
165	0.692	3.121	3.720	16.912	3.813	20.632
180	0.692	3.113	3.720	16.912	3.805	20.632
195	0.904	3.070	3.749	16.105	3.974	19.854
210	1.008	3.073	3.033	19.716	4.081	22.749
225	1.190	3.079	2.080	20.546	4.268	22.626
240	1.342	3.245	1.577	20.621	4.586	22.198
255	1.455	3.591	1.316	20.734	5.045	22.050
270	1.011	4.358	2.951	30.239	5.369	33.190
285	0.971	3.830	3.108	31.379	4.801	34.487
300	0.964	3.381	3.076	31.113	4.346	34.189
315	0.928	3.106	3.276	34.948	4.034	38.224
330	0.893	3.058	3.369	32.871	3.951	36.240
345	0.830	3.066	3.565	32.280	3.896	35.844
360	0.746	3.077	3.620	29.697	3.823	33.317

Table A.4. L_1 Halo orbit results for $i = 30°$ inclination of the LEO

θ (deg)	ΔV_1 (km/s)	ΔV_2 (km/s)	TOF_1 (days)	TOF_2 (days)	ΔV_T (km/s)	TOF_T (days)
0	0.758	3.072	3.797	31.852	3.830	35.649
15	0.641	3.071	3.958	27.182	3.712	31.139
30	0.675	3.137	3.764	26.061	3.813	29.825
45	0.757	3.394	3.492	32.552	4.151	36.044
60	0.741	3.932	3.482	31.666	4.673	35.148
75	0.627	4.650	3.768	29.580	5.277	33.348
90	0.559	5.375	3.922	27.427	5.935	31.350
105	1.000	5.523	3.047	42.710	6.522	45.757
120	0.693	5.101	3.701	17.091	5.794	20.793
135	0.683	4.244	3.712	17.091	4.927	20.804
150	0.687	3.537	3.717	17.024	4.224	20.741
165	0.702	3.122	3.642	17.199	3.824	20.841
180	0.687	3.111	3.713	17.032	3.798	20.745
195	0.938	3.073	3.763	15.336	4.011	19.100
210	1.054	3.100	2.873	19.583	4.154	22.455
225	1.187	3.301	2.167	20.042	4.488	22.209
240	1.259	3.770	1.935	20.212	5.030	22.146
255	1.352	4.311	1.685	20.426	5.663	22.111
270	0.992	5.060	3.155	31.910	6.053	35.066
285	1.034	4.439	2.858	29.922	5.473	32.780
300	0.991	3.909	3.113	35.217	4.900	38.330
315	1.001	3.376	3.011	35.221	4.377	38.232
330	1.000	3.064	2.973	35.246	4.064	38.219
345	0.863	3.065	3.412	31.203	3.929	34.615
360	0.758	3.072	3.797	31.852	3.830	35.649

Table A.5. L_1 Halo orbit results for $i = 40°$ inclination of the LEO

θ (deg)	ΔV_1 (km/s)	ΔV_2 (km/s)	TOF_1 (days)	TOF_2 (days)	ΔV_T (km/s)	TOF_T (days)
0	0.768	3.078	3.838	32.127	3.846	35.965
15	0.701	3.068	3.919	26.948	3.769	30.867
30	0.749	3.223	3.678	25.926	3.972	29.604
45	0.835	3.595	3.440	34.093	4.429	37.533
60	0.831	4.216	3.397	33.373	5.048	36.771
75	0.789	4.949	3.446	32.027	5.738	35.473
90	0.658	5.787	3.753	29.614	6.445	33.367
105	0.711	6.039	3.686	17.197	6.751	20.883
120	0.701	5.095	3.700	17.197	5.795	20.897
135	0.694	4.235	3.711	17.180	4.929	20.890
150	0.690	3.539	3.715	17.170	4.229	20.884
165	0.690	3.125	3.715	17.151	3.815	20.866
180	0.709	3.108	3.643	17.304	3.818	20.947
195	0.980	3.066	3.771	14.677	4.046	18.447
210	1.087	3.152	2.804	19.303	4.239	22.107
225	1.146	3.552	2.479	19.582	4.698	22.061
240	1.207	4.147	2.263	19.830	5.354	22.093
255	1.285	4.810	2.016	20.098	6.094	22.114
270	1.064	5.601	2.874	30.037	6.666	32.911
285	1.038	4.936	3.070	35.265	5.975	38.335
300	1.060	4.217	2.920	35.263	5.278	38.184
315	1.069	3.577	2.839	35.267	4.646	38.105
330	1.067	3.137	2.793	35.323	4.204	38.116
345	0.889	3.086	3.348	30.617	3.976	33.965
360	0.768	3.078	3.838	32.127	3.846	35.965

Table A.6. L_1 Halo orbit results for $i = 50°$ inclination of the LEO

θ (deg)	ΔV_1 (km/s)	ΔV_2 (km/s)	TOF_1 (days)	TOF_2 (days)	ΔV_T (km/s)	TOF_T (days)
0	0.798	3.072	3.832	32.246	3.870	36.078
15	0.752	3.080	3.924	27.095	3.832	31.019
30	0.803	3.296	3.660	25.977	4.099	29.637
45	0.883	3.756	3.471	35.015	4.639	38.486
60	0.885	4.447	3.423	34.455	5.332	37.878
75	0.870	5.226	3.391	33.490	6.096	36.880
90	0.800	6.082	3.504	31.824	6.881	35.328
105	0.721	6.030	3.694	17.375	6.752	21.069
120	0.715	5.084	3.706	17.312	5.800	21.018
135	0.708	4.229	3.717	17.312	4.937	21.029
150	0.710	3.531	3.716	17.265	4.241	20.981
165	0.710	3.123	3.706	17.291	3.833	20.997
180	0.712	3.113	3.707	17.271	3.825	20.978
195	1.020	3.072	3.724	14.400	4.091	18.124
210	1.088	3.235	2.989	18.789	4.323	21.777
225	1.125	3.735	2.766	19.109	4.860	21.875
240	1.174	4.413	2.571	19.413	5.587	21.984
255	1.236	5.164	2.337	19.734	6.400	22.070
270	1.077	6.046	3.047	35.275	7.123	38.322
285	1.108	5.222	2.892	35.176	6.330	38.068
300	1.127	4.424	2.787	35.248	5.551	38.035
315	1.135	3.712	2.710	35.051	4.848	37.761
330	1.134	3.200	2.682	35.207	4.334	37.889
345	0.911	3.113	3.337	30.359	4.024	33.696
360	0.798	3.072	3.832	32.246	3.870	36.078

Table A.7. L_1 Halo orbit results for $i = 60°$ inclination of the LEO

θ (deg)	ΔV_1 (km/s)	ΔV_2 (km/s)	TOF_1 (days)	TOF_2 (days)	ΔV_T (km/s)	TOF_T (days)
0	0.827	3.074	3.848	32.458	3.901	36.306
15	0.810	3.083	3.856	26.782	3.893	30.637
30	0.861	3.339	3.617	25.931	4.199	29.547
45	0.901	3.887	3.432	25.452	4.787	28.884
60	0.937	4.608	3.441	35.361	5.545	38.802
75	0.926	5.444	3.409	34.588	6.370	37.997
90	0.894	6.329	3.406	33.419	7.223	36.825
105	0.747	6.010	3.696	17.439	6.757	21.136
120	0.741	5.068	3.710	17.439	5.809	21.149
135	0.736	4.215	3.721	17.439	4.950	21.160
150	0.734	3.523	3.728	17.381	4.257	21.110
165	0.732	3.120	3.729	17.368	3.852	21.097
180	0.735	3.118	3.719	17.368	3.853	21.087
195	1.060	3.072	3.703	14.136	4.131	17.839
210	1.097	3.302	3.171	18.214	4.399	21.385
225	1.124	3.860	2.990	18.624	4.984	21.614
240	1.157	4.599	2.841	18.929	5.756	21.770
255	1.200	5.420	2.652	19.268	6.620	21.920
270	1.147	6.311	2.871	35.252	7.459	38.123
285	1.178	5.414	2.745	35.177	6.592	37.922
300	1.195	4.558	2.663	35.045	5.754	37.708
315	1.202	3.802	2.617	35.079	5.003	37.696
330	1.200	3.245	2.595	35.156	4.446	37.751
345	0.935	3.137	3.358	30.288	4.072	33.646
360	0.827	3.074	3.848	32.458	3.901	36.306

Table A.8. L_1 Halo orbit results for $i = 70°$ inclination of the LEO

θ (deg)	ΔV_1 (km/s)	ΔV_2 (km/s)	TOF_1 (days)	TOF_2 (days)	ΔV_T (km/s)	TOF_T (days)
0	0.851	3.092	3.931	28.563	3.943	32.494
15	0.854	3.094	3.870	26.925	3.948	30.795
30	0.902	3.378	3.637	26.062	4.281	29.698
45	0.942	3.953	3.454	25.579	4.895	29.033
60	0.960	4.728	3.356	25.337	5.688	28.693
75	0.950	5.623	3.350	25.290	6.574	28.640
90	0.960	6.523	3.403	34.733	7.483	38.136
105	0.779	5.982	3.702	17.621	6.760	21.323
120	0.775	5.043	3.715	17.621	5.818	21.336
135	0.771	4.194	3.727	17.557	4.965	21.284
150	0.773	3.510	3.717	17.540	4.283	21.257
165	0.773	3.113	3.719	17.524	3.885	21.243
180	0.773	3.121	3.719	17.513	3.894	21.233
195	1.098	3.072	3.622	14.604	4.170	18.226
210	1.120	3.345	3.232	17.927	4.465	21.159
225	1.130	3.949	3.209	18.003	5.079	21.212
240	1.151	4.729	3.087	18.343	5.880	21.430
255	1.180	5.598	2.930	18.709	6.777	21.639
270	1.221	6.482	2.710	35.071	7.704	37.780
285	1.247	5.537	2.624	35.124	6.784	37.748
300	1.263	4.643	2.567	35.071	5.906	37.638
315	1.269	3.857	2.533	35.061	5.126	37.594
330	1.073	3.466	2.946	28.872	4.538	31.819
345	0.953	3.167	3.429	30.447	4.120	33.877
360	0.851	3.092	3.931	28.563	3.943	32.494

Table A.9. L_1 Halo orbit results for $i = 80°$ inclination of the LEO

θ (deg)	ΔV_1 (km/s)	ΔV_2 (km/s)	TOF_1 (days)	TOF_2 (days)	ΔV_T (km/s)	TOF_T (days)
0	0.908	3.068	3.821	32.400	3.977	36.221
15	0.908	3.094	3.829	26.794	4.002	30.624
30	0.945	3.401	3.647	26.158	4.346	29.805
45	0.996	3.977	3.412	25.541	4.974	28.953
60	1.006	4.778	3.350	25.401	5.784	28.751
75	1.005	5.689	3.314	25.314	6.694	28.629
90	0.988	6.664	3.330	25.337	7.652	28.666
105	0.818	5.942	3.717	17.804	6.760	21.520
120	0.816	5.009	3.723	17.765	5.825	21.487
135	0.813	4.167	3.729	17.730	4.981	21.459
150	0.812	3.493	3.730	17.680	4.305	21.410
165	0.810	3.108	3.735	17.646	3.918	21.381
180	0.809	3.129	3.737	17.621	3.938	21.358
195	1.132	3.072	3.503	16.385	4.204	19.888
210	1.134	3.384	3.445	16.916	4.518	20.361
225	1.142	4.010	3.393	17.206	5.152	20.598
240	1.153	4.818	3.310	17.564	5.971	20.874
255	1.168	5.720	3.207	17.924	6.888	21.131
270	1.188	6.665	3.069	18.320	7.852	21.389
285	1.321	5.599	2.502	34.966	6.920	37.468
300	1.331	4.687	2.477	34.995	6.018	37.473
315	1.336	3.885	2.463	34.928	5.222	37.390
330	1.098	3.506	2.990	28.898	4.604	31.888
345	0.996	3.168	3.410	30.305	4.164	33.715
360	0.908	3.068	3.821	32.400	3.977	36.221

Table A.10. L_1 Halo orbit results for $i = 90°$ inclination of the LEO

θ (deg)	ΔV_1 (km/s)	ΔV_2 (km/s)	TOF_1 (days)	TOF_2 (days)	ΔV_T (km/s)	TOF_T (days)
0	0.942	3.077	3.863	33.000	4.020	36.863
15	0.932	3.112	3.918	27.339	4.044	31.256
30	0.998	3.399	3.609	26.101	4.397	29.710
45	1.029	3.999	3.454	25.712	5.029	29.165
60	1.051	4.793	3.341	25.468	5.844	28.809
75	1.062	5.700	3.263	25.318	6.763	28.581
90	0.866	6.864	3.721	18.027	7.730	21.748
105	0.867	5.888	3.730	18.017	6.755	21.747
120	0.863	4.965	3.737	17.943	5.827	21.679
135	0.857	4.134	3.743	17.842	4.991	21.585
150	0.856	3.470	3.748	17.804	4.326	21.552
165	0.861	3.099	3.730	17.825	3.959	21.555
180	0.855	3.139	3.742	17.779	3.994	21.521
195	1.154	3.082	3.548	16.253	4.236	19.801
210	1.155	3.408	3.562	16.068	4.563	19.630
225	1.157	4.050	3.556	16.018	5.207	19.574
240	1.156	4.881	3.543	16.069	6.037	19.612
255	1.154	5.811	3.548	15.807	6.966	19.355
270	1.173	6.764	3.375	17.101	7.936	20.476
285	1.399	5.608	2.377	34.839	7.007	37.215
300	1.402	4.694	2.388	34.839	6.096	37.226
315	1.405	3.890	2.396	34.839	5.295	37.235
330	1.131	3.528	3.012	28.871	4.659	31.883
345	1.023	3.183	3.455	30.413	4.207	33.867
360	0.942	3.077	3.863	33.000	4.020	36.863

A.2 L_1 Lyapunov Orbit

Results for L_1 halo orbit with initial conditions given in Table 4.6 are presented in Tables A.11 - A.20.

Table A.11. L_1 Lyapunov orbit results for $i = 0°$ inclination of the LEO

θ (deg)	ΔV_1 (km/s)	ΔV_2 (km/s)	TOF_1 (days)	TOF_2 (days)	ΔV_T (km/s)	TOF_T (days)
0	0.768	3.068	3.265	19.730	3.836	22.995
15	0.678	3.062	3.445	19.472	3.740	22.917
30	0.601	3.062	3.492	18.860	3.663	22.352
45	0.539	3.059	3.486	18.655	3.598	22.141
60	0.535	3.134	3.481	19.003	3.669	22.484
75	0.542	3.569	3.475	18.972	4.111	22.447
90	1.225	2.983	1.704	28.084	4.209	29.789
105	1.231	3.155	1.694	28.138	4.386	29.831
120	1.240	3.687	1.690	28.144	4.927	29.834
135	0.636	4.403	3.675	8.268	5.040	11.943
150	0.615	3.674	3.684	8.329	4.290	12.013
165	0.590	3.198	3.686	8.464	3.788	12.149
180	0.560	3.061	3.676	8.946	3.621	12.622
195	0.615	3.140	3.706	9.553	3.755	13.259
210	0.920	3.057	2.697	12.439	3.977	15.136
225	1.066	3.020	2.194	13.436	4.086	15.630
240	1.153	3.000	1.918	14.086	4.153	16.004
255	1.204	2.988	1.765	14.595	4.192	16.360
270	1.227	2.982	1.700	15.031	4.210	16.731
285	1.226	2.983	1.705	15.475	4.209	17.180
300	1.200	2.990	1.783	15.936	4.189	17.719
315	1.145	3.003	1.948	16.494	4.148	18.442
330	1.056	3.024	2.239	17.188	4.079	19.427
345	0.920	3.053	2.717	18.288	3.973	21.004
360	0.768	3.068	3.265	19.730	3.836	22.995

Table A.12. L_1 Lyapunov orbit results for $i = 10°$ inclination of the LEO

θ (deg)	ΔV_1 (km/s)	ΔV_2 (km/s)	TOF_1 (days)	TOF_2 (days)	ΔV_T (km/s)	TOF_T (days)
0	0.765	3.454	3.275	19.733	4.219	23.008
15	0.782	3.216	3.251	19.685	3.998	22.936
30	0.730	3.517	3.387	19.666	4.247	23.053
45	0.678	3.842	3.460	19.350	4.519	22.810
60	0.625	4.153	3.485	18.878	4.778	22.364
75	0.574	4.431	3.480	18.648	5.004	22.129
90	0.561	4.724	3.468	19.032	5.285	22.500
105	0.570	5.388	3.454	18.946	5.959	22.399
120	0.658	5.285	3.664	8.235	5.944	11.899
135	0.641	4.410	3.675	8.268	5.051	11.943
150	0.621	3.684	3.684	8.329	4.305	12.013
165	0.579	3.231	3.682	8.620	3.810	12.302
180	0.560	3.445	3.676	8.946	4.005	12.622
195	0.578	3.227	3.681	9.263	3.805	12.944
210	0.666	3.559	3.635	9.929	4.225	13.564
225	0.861	3.839	2.971	11.864	4.699	14.836
240	0.992	4.129	2.521	12.773	5.121	15.294
255	1.097	4.387	2.184	13.447	5.484	15.631
270	1.175	4.602	1.946	13.976	5.777	15.922
285	1.177	4.372	1.948	16.525	5.549	18.473
300	1.106	4.107	2.158	17.036	5.213	19.194
315	1.021	3.811	2.427	17.622	4.832	20.049
330	0.926	3.502	2.745	18.352	4.428	21.097
345	0.841	3.212	3.039	19.112	4.053	22.151
360	0.765	3.454	3.275	19.733	4.219	23.008

Table A.13. L_1 Lyapunov orbit results for $i = 20°$ inclination of the LEO

θ (deg)	ΔV_1 (km/s)	ΔV_2 (km/s)	TOF_1 (days)	TOF_2 (days)	ΔV_T (km/s)	TOF_T (days)
0	0.754	4.407	3.306	19.799	5.161	23.105
15	0.818	3.244	3.182	19.468	4.062	22.650
30	0.782	3.673	3.319	19.773	4.455	23.092
45	0.741	4.173	3.411	19.635	4.914	23.046
60	0.697	4.681	3.459	19.228	5.378	22.687
75	0.649	5.164	3.477	18.829	5.812	22.306
90	0.599	5.596	3.469	18.644	6.195	22.113
105	0.586	6.007	3.455	19.013	6.594	22.469
120	0.665	5.308	3.663	8.268	5.973	11.931
135	0.656	4.429	3.675	8.268	5.085	11.942
150	0.623	3.723	3.682	8.415	4.346	12.097
165	0.587	3.256	3.674	8.788	3.842	12.462
180	0.560	4.392	3.676	8.946	4.952	12.622
195	0.584	3.256	3.675	9.085	3.840	12.761
210	0.623	3.694	3.692	9.473	4.317	13.165
225	0.750	4.201	3.428	10.681	4.951	14.109
240	0.905	4.679	2.911	11.979	5.584	14.889
255	1.029	5.138	2.497	12.812	6.167	15.309
270	1.131	5.550	2.176	13.436	6.681	15.612
285	1.147	5.114	2.137	17.002	6.260	19.139
300	1.066	4.647	2.380	17.507	5.713	19.887
315	0.978	4.155	2.658	18.162	5.133	20.820
330	0.895	3.668	2.926	18.800	4.563	21.726
345	0.840	3.244	3.100	19.290	4.084	22.390
360	0.754	4.407	3.306	19.799	5.161	23.105

Table A.14. L_1 Lyapunov orbit results for $i = 30°$ inclination of the LEO

θ (deg)	ΔV_1 (km/s)	ΔV_2 (km/s)	TOF_1 (days)	TOF_2 (days)	ΔV_T (km/s)	TOF_T (days)
0	0.741	5.625	3.339	19.810	6.367	23.149
15	0.850	3.253	3.159	19.468	4.102	22.628
30	0.827	3.745	3.264	19.736	4.572	23.000
45	0.794	4.355	3.362	19.748	5.149	23.110
60	0.757	4.998	3.425	19.508	5.755	22.933
75	0.714	5.632	3.458	19.134	6.347	22.592
90	0.665	6.230	3.466	18.772	6.895	22.238
105	0.696	6.287	3.649	8.268	6.982	11.917
120	0.685	5.333	3.663	8.268	6.018	11.931
135	0.651	4.484	3.673	8.415	5.135	12.088
150	0.625	3.771	3.677	8.594	4.396	12.271
165	0.605	3.266	3.673	8.878	3.871	12.552
180	0.560	5.605	3.676	8.946	6.165	12.622
195	0.605	3.266	3.674	9.016	3.871	12.690
210	0.627	3.760	3.677	9.317	4.387	12.994
225	0.681	4.394	3.697	9.564	5.075	13.261
240	0.828	5.019	3.258	11.152	5.848	14.410
255	0.965	5.626	2.806	12.180	6.591	14.986
270	1.079	6.201	2.433	12.914	7.280	15.347
285	1.122	5.592	2.316	17.425	6.714	19.741
300	1.039	4.976	2.570	17.981	6.015	20.551
315	0.961	4.345	2.814	18.537	5.306	21.351
330	0.896	3.744	3.012	19.012	4.639	22.024
345	0.857	3.256	3.122	19.368	4.113	22.489
360	0.741	5.625	3.339	19.810	6.367	23.149

Table A.15. L_1 Lyapunov orbit results for $i = 40°$ inclination of the LEO

θ (deg)	ΔV_1 (km/s)	ΔV_2 (km/s)	TOF_1 (days)	TOF_2 (days)	ΔV_T (km/s)	TOF_T (days)
0	0.727	6.944	3.370	19.775	7.671	23.145
15	0.884	3.256	3.141	19.403	4.140	22.544
30	0.871	3.781	3.219	19.629	4.653	22.847
45	0.844	4.463	3.319	19.815	5.307	23.134
60	0.812	5.202	3.387	19.664	6.014	23.051
75	0.773	5.952	3.431	19.375	6.725	22.806
90	0.728	6.680	3.451	18.973	7.408	22.424
105	0.706	6.330	3.649	8.329	7.036	11.978
120	0.698	5.376	3.663	8.329	6.075	11.992
135	0.673	4.520	3.671	8.464	5.193	12.135
150	0.649	3.797	3.674	8.666	4.446	12.341
165	0.632	3.271	3.674	8.920	3.903	12.594
180	0.560	6.919	3.676	8.946	7.478	12.622
195	0.633	3.270	3.674	8.984	3.902	12.658
210	0.645	3.797	3.668	9.189	4.443	12.857
225	0.681	4.486	3.683	9.473	5.167	13.156
240	0.739	5.262	3.644	9.796	6.002	13.439
255	0.889	5.976	3.157	11.380	6.864	14.537
270	1.015	6.675	2.737	12.295	7.690	15.032
285	1.099	5.923	2.490	17.812	7.023	20.302
300	1.026	5.188	2.718	18.310	6.214	21.027
315	0.962	4.458	2.918	18.800	5.419	21.718
330	0.913	3.782	3.059	19.194	4.695	22.254
345	0.886	3.259	3.127	19.375	4.145	22.503
360	0.727	6.944	3.370	19.775	7.671	23.145

Table A.16. L_1 Lyapunov orbit results for $i = 50°$ inclination of the LEO

θ (deg)	ΔV_1 (km/s)	ΔV_2 (km/s)	TOF_1 (days)	TOF_2 (days)	ΔV_T (km/s)	TOF_T (days)
0	0.709	8.287	3.402	19.662	8.996	23.064
15	0.922	3.258	3.136	19.359	4.180	22.495
30	0.915	3.802	3.187	19.519	4.717	22.706
45	0.894	4.530	3.276	19.792	5.423	23.068
60	0.865	5.338	3.347	19.775	6.203	23.122
75	0.830	6.174	3.395	19.498	7.004	22.893
90	0.788	7.004	3.427	19.224	7.792	22.651
105	0.729	6.368	3.648	8.356	7.098	12.003
120	0.710	5.429	3.659	8.451	6.138	12.111
135	0.690	4.563	3.667	8.594	5.253	12.261
150	0.675	3.818	3.668	8.788	4.493	12.457
165	0.665	3.272	3.674	8.920	3.937	12.594
180	0.560	8.255	3.676	8.946	8.815	12.622
195	0.664	3.273	3.674	8.946	3.937	12.620
210	0.673	3.818	3.670	9.085	4.491	12.755
225	0.691	4.551	3.668	9.317	5.243	12.985
240	0.725	5.378	3.679	9.505	6.103	13.184
255	0.781	6.250	3.600	9.929	7.030	13.529
270	0.929	7.033	3.113	11.454	7.962	14.568
285	1.081	6.156	2.657	18.212	7.237	20.869
300	1.022	5.331	2.844	18.626	6.352	21.470
315	0.973	4.529	2.993	19.006	5.502	21.999
330	0.937	3.807	3.095	19.290	4.744	22.385
345	0.920	3.261	3.130	19.350	4.182	22.480
360	0.709	8.287	3.402	19.662	8.996	23.064

Table A.17. L_1 Lyapunov orbit results for $i = 60°$ inclination of the LEO

θ (deg)	ΔV_1 (km/s)	ΔV_2 (km/s)	TOF_1 (days)	TOF_2 (days)	ΔV_T (km/s)	TOF_T (days)
0	0.684	9.614	3.438	19.495	10.298	22.933
15	0.963	3.260	3.130	19.350	4.223	22.480
30	0.959	3.815	3.169	19.505	4.774	22.674
45	0.942	4.572	3.237	19.685	5.514	22.922
60	0.917	5.428	3.306	19.815	6.345	23.121
75	0.886	6.326	3.356	19.674	7.212	23.030
90	0.849	7.232	3.393	19.480	8.081	22.874
105	0.742	6.419	3.645	8.464	7.161	12.108
120	0.732	5.469	3.657	8.530	6.201	12.187
135	0.718	4.591	3.665	8.666	5.309	12.332
150	0.707	3.830	3.669	8.849	4.537	12.518
165	0.700	3.274	3.674	8.946	3.974	12.620
180	0.560	9.573	3.676	8.946	10.133	12.622
195	0.701	3.273	3.674	8.946	3.974	12.620
210	0.706	3.829	3.669	9.043	4.535	12.713
225	0.715	4.591	3.659	9.189	5.306	12.848
240	0.735	5.453	3.658	9.399	6.188	13.057
255	0.758	6.373	3.664	9.505	7.131	13.169
270	0.782	7.327	3.656	9.567	8.109	13.223
285	1.065	6.319	2.816	18.610	7.384	21.426
300	1.023	5.427	2.954	18.936	6.451	21.889
315	0.992	4.574	3.051	19.194	5.566	22.245
330	0.971	3.818	3.108	19.315	4.789	22.423
345	0.961	3.261	3.130	19.350	4.222	22.480
360	0.684	9.614	3.438	19.495	10.298	22.933

Table A.18. L_1 Lyapunov orbit results for $i = 70°$ inclination of the LEO

θ (deg)	ΔV_1 (km/s)	ΔV_2 (km/s)	TOF_1 (days)	TOF_2 (days)	ΔV_T (km/s)	TOF_T (days)
0	0.643	10.902	3.473	19.138	11.545	22.612
15	1.007	3.260	3.130	19.350	4.266	22.480
30	1.003	3.822	3.154	19.468	4.825	22.622
45	0.991	4.598	3.201	19.604	5.588	22.806
60	0.970	5.485	3.257	19.742	6.455	22.999
75	0.942	6.426	3.309	19.795	7.368	23.104
90	0.765	7.450	3.627	8.530	8.216	12.157
105	0.758	6.464	3.641	8.594	7.222	12.234
120	0.753	5.506	3.653	8.666	6.259	12.319
135	0.747	4.613	3.659	8.788	5.360	12.447
150	0.742	3.837	3.666	8.907	4.579	12.573
165	0.738	3.274	3.674	8.946	4.013	12.620
180	0.560	10.846	3.676	8.946	11.406	12.622
195	0.739	3.273	3.674	8.946	4.013	12.620
210	0.741	3.837	3.668	8.984	4.578	12.652
225	0.745	4.613	3.660	9.085	5.358	12.746
240	0.755	5.500	3.654	9.263	6.255	12.916
255	0.763	6.450	3.643	9.364	7.213	13.006
270	0.779	7.421	3.640	9.473	8.200	13.112
285	1.052	6.428	2.967	19.019	7.480	21.986
300	1.033	5.488	3.039	19.194	6.521	22.233
315	1.017	4.601	3.091	19.297	5.618	22.388
330	1.005	3.827	3.124	19.350	4.832	22.475
345	1.002	3.263	3.137	19.438	4.265	22.575
360	0.643	10.902	3.473	19.138	11.545	22.612

Table A.19. L_1 Lyapunov orbit results for $i = 80°$ inclination of the LEO

θ (deg)	ΔV_1 (km/s)	ΔV_2 (km/s)	TOF_1 (days)	TOF_2 (days)	ΔV_T (km/s)	TOF_T (days)
0	0.573	12.128	3.477	18.638	12.700	22.115
15	1.050	3.260	3.127	19.356	4.311	22.483
30	1.049	3.825	3.136	19.403	4.874	22.539
45	1.039	4.611	3.167	19.519	5.650	22.685
60	1.022	5.517	3.206	19.640	6.538	22.847
75	0.999	6.483	3.249	19.745	7.482	22.993
90	0.781	7.486	3.622	8.666	8.268	12.289
105	0.778	6.496	3.632	8.788	7.274	12.420
120	0.778	5.531	3.647	8.849	6.308	12.496
135	0.779	4.625	3.658	8.878	5.404	12.536
150	0.777	3.841	3.668	8.946	4.618	12.614
165	0.777	3.274	3.674	8.946	4.051	12.620
180	0.560	12.056	3.676	8.946	12.616	12.622
195	0.776	3.275	3.674	8.920	4.051	12.594
210	0.777	3.840	3.668	8.946	4.617	12.614
225	0.778	4.625	3.659	9.016	5.403	12.675
240	0.778	5.528	3.648	9.085	6.306	12.733
255	0.778	6.493	3.634	9.149	7.271	12.783
270	0.776	7.489	3.619	9.149	8.265	12.767
285	1.048	6.487	3.087	19.356	7.535	22.443
300	1.044	5.523	3.114	19.416	6.567	22.531
315	1.044	4.617	3.127	19.403	5.660	22.530
330	1.043	3.831	3.136	19.403	4.874	22.539
345	1.046	3.263	3.137	19.438	4.308	22.575
360	0.573	12.128	3.477	18.638	12.700	22.115

Table A.20. L_1 Lyapunov orbit results for $i = 90°$ inclination of the LEO

θ (deg)	ΔV_1 (km/s)	ΔV_2 (km/s)	TOF_1 (days)	TOF_2 (days)	ΔV_T (km/s)	TOF_T (days)
0	0.553	13.184	3.462	18.813	13.737	22.275
15	1.094	3.260	3.127	19.375	4.354	22.503
30	1.093	3.826	3.122	19.356	4.919	22.477
45	1.091	4.612	3.113	19.356	5.703	22.468
60	1.088	5.519	3.101	19.356	6.607	22.457
75	1.084	6.488	3.087	19.356	7.572	22.443
90	0.800	7.503	3.617	8.946	8.304	12.562
105	0.805	6.507	3.632	9.016	7.312	12.648
120	0.808	5.538	3.648	9.043	6.346	12.691
135	0.811	4.630	3.658	9.016	5.441	12.675
150	0.813	3.842	3.668	8.984	4.655	12.652
165	0.816	3.274	3.669	8.973	4.090	12.642
180	0.560	13.188	3.676	8.946	13.748	12.622
195	0.814	3.275	3.674	8.920	4.089	12.594
210	0.813	3.841	3.668	8.920	4.654	12.588
225	0.811	4.629	3.657	8.907	5.440	12.564
240	0.808	5.537	3.647	8.920	6.344	12.567
255	0.804	6.507	3.632	8.920	7.310	12.552
270	0.799	7.504	3.617	8.920	8.303	12.537
285	1.048	6.506	3.188	19.635	7.554	22.823
300	1.059	5.534	3.176	19.570	6.593	22.746
315	1.070	4.622	3.160	19.505	5.693	22.665
330	1.080	3.832	3.146	19.413	4.912	22.559
345	1.087	3.264	3.136	19.359	4.351	22.495
360	0.553	13.184	3.462	18.813	13.737	22.275

Appendix B
L_2 LPO Solutions

The results obtained by solving the Lambert's problem on the manifold of L_2 LPO are presented. The tables are generated as a result of variations in true anomaly θ_{LEO} and inclination i_{LEO}. Each table includes the ΔV_1 for the departure from manifold, ΔV_2 injection into parking orbit, the TOF_1 as the time-of-flight for the transfer trajectory to LEO, TOF_2 as the time of flight required for manifold coast till the optimal patch point, ΔV_T as the total coast for the trajectory and TOF_T as the total time of flight taken for the entire transfer.

B.1 L_2 Halo Orbit

Results for L_2 halo orbit with initial conditions given in Table 4.7 are presented in Tables B.1 - B.10.

Table B.1. L_2 Halo orbit results for $i = 0°$ inclination of the LEO

θ (deg)	ΔV_1 (km/s)	ΔV_2 (km/s)	TOF_1 (days)	TOF_2 (days)	ΔV_T (km/s)	TOF_T (days)
0	0.481	3.141	20.340	35.879	3.622	56.219
15	0.497	3.141	19.392	34.570	3.637	53.962
30	0.515	3.140	18.396	33.196	3.655	51.592
45	0.537	3.138	17.398	31.781	3.675	49.179
60	0.561	3.136	16.380	30.346	3.698	46.725
75	0.591	3.133	15.282	28.775	3.724	44.056
90	0.622	3.132	14.221	27.301	3.754	41.522
105	0.660	3.129	13.078	25.653	3.789	38.731
120	0.703	3.126	11.875	23.917	3.829	35.792
135	0.754	3.122	10.617	22.035	3.876	32.652
150	0.815	3.120	9.307	19.919	3.935	29.226
165	0.894	3.119	7.883	17.201	4.013	25.085
180	1.026	3.113	7.945	15.171	4.138	23.115
195	1.001	3.225	6.192	1.771	4.226	7.963
210	0.972	3.707	6.265	2.027	4.679	8.292
225	0.428	4.726	29.795	43.048	5.153	72.843
240	0.423	3.924	26.024	43.577	4.347	69.600
255	0.422	3.354	25.885	43.604	3.776	69.488
270	0.422	3.145	25.706	43.549	3.567	69.255
285	0.428	3.148	25.019	42.464	3.576	67.483
300	0.436	3.146	24.093	41.155	3.582	65.248
315	0.445	3.147	23.203	39.900	3.591	63.104
330	0.456	3.142	22.099	38.398	3.598	60.497
345	0.467	3.142	21.260	37.184	3.609	58.443
360	0.481	3.141	20.340	35.879	3.622	56.219

Table B.2. L_2 Halo orbit results for $i = 10°$ inclination of the LEO

θ (deg)	ΔV_1 (km/s)	ΔV_2 (km/s)	TOF_1 (days)	TOF_2 (days)	ΔV_T (km/s)	TOF_T (days)
0	0.481	3.143	21.111	35.737	3.624	56.847
15	0.508	3.173	18.972	36.275	3.681	55.247
30	0.516	3.416	18.710	35.734	3.932	54.443
45	0.529	3.723	18.466	34.886	4.252	53.352
60	0.545	4.027	17.828	33.843	4.572	51.670
75	0.566	4.298	17.436	32.681	4.864	50.118
90	0.590	4.520	16.659	31.373	5.110	48.032
105	0.806	4.286	11.638	23.124	5.092	34.763
120	0.861	4.011	10.566	21.508	4.872	32.074
135	0.921	3.708	9.446	19.820	4.629	29.265
150	0.986	3.403	8.439	18.112	4.388	26.551
165	1.044	3.154	7.690	16.564	4.199	24.255
180	0.965	3.114	6.284	2.062	4.079	8.346
195	0.954	3.221	6.315	2.307	4.175	8.621
210	0.962	3.705	6.295	2.181	4.667	8.476
225	0.976	4.442	6.264	1.982	5.417	8.246
240	0.465	4.778	36.423	42.494	5.243	78.917
255	0.472	4.716	34.582	41.197	5.188	75.779
270	0.475	4.565	32.581	40.009	5.040	72.589
285	0.486	4.335	31.725	38.908	4.821	70.633
300	0.491	4.061	30.202	37.879	4.551	68.081
315	0.499	3.751	29.303	36.962	4.250	66.265
330	0.503	3.442	28.213	36.176	3.945	64.389
345	0.498	3.195	26.623	35.679	3.694	62.302
360	0.481	3.142	20.919	35.743	3.623	56.662

Table B.3. L_2 Halo orbit results for $i = 20°$ inclination of the LEO

θ (deg)	ΔV_1 (km/s)	ΔV_2 (km/s)	TOF_1 (days)	TOF_2 (days)	ΔV_T (km/s)	TOF_T (days)
0	0.492	3.141	19.076	36.022	3.633	55.098
15	0.507	3.241	18.906	36.688	3.748	55.594
30	0.514	3.621	18.954	36.309	4.135	55.263
45	0.525	4.106	18.900	35.660	4.631	54.560
60	0.537	4.608	18.311	34.839	5.145	53.150
75	0.553	5.086	17.811	33.843	5.640	51.654
90	0.572	5.515	17.316	32.733	6.087	50.049
105	0.872	5.071	10.486	21.485	5.942	31.971
120	0.930	4.590	9.461	19.888	5.520	29.349
135	0.990	4.090	8.568	18.345	5.080	26.913
150	1.051	3.607	7.750	16.722	4.658	24.472
165	0.918	3.382	6.458	4.086	4.301	10.543
180	0.937	3.106	6.387	3.098	4.043	9.484
195	0.937	3.235	6.388	3.072	4.172	9.460
210	0.955	3.723	6.337	2.550	4.678	8.887
225	0.973	4.457	6.292	2.287	5.430	8.579
240	0.988	5.337	6.260	2.192	6.324	8.452
255	0.479	5.906	32.557	40.009	6.385	72.566
270	0.485	5.552	31.025	38.904	6.037	69.929
285	0.493	5.119	29.933	37.913	5.612	67.846
300	0.498	4.638	28.826	37.036	5.136	65.862
315	0.505	4.132	28.124	36.292	4.637	64.416
330	0.505	3.647	26.959	35.714	4.152	62.672
345	0.496	3.267	25.143	35.392	3.763	60.535
360	0.492	3.141	19.076	36.022	3.633	55.098

Table B.4. L_2 Halo orbit results for $i = 30°$ inclination of the LEO

θ (deg)	ΔV_1 (km/s)	ΔV_2 (km/s)	TOF_1 (days)	TOF_2 (days)	ΔV_T (km/s)	TOF_T (days)
0	0.490	3.143	20.661	35.705	3.633	56.366
15	0.511	3.273	19.070	36.860	3.784	55.930
30	0.517	3.723	18.991	36.605	4.240	55.596
45	0.525	4.318	18.762	36.124	4.844	54.887
60	0.537	4.955	18.617	35.451	5.492	54.068
75	0.549	5.587	18.187	34.651	6.136	52.837
90	0.564	6.181	17.751	33.687	6.745	51.439
105	0.928	5.569	9.647	20.258	6.497	29.904
120	0.985	4.937	8.756	18.774	5.923	27.530
135	1.044	4.300	8.032	17.335	5.344	25.368
150	1.095	3.709	7.499	15.946	4.804	23.445
165	0.931	3.369	6.460	4.456	4.301	10.916
180	0.936	3.102	6.432	3.680	4.038	10.111
195	0.937	3.250	6.428	3.577	4.187	10.005
210	0.954	3.750	6.380	3.005	4.704	9.386
225	0.976	4.481	6.320	2.494	5.457	8.814
240	0.991	5.359	6.282	2.266	6.350	8.548
255	0.486	6.745	30.942	39.084	7.231	70.026
270	0.495	6.214	29.850	38.077	6.709	67.926
285	0.502	5.617	28.905	37.213	6.119	66.118
300	0.504	4.986	27.663	36.511	5.490	64.174
315	0.508	4.345	27.045	35.890	4.853	62.935
330	0.511	3.745	26.650	35.447	4.257	62.098
345	0.501	3.296	24.861	35.269	3.797	60.130
360	0.490	3.143	20.661	35.705	3.633	56.366

Table B.5. L_2 Halo orbit results for $i = 40°$ inclination of the LEO

θ (deg)	ΔV_1 (km/s)	ΔV_2 (km/s)	TOF_1 (days)	TOF_2 (days)	ΔV_T (km/s)	TOF_T (days)
0	0.503	3.147	23.895	35.253	3.649	59.149
15	0.518	3.290	18.956	36.950	3.808	55.906
30	0.523	3.780	18.906	36.758	4.303	55.664
45	0.530	4.447	18.830	36.420	4.976	55.250
60	0.539	5.181	18.665	35.918	5.720	54.583
75	0.549	5.927	18.477	35.235	6.477	53.712
90	0.561	6.652	18.111	34.464	7.213	52.575
105	0.980	5.909	9.055	19.299	6.889	28.354
120	1.038	5.160	8.319	17.926	6.198	26.245
135	1.090	4.429	7.749	16.639	5.519	24.388
150	0.954	3.917	6.496	7.497	4.871	13.993
165	0.947	3.361	6.462	4.251	4.308	10.713
180	0.947	3.101	6.452	4.076	4.048	10.528
195	0.949	3.261	6.448	3.879	4.210	10.327
210	0.961	3.774	6.414	3.439	4.736	9.853
225	0.980	4.512	6.359	2.892	5.492	9.251
240	0.996	5.389	6.313	2.688	6.385	9.001
255	1.008	6.344	6.283	2.437	7.352	8.720
270	0.504	6.683	28.859	37.414	7.187	66.273
285	0.508	5.958	27.821	36.710	6.465	64.531
300	0.513	5.208	27.227	36.111	5.721	63.339
315	0.516	4.470	26.742	35.631	4.987	62.373
330	0.514	3.803	25.987	35.321	4.317	61.309
345	0.504	3.315	24.091	35.281	3.818	59.371
360	0.506	3.150	24.684	35.194	3.656	59.878

Table B.6. L_2 Halo orbit results for $i = 50°$ inclination of the LEO

θ (deg)	ΔV_1 (km/s)	ΔV_2 (km/s)	TOF_1 (days)	TOF_2 (days)	ΔV_T (km/s)	TOF_T (days)
0	0.519	3.140	18.691	36.298	3.659	54.990
15	0.526	3.302	19.770	37.028	3.828	56.798
30	0.531	3.814	19.384	36.905	4.345	56.289
45	0.536	4.529	19.155	36.671	5.064	55.827
60	0.543	5.332	18.932	36.275	5.875	55.207
75	0.551	6.164	18.690	35.745	6.715	54.436
90	0.560	6.991	18.469	35.114	7.551	53.583
105	1.033	6.143	8.547	18.412	7.176	26.960
120	1.086	5.311	7.986	17.226	6.397	25.213
135	1.128	4.513	7.637	16.135	5.641	23.772
150	0.972	3.930	6.467	5.167	4.902	11.634
165	0.967	3.355	6.466	4.439	4.323	10.904
180	0.966	3.100	6.464	4.390	4.066	10.853
195	0.967	3.268	6.460	4.160	4.235	10.620
210	0.975	3.794	6.438	3.822	4.769	10.259
225	0.989	4.543	6.393	3.290	5.532	9.683
240	1.003	5.424	6.350	3.074	6.427	9.424
255	1.014	6.379	6.317	2.807	7.393	9.124
270	0.513	7.020	28.082	36.882	7.533	64.964
285	0.517	6.192	27.304	36.294	6.709	63.598
300	0.523	5.355	27.071	35.809	5.878	62.880
315	0.523	4.551	26.376	35.433	5.074	61.810
330	0.520	3.837	25.593	35.217	4.357	60.810
345	0.516	3.318	24.944	35.149	3.834	60.093
360	0.519	3.140	18.691	36.298	3.659	54.990

Table B.7. L_2 Halo orbit results for $i = 60°$ inclination of the LEO

θ (deg)	ΔV_1 (km/s)	ΔV_2 (km/s)	TOF_1 (days)	TOF_2 (days)	ΔV_T (km/s)	TOF_T (days)
0	0.516	3.147	21.975	35.439	3.663	57.415
15	0.537	3.307	19.381	37.068	3.844	56.449
30	0.540	3.835	19.270	36.988	4.375	56.257
45	0.544	4.580	19.076	36.807	5.124	55.883
60	0.549	5.432	19.127	36.538	5.981	55.665
75	0.555	6.327	18.995	36.154	6.882	55.149
90	0.561	7.230	18.678	35.667	7.792	54.346
105	1.085	6.307	8.200	17.681	7.392	25.881
120	1.129	5.414	7.839	16.692	6.543	24.530
135	0.996	4.714	6.800	11.346	5.710	18.146
150	0.994	3.936	6.467	4.886	4.930	11.353
165	0.990	3.352	6.468	4.442	4.342	10.910
180	0.988	3.100	6.468	4.313	4.088	10.782
195	0.989	3.273	6.467	4.451	4.263	10.918
210	0.995	3.807	6.451	4.103	4.802	10.555
225	1.003	4.568	6.421	3.746	5.571	10.167
240	1.013	5.456	6.384	3.376	6.469	9.760
255	1.022	6.414	6.353	3.176	7.436	9.529
270	0.522	7.259	27.207	36.366	7.781	63.573
285	0.527	6.354	26.835	35.924	6.880	62.759
300	0.528	5.458	26.164	35.565	5.986	61.730
315	0.530	4.604	25.970	35.321	5.133	61.291
330	0.531	3.854	25.990	35.122	4.385	61.111
345	0.524	3.323	24.856	35.115	3.847	59.971
360	0.516	3.147	21.975	35.439	3.663	57.415

Table B.8. L_2 Halo orbit results for $i = 70°$ inclination of the LEO

θ (deg)	ΔV_1 (km/s)	ΔV_2 (km/s)	TOF_1 (days)	TOF_2 (days)	ΔV_T (km/s)	TOF_T (days)
0	0.531	3.139	20.022	35.844	3.670	55.865
15	0.548	3.311	19.492	37.096	3.859	56.588
30	0.549	3.848	19.601	37.064	4.398	56.665
45	0.552	4.613	19.431	36.964	5.165	56.395
60	0.556	5.496	19.145	36.753	6.052	55.897
75	0.559	6.434	19.192	36.530	6.994	55.722
90	0.563	7.391	19.053	36.197	7.954	55.250
105	1.135	6.418	7.942	17.006	7.553	24.948
120	1.013	5.637	7.040	12.629	6.650	19.670
135	1.021	4.734	6.607	9.677	5.754	16.284
150	1.018	3.940	6.466	4.768	4.958	11.234
165	1.015	3.350	6.472	4.822	4.365	11.294
180	1.014	3.100	6.473	4.574	4.113	11.046
195	1.015	3.276	6.472	4.616	4.291	11.088
210	1.017	3.817	6.461	4.385	4.834	10.846
225	1.022	4.586	6.440	4.103	5.608	10.544
240	1.027	5.482	6.413	3.801	6.510	10.214
255	1.031	6.446	6.388	3.691	7.477	10.079
270	0.532	7.418	26.663	35.910	7.950	62.573
285	0.537	6.459	26.607	35.608	6.996	62.215
300	0.536	5.522	25.881	35.385	6.058	61.265
315	0.537	4.636	25.675	35.193	5.173	60.868
330	0.539	3.866	25.770	35.077	4.405	60.847
345	0.530	3.329	24.228	35.150	3.859	59.378
360	0.531	3.139	20.022	35.844	3.670	55.865

Table B.9. L_2 Halo orbit results for $i = 80°$ inclination of the LEO

θ (deg)	ΔV_1 (km/s)	ΔV_2 (km/s)	TOF_1 (days)	TOF_2 (days)	ΔV_T (km/s)	TOF_T (days)
0	0.546	3.148	25.436	35.020	3.694	60.455
15	0.560	3.313	19.478	37.132	3.873	56.610
30	0.559	3.856	19.960	37.113	4.415	57.072
45	0.561	4.631	19.585	37.064	5.192	56.649
60	0.562	5.533	19.672	36.998	6.095	56.670
75	0.564	6.496	19.409	36.881	7.059	56.291
90	0.566	7.483	19.263	36.718	8.049	55.981
105	1.179	6.490	7.794	16.307	7.669	24.101
120	1.043	5.660	6.644	10.219	6.703	16.864
135	1.044	4.744	6.455	4.949	5.788	11.404
150	1.043	3.941	6.466	4.723	4.984	11.189
165	1.042	3.349	6.472	4.611	4.390	11.082
180	1.041	3.099	6.479	5.203	4.141	11.682
195	1.042	3.278	6.473	4.667	4.319	11.140
210	1.042	3.821	6.466	4.611	4.864	11.077
225	1.044	4.597	6.453	4.561	5.641	11.014
240	1.045	5.499	6.434	4.320	6.544	10.754
255	1.046	6.467	6.414	4.199	7.513	10.613
270	0.545	7.507	26.294	35.433	8.052	61.727
285	0.547	6.518	26.229	35.262	7.065	61.491
300	0.546	5.556	25.759	35.177	6.102	60.936
315	0.547	4.652	25.753	35.077	5.199	60.830
330	0.544	3.876	25.172	35.077	4.420	60.249
345	0.539	3.332	24.146	35.119	3.871	59.265
360	0.546	3.148	25.436	35.020	3.694	60.455

Table B.10. L_2 Halo orbit results for $i = 90°$ inclination of the LEO

θ (deg)	ΔV_1 (km/s)	ΔV_2 (km/s)	TOF_1 (days)	TOF_2 (days)	ΔV_T (km/s)	TOF_T (days)
0	0.573	3.142	18.785	37.108	3.715	55.893
15	0.569	3.316	20.709	37.120	3.885	57.829
30	0.570	3.858	20.022	37.154	4.428	57.176
45	0.571	4.637	19.355	37.188	5.207	56.543
60	0.570	5.544	19.522	37.180	6.114	56.702
75	0.569	6.516	19.783	37.183	7.085	56.966
90	0.568	7.514	19.660	37.209	8.082	56.869
105	1.065	6.641	6.424	5.073	7.707	11.497
120	1.066	5.666	6.438	4.643	6.732	11.081
135	1.067	4.747	6.453	4.643	5.814	11.096
150	1.068	3.942	6.466	4.768	5.010	11.233
165	1.069	3.348	6.474	4.822	4.417	11.296
180	1.069	3.100	6.497	6.625	4.168	13.122
195	1.068	3.278	6.530	7.890	4.346	14.420
210	1.067	3.824	6.567	8.772	4.891	15.340
225	1.066	4.601	6.602	9.424	5.667	16.026
240	1.064	5.507	6.652	10.130	6.570	16.781
255	1.061	6.476	6.721	10.847	7.538	17.568
270	0.558	7.535	26.049	34.968	8.093	61.017
285	0.558	6.537	25.880	34.943	7.095	60.823
300	0.556	5.566	25.698	34.973	6.122	60.671
315	0.557	4.657	25.721	34.973	5.213	60.694
330	0.554	3.877	25.175	35.009	4.431	60.184
345	0.552	3.330	24.685	35.051	3.881	59.736
360	0.545	3.160	22.658	35.301	3.705	57.960

B.2 L_2 Lyapunov Orbit

Results for L_2 Lyapunov orbit with initial conditions given in Table 4.8 are presented in Tables B.11 - B.20.

Table B.11. L_2 Lyapunov orbit results for $i = 0°$ inclination of the LEO

θ (deg)	ΔV_1 (km/s)	ΔV_2 (km/s)	TOF_1 (days)	TOF_2 (days)	ΔV_T (km/s)	TOF_T (days)
0	0.488	3.141	21.109	35.653	3.629	56.763
15	0.505	3.140	20.330	34.206	3.645	54.536
30	0.537	3.125	19.346	33.497	3.661	52.843
45	0.545	3.138	18.455	31.392	3.683	49.847
60	0.570	3.136	17.488	29.886	3.706	47.374
75	0.598	3.135	16.566	28.356	3.733	44.922
90	0.629	3.133	15.571	26.753	3.762	42.324
105	0.664	3.132	14.324	25.191	3.796	39.515
120	0.704	3.129	13.164	23.401	3.833	36.565
135	0.749	3.126	11.884	21.543	3.875	33.427
150	0.801	3.122	10.473	19.456	3.923	29.929
165	0.862	3.117	8.913	16.886	3.979	25.799
180	0.932	3.097	6.440	4.223	4.028	10.664
195	0.956	3.252	6.367	2.170	4.208	8.537
210	0.980	3.749	6.307	1.472	4.729	7.779
225	0.429	4.719	26.396	43.491	5.148	69.886
240	0.427	3.924	26.413	43.491	4.351	69.904
255	0.425	3.355	26.518	43.471	3.780	69.989
270	0.425	3.146	26.665	43.441	3.571	70.106
285	0.433	3.145	25.414	42.258	3.578	67.673
300	0.441	3.144	24.787	40.905	3.585	65.693
315	0.451	3.143	23.564	39.716	3.594	63.280
330	0.462	3.143	22.929	38.316	3.604	61.244
345	0.474	3.142	21.960	37.008	3.616	58.969
360	0.489	3.141	20.955	35.693	3.629	56.648

Table B.12. L_2 Lyapunov orbit results for $i = 10°$ inclination of the LEO

θ (deg)	ΔV_1 (km/s)	ΔV_2 (km/s)	TOF_1 (days)	TOF_2 (days)	ΔV_T (km/s)	TOF_T (days)
0	0.488	3.519	21.109	35.653	4.007	56.763
15	0.494	3.305	20.842	35.329	3.799	56.171
30	0.504	3.604	20.490	34.565	4.108	55.055
45	0.517	3.927	19.979	33.645	4.444	53.624
60	0.533	4.237	19.266	32.620	4.769	51.886
75	0.551	4.514	18.665	31.399	5.065	50.064
90	0.572	4.743	17.891	30.105	5.315	47.996
105	0.765	4.500	11.756	21.248	5.266	33.004
120	0.809	4.217	10.528	19.516	5.026	30.044
135	0.852	3.902	9.386	17.700	4.754	27.085
150	0.896	3.573	8.212	15.571	4.469	23.782
165	0.930	3.265	7.027	12.324	4.195	19.352
180	0.932	3.478	6.439	4.069	4.410	10.509
195	0.949	3.273	6.397	2.659	4.222	9.056
210	0.981	3.757	6.312	1.757	4.738	8.069
225	0.997	4.502	6.277	1.259	5.499	7.535
240	0.431	4.988	26.493	43.125	5.420	69.618
255	0.440	4.913	25.466	41.846	5.353	67.311
270	0.449	4.751	24.777	40.590	5.199	65.367
285	0.458	4.520	23.536	39.557	4.978	63.093
300	0.466	4.241	22.903	38.477	4.707	61.380
315	0.474	3.929	22.129	37.540	4.403	59.669
330	0.481	3.606	21.827	36.574	4.087	58.401
345	0.488	3.305	21.323	35.887	3.793	57.210
360	0.488	3.519	21.109	35.653	4.007	56.763

Table B.13. L_2 Lyapunov orbit results for $i = 20°$ inclination of the LEO

θ (deg)	ΔV_1 (km/s)	ΔV_2 (km/s)	TOF_1 (days)	TOF_2 (days)	ΔV_T (km/s)	TOF_T (days)
0	0.488	4.457	21.233	35.634	4.945	56.867
15	0.496	3.337	21.394	35.369	3.833	56.763
30	0.504	3.764	20.895	34.938	4.268	55.833
45	0.514	4.265	20.403	34.310	4.779	54.713
60	0.527	4.772	19.979	33.422	5.299	53.400
75	0.541	5.254	19.331	32.487	5.796	51.817
90	0.559	5.687	18.605	31.372	6.246	49.977
105	0.815	5.234	10.683	19.703	6.050	30.386
120	0.857	4.747	9.609	18.042	5.604	27.651
135	0.895	4.234	8.578	16.267	5.129	24.845
150	0.929	3.727	7.555	14.056	4.656	21.611
165	0.945	3.294	6.661	10.176	4.238	16.837
180	0.932	4.421	6.440	4.112	5.353	10.552
195	0.949	3.294	6.424	3.351	4.243	9.774
210	0.981	3.782	6.337	1.913	4.763	8.250
225	1.001	4.519	6.288	1.481	5.521	7.769
240	1.014	5.405	6.260	1.191	6.420	7.451
255	0.454	6.053	24.737	40.639	6.507	65.376
270	0.463	5.693	23.931	39.501	6.157	63.432
285	0.471	5.259	23.555	38.386	5.731	61.941
300	0.479	4.775	22.353	37.655	5.254	60.008
315	0.486	4.266	21.831	36.856	4.752	58.687
330	0.490	3.765	21.506	36.170	4.255	57.677
345	0.493	3.337	21.358	35.659	3.830	57.017
360	0.488	4.457	21.233	35.634	4.945	56.867

Table B.14. L_2 Lyapunov orbit results for $i = 30°$ inclination of the LEO

θ (deg)	ΔV_1 (km/s)	ΔV_2 (km/s)	TOF_1 (days)	TOF_2 (days)	ΔV_T (km/s)	TOF_T (days)
0	0.488	5.664	21.296	35.645	6.152	56.941
15	0.501	3.347	21.105	35.514	3.848	56.619
30	0.506	3.840	21.285	35.102	4.347	56.387
45	0.515	4.451	20.886	34.615	4.967	55.501
60	0.526	5.095	20.234	34.016	5.621	54.251
75	0.538	5.730	19.990	33.131	6.268	53.121
90	0.552	6.327	19.327	32.204	6.879	51.531
105	0.858	5.705	9.925	18.535	6.563	28.460
120	0.897	5.065	8.934	16.931	5.961	25.865
135	0.930	4.415	8.028	15.169	5.345	23.197
150	0.954	3.799	7.165	12.866	4.753	20.031
165	0.959	3.303	6.521	8.361	4.262	14.881
180	0.932	5.631	6.439	4.004	6.563	10.443
195	0.960	3.303	6.432	3.583	4.263	10.015
210	0.983	3.814	6.371	2.485	4.797	8.855
225	1.008	4.545	6.306	1.816	5.553	8.122
240	1.022	5.428	6.272	1.352	6.450	7.623
255	0.467	6.865	24.242	39.672	7.332	63.914
270	0.476	6.333	23.737	38.607	6.809	62.344
285	0.485	5.734	22.683	37.828	6.218	60.511
300	0.491	5.098	22.308	37.025	5.589	59.333
315	0.496	4.452	21.774	36.404	4.948	58.178
330	0.499	3.840	21.149	36.012	4.339	57.162
345	0.499	3.347	21.230	35.634	3.846	56.863
360	0.488	5.664	21.296	35.645	6.152	56.941

Table B.15. L_2 Lyapunov orbit results for $i = 40°$ inclination of the LEO

θ (deg)	ΔV_1 (km/s)	ΔV_2 (km/s)	TOF_1 (days)	TOF_2 (days)	ΔV_T (km/s)	TOF_T (days)
0	0.487	6.976	21.361	35.659	7.463	57.020
15	0.507	3.353	21.633	35.399	3.859	57.032
30	0.512	3.881	22.162	35.038	4.393	57.201
45	0.519	4.564	21.146	34.848	5.083	55.994
60	0.528	5.305	20.686	34.365	5.833	55.052
75	0.538	6.055	20.292	33.711	6.593	54.002
90	0.550	6.782	19.664	32.951	7.332	52.615
105	0.898	6.025	9.310	17.541	6.923	26.850
120	0.933	5.270	8.431	15.991	6.203	24.422
135	0.961	4.524	7.643	14.271	5.484	21.915
150	0.977	3.836	6.916	11.832	4.813	18.748
165	0.977	3.307	6.461	6.438	4.284	12.898
180	0.917	6.959	7.374	13.529	7.875	20.903
195	0.977	3.307	6.434	3.746	4.284	10.180
210	0.992	3.840	6.398	2.871	4.832	9.269
225	1.015	4.578	6.332	1.977	5.593	8.309
240	1.031	5.458	6.291	1.572	6.489	7.862
255	1.043	6.414	6.259	1.412	7.458	7.671
270	0.489	6.787	23.103	37.995	7.276	61.098
285	0.496	6.058	22.547	37.247	6.555	59.794
300	0.502	5.307	22.125	36.608	5.809	58.734
315	0.505	4.565	21.790	36.121	5.070	57.911
330	0.506	3.881	21.847	35.655	4.387	57.502
345	0.506	3.352	21.453	35.518	3.858	56.972
360	0.487	6.976	21.361	35.659	7.463	57.020

Table B.16. L_2 Lyapunov orbit results for $i = 50°$ inclination of the LEO

θ (deg)	ΔV_1 (km/s)	ΔV_2 (km/s)	TOF_1 (days)	TOF_2 (days)	ΔV_T (km/s)	TOF_T (days)
0	0.487	8.313	21.321	35.736	8.799	57.056
15	0.515	3.354	21.633	35.399	3.870	57.032
30	0.519	3.903	21.518	35.281	4.422	56.799
45	0.525	4.634	21.257	35.033	5.159	56.290
60	0.532	5.446	21.053	34.630	5.977	55.683
75	0.540	6.282	20.763	34.102	6.822	54.864
90	0.549	7.111	20.129	33.538	7.659	53.667
105	0.936	6.247	8.752	16.593	7.184	25.345
120	0.967	5.406	8.029	15.159	6.373	23.188
135	0.990	4.591	7.330	13.409	5.580	20.739
150	1.000	3.857	6.760	10.943	4.857	17.703
165	0.998	3.309	6.443	4.939	4.307	11.382
180	0.903	8.305	7.825	14.719	9.207	22.545
195	0.998	3.309	6.436	3.981	4.307	10.418
210	1.007	3.858	6.414	3.237	4.865	9.651
225	1.026	4.610	6.360	2.333	5.636	8.693
240	1.041	5.492	6.314	1.894	6.534	8.208
255	1.053	6.448	6.280	1.779	7.501	8.058
270	0.502	7.115	22.941	37.352	7.616	60.293
285	0.508	6.285	22.555	36.733	6.793	59.288
300	0.513	5.447	21.840	36.347	5.960	58.188
315	0.515	4.635	22.032	35.815	5.150	57.848
330	0.515	3.903	21.737	35.585	4.419	57.322
345	0.515	3.355	21.715	35.426	3.869	57.141
360	0.487	8.313	21.321	35.736	8.799	57.056

Table B.17. L_2 Lyapunov orbit results for $i = 60°$ inclination of the LEO

θ (deg)	ΔV_1 (km/s)	ΔV_2 (km/s)	TOF_1 (days)	TOF_2 (days)	ΔV_T (km/s)	TOF_T (days)
0	0.486	9.632	21.351	35.836	10.118	57.186
15	0.524	3.357	21.972	35.345	3.881	57.317
30	0.528	3.917	21.341	35.399	4.444	56.740
45	0.532	4.679	21.559	35.109	5.211	56.668
60	0.536	5.540	21.576	34.796	6.076	56.371
75	0.542	6.439	21.231	34.450	6.981	55.681
90	0.548	7.344	20.873	33.979	7.892	54.852
105	0.975	6.399	8.265	15.664	7.374	23.930
120	1.001	5.495	7.631	14.263	6.496	21.893
135	1.018	4.632	7.077	12.542	5.650	19.620
150	1.024	3.870	6.630	9.906	4.894	16.536
165	1.022	3.310	6.437	4.069	4.332	10.507
180	0.882	9.635	8.414	15.960	10.517	24.374
195	1.022	3.310	6.436	3.909	4.332	10.345
210	1.027	3.870	6.422	3.530	4.897	9.952
225	1.038	4.639	6.387	2.822	5.677	9.209
240	1.051	5.528	6.345	2.333	6.579	8.678
255	1.061	6.486	6.310	2.101	7.547	8.411
270	0.515	7.346	22.436	36.882	7.861	59.318
285	0.520	6.441	22.326	36.366	6.960	58.692
300	0.523	5.540	21.987	35.999	6.063	57.986
315	0.525	4.679	21.719	35.742	5.205	57.462
330	0.526	3.917	21.435	35.607	4.442	57.043
345	0.524	3.356	21.715	35.426	3.880	57.141
360	0.486	9.632	21.351	35.836	10.118	57.186

Table B.18. L_2 Lyapunov orbit results for $i = 70°$ inclination of the LEO

θ (deg)	ΔV_1 (km/s)	ΔV_2 (km/s)	TOF_1 (days)	TOF_2 (days)	ΔV_T (km/s)	TOF_T (days)
0	0.484	10.909	21.531	36.000	11.393	57.531
15	0.534	3.357	21.972	35.345	3.891	57.317
30	0.536	3.926	22.185	35.244	4.462	57.429
45	0.539	4.707	21.785	35.203	5.246	56.988
60	0.542	5.599	21.647	35.018	6.142	56.665
75	0.546	6.542	21.439	34.782	7.088	56.221
90	0.550	7.500	21.243	34.464	8.049	55.707
105	1.013	6.498	7.789	14.664	7.511	22.452
120	1.034	5.551	7.279	13.281	6.585	20.560
135	1.046	4.657	6.863	11.584	5.703	18.447
150	1.049	3.877	6.552	8.961	4.926	15.513
165	1.048	3.311	6.438	4.248	4.359	10.686
180	0.851	10.925	9.270	17.493	11.776	26.763
195	1.047	3.311	6.440	4.524	4.359	10.963
210	1.051	3.877	6.427	3.725	4.927	10.152
225	1.056	4.658	6.405	3.468	5.714	9.873
240	1.063	5.559	6.375	2.876	6.622	9.251
255	1.069	6.522	6.345	2.691	7.591	9.036
270	0.527	7.501	22.406	36.311	8.029	58.716
285	0.531	6.543	22.383	35.937	7.074	58.320
300	0.534	5.600	22.155	35.711	6.133	57.867
315	0.535	4.707	22.061	35.528	5.242	57.589
330	0.535	3.925	22.093	35.384	4.460	57.477
345	0.535	3.356	21.567	35.448	3.891	57.015
360	0.484	10.909	21.531	36.000	11.393	57.531

Table B.19. L_2 Lyapunov orbit results for $i = 80°$ inclination of the LEO

θ (deg)	ΔV_1 (km/s)	ΔV_2 (km/s)	TOF_1 (days)	TOF_2 (days)	ΔV_T (km/s)	TOF_T (days)
0	0.480	12.123	21.698	36.442	12.603	58.140
15	0.545	3.357	21.972	35.345	3.902	57.317
30	0.547	3.929	21.622	35.399	4.475	57.022
45	0.547	4.722	21.778	35.302	5.269	57.080
60	0.548	5.633	21.795	35.200	6.181	56.995
75	0.549	6.601	21.972	35.017	7.150	56.989
90	0.551	7.590	21.757	34.896	8.141	56.653
105	1.053	6.550	7.276	13.315	7.604	20.591
120	1.067	5.580	6.922	11.942	6.647	18.864
135	1.074	4.670	6.643	10.110	5.744	16.753
150	1.075	3.880	6.480	7.467	4.956	13.947
165	1.075	3.311	6.444	5.073	4.386	11.517
180	0.441	12.462	27.158	43.322	12.903	70.479
195	1.074	3.312	6.465	6.616	4.386	13.081
210	1.076	3.880	6.430	4.035	4.956	10.464
225	1.077	4.670	6.416	3.803	5.747	10.218
240	1.079	5.578	6.396	3.530	6.657	9.926
255	1.081	6.548	6.374	3.385	7.629	9.759
270	0.540	7.591	22.318	35.824	8.130	58.142
285	0.542	6.601	22.145	35.680	7.143	57.825
300	0.544	5.633	22.038	35.528	6.177	57.567
315	0.545	4.723	22.159	35.401	5.267	57.560
330	0.545	3.929	22.045	35.366	4.475	57.411
345	0.545	3.357	21.972	35.345	3.902	57.317
360	0.480	12.123	21.698	36.442	12.603	58.140

Table B.20. L_2 Lyapunov orbit results for $i = 90°$ inclination of the LEO

θ (deg)	ΔV_1 (km/s)	ΔV_2 (km/s)	TOF_1 (days)	TOF_2 (days)	ΔV_T (km/s)	TOF_T (days)
0	0.441	13.258	27.209	43.312	13.698	70.521
15	0.555	3.358	23.066	35.137	3.913	58.203
30	0.555	3.931	22.558	35.234	4.486	57.791
45	0.554	4.728	22.649	35.220	5.282	57.869
60	0.554	5.644	22.006	35.366	6.198	57.372
75	0.553	6.620	22.432	35.260	7.174	57.692
90	0.553	7.619	21.952	35.366	8.173	57.318
105	1.098	6.557	6.396	5.366	7.655	11.763
120	1.100	5.585	6.408	4.754	6.684	11.163
135	1.101	4.673	6.419	4.144	5.773	10.563
150	1.101	3.881	6.430	4.066	4.983	10.496
165	1.102	3.311	6.449	5.627	4.413	12.077
180	0.441	13.258	27.210	43.312	13.698	70.522
195	1.101	3.312	6.485	7.408	4.413	13.893
210	1.100	3.882	6.505	8.109	4.982	14.614
225	1.098	4.675	6.527	8.740	5.773	15.268
240	1.096	5.588	6.565	9.465	6.684	16.030
255	1.094	6.561	6.610	10.110	7.655	16.720
270	0.553	7.619	21.952	35.366	8.172	57.318
285	0.554	6.620	22.245	35.265	7.174	57.510
300	0.555	5.643	21.922	35.345	6.198	57.267
315	0.556	4.727	21.605	35.399	5.283	57.005
330	0.556	3.931	21.961	35.345	4.486	57.306
345	0.555	3.357	22.321	35.265	3.913	57.586
360	0.441	13.258	27.209	43.312	13.698	70.521

References

[1] Abraham, A. J., D. B. Spencer, and T. J. Hart (2014) "Particle Swarm Optimization of 2-Maneuver, Impulsive Transfers From LEO to Lagrange Point Orbits via Shooting," Proceedings of the 24th International Symposium on Space Flight Dynamics.

[2] Abraham, A. J. (2014) *Particle Swarm Optimization of Low-Thrust, Geocentric-to-Halo-Orbit Transfers*, Ph.d. dissertation, Department of Mechanical Engineering, Lehigh University, Bethlehem, PA.

[3] Koon, W. S., M. W. Lo, J. E. Marsden, and S. D. Ross (2008) *Dynamical Systems, the Three-Body Problem and Space Mission Design*, Marsden Books.

[4] Poincaré, H. (1893) *Les Methodes Nouvelles de la Mecanique Celeste*, Gauthier-Villars.

[5] Farquhar, R. W. (1972) "A Halo-Orbit Lunar Station," *Astronautics & Aeronautics*, **10**, pp. 59–63.

[6] Lo, M. W. and S. D. Ross (2001) "The Lunar L1 Gateway: Portal to the Stars and Beyond," AIAA SPACE 2001 Conference, Alburquerque, New Mexico.

[7] Dunham, D. and R.W.Farquhar (2011) *Libration Point Missions, 1978 – 2002*, World Scientific.

[8] Koon, W. S., M. W. Lo, J. Marsden, and S. Ross (1999) "The Genesis Trajectory and Heteroclinic Cycles," *Advances in Astronautical Sciences*, **103**, pp. 2327–2343.

[9] Vallado, D. A. (2001) *Fundamentals of Astrodynamics and Applications*, 2nd ed., Microcosm Press and Kluwer Academic Publishers, El Segundo, California.

[10] Parker, J. S. and R. L. Anderson (2014) *Low-Energy Lunar Trajectory Design*, John Wiley and Sons.

[11] Howell, K. C. (1984) "Three-Dimensional, Periodic, 'Halo' Orbits," *Celestial Mechanics*, **32**, pp. 53 – 71.

[12] Pavlak, T. A. (2010) *Mission Design Applications In The Earth-Moon System: Transfer Trajectories and Stationkeeping*, Master's thesis, School of Aeronautics and Astronautics, Purdue University, West Lafayette, IN.

[13] Parker, J. S. (2003) *Low-Energy Ballistic Lunar Transfers*, Ph.d. dissertation, Department of Aerospace Engineering Sciences, University of Colorado, Boulder,CO.

[14] Rausch, R. R. (2005) *Earth to Halo Orbit Transfer Trajectories*, Master's thesis, School of Aeronautics and Astronautics, Purdue University, West Lafayette, IN.

[15] Richardson, D. L. (1980) "Analytic construction of periodic orbits about the collinear points," *Celestial Mechanics*, **22**, pp. 241–253.

[16] Strogatz, S. H. (1994) *Nonlinear Dynamics and Chaos*, Westview Press.

[17] Wiggins, S. (1990) *Introduction to Applied Nonlinear Dynamical Systems and Chaos*, Springer.

[18] Guckenheimer, J. and P. Holmes (1991) *Nonlinear Oscillations*, John Wiley and Sons.

[19] Grebow, D. (2006) *Generating Periodic Orbits in the Circular Restricted Three-Body Problem with Applications to Lunar South Pole Coverage*, Master's thesis, School of Aeronautics and Astronautics, Purdue University, West Lafayette, IN.

[20] Perko, L. (2001) *Differential Equations and Dynamical Systems*, 3rd ed., Springer, 175 Fifth Avenue, New York, NY, 10010, USA.

[21] Breakwell, J. and J. Brown (1979) "The "Halo" Family of 3-Dimensional Periodic Orbits in the Earth-Moon Restricted 3-Body Problem," *Celestial Mechanics*, **20**, pp. 389–404.

[22] Gordon, D. P. (2008) *Transfers to Earth-Moon L2 Orbits Using Lunar Proximity and Invariant Manifolds*, Master's thesis, School of Aeronautics and Astronautics, Purdue University, West Lafayette, IN.

[23] Butenko, S. and P. M. Pardalos (2014) *Numerical Methods and Optimization: An Introduction*, CRC Press, Oxfordshire, UK.

[24] Nocedal, J. and S. J. Wright (2006) *Numerical Optimization*, Springer, New York.

[25] Hare, W., J. Nutini, and S. Tesfamariam (2013) "A survey of non-gradient optimization methods in structural engineering," *Advances in Engineering Software*, **59**, pp. 19 – 28.

[26] Kennedy, J. and R. Eberhart (1995) "Particle Swarm Optimization," in *Proceedings of IEEE International Conference on Neural Networks*, vol. 4, Western Australia, pp. 1942–1948.

[27] Poli, R. (2008) "Analysis of the Publications on the Applications of Particle Swarm Optimization," *Journal of Artifical Evolution and Applications*, **2008**, pp. 4:1–4:10.

[28] Pontani, M. and B. A. Conway (2010) "Particle Swarm Optimization Applied to Space Trajectories," *Journal of Guidance, Control, and Dynamics*, **33**(5), pp. 1429–1441.

[29] Conway, B. A. (ed.) (2010) *Spacecraft Trajectory Optimization*, Cambridge.

[30] Curtis, H. D. (2014) *Orbital Mechanics for Engineering Students*, 3rd ed., Elsevier, Oxford, UK.

[31] Prussing, J. E. and B. A. Conway (2013) *Orbital Mechanics*, 2nd ed., Oxford University Press.